INTERNATIONAL SCIENTIFIC JOURNAL

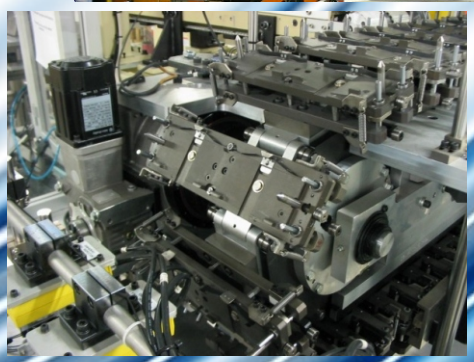
trans & MOTAUTO WORLD

ISSN PRINT 2367-8399
ISSN WEB 2534-8493

YEAR VII, ISSUE 2/2022









SCIENTIFIC TECHNICAL UNION OF MECHANICAL INGENEERING "INDUSTRY 4.0"
108 RAKOVSKI STR., SOFIA 1000, BULGARIA

INTERNATIONAL SCIENTIFIC JOURNAL

TRANS MOTAUTO WORLD

PUBLISHER:

SCIENTIFIC TECHNICAL UNION OF MECHANICAL ENGINEERING INDUSTRY-4.0

108, Rakovski Str., 1000 Sofia, Bulgaria
tel. (+359 2) 987 72 90,
tel./fax (+359 2) 986 22 40**,**
office@stumejournals.com
www.stumejournals.com

ISSN PRINT 2367-8399
ISSN WEB 2534-8493
YEAR VII, ISSUE 2 / 2022

EDITORIAL BOARD

CHIEF EDITOR
Prof. Petar Kolev, Bulgaria

MEMBERS:

Prof. Ahmet H. Ertas, TR	Prof. Massimo Borghi, IT
Prof. Aleksandar Kostikj, MK	Prof. Miho Mihow, BG
Prof. Andrey Ferenets, RU	Prof. Murat Dogruel, TR
Prof. Angel Dimitrov, BG	Prof. Natalia Sidenko, LV
Prof. Beti Angelevska, MK	Prof. Natasa Tomic-Petrovic, RS
Prof. Dainis Berjoza, LV	Prof. Nikolay Georgiev, BG
Prof. Dan Scarpete, RO	Prof. Nikolay Ovchenkov, RU
Prof. Daniela Todorova, BG	Prof. Oleg Sharkov, RU
Prof. Emilia Andreeva-Moschen, AT	Prof. Pepo Yordanov, BG
Prof. Hristo Stanchev, BG	Prof. Polatbeg Zhunisbekov, KZ
Prof. Igor Penkov, EE	Prof. Rinat Kurmaev, RU
Prof. Igor Smirnov, UA	Prof. Rosen Ivanov, BG
Prof. Igor Taratorkin, RU	Prof. Sanjin Troha, HR
Prof. Iliyan Lilov, BG	Prof. Teymuraz Kochadze, GE
Prof. Lech Sitnik, PL	Prof. Tomaz Morchadze, GE
Prof. Ljudmila Boyko, UA	Prof. Vadim Zhmud, RU
Prof. Madaminjon Aripdzanov, UZ	Prof. Valyo Nikolov, BG
Prof. Martin Kendra, SK	Prof. Zoran Jovanovic, RS

RESPONSIBLE SECRETARY:
Prof. Nikolay Tonchev, Bulgaria

C O N T E N T S

TRANSPORT TECHNICS. INVESTIGATION OF ELEMENTS. RELIABILITY

Extension of geometry and investigation of deformation on crossed helical gears to increase load capacity and performance
Linda Becker, Christian Kirchhoff, Peter Tenberge, Dietmar Vill 42

Acoustic emission method of diagnostic of elevating rudder covering in places of lightning strikes impact
Leonid Vinogradov, Muharbij Banov, Alekseij Nasibulin 47

Application of hardfacing arc methods in Bulgarian ship repair SME
Yordan Denev 50

TRANSPORT. SAFETY AND ECOLOGY. LOGISTICS AND MANAGEMENT

Perspectives of the auto world during the pandemic – international and national view
Nataša Tomić-Petrović 53

Practical UML subset for railway engineers to support formal modeling
Gábor Lukács, Tamás Bartha 56

Unaccompanied combined transport with rail legs in Romania
Nicolae Mugure Tănăsuică 60

Comparative Analysis of Methods for Defining the Speed of the Vehicle in Vehicle- Pedestrian Collisions
Zovak Goran, Kučinić Tomislav, Cindrić Josip, Velić Želimir 71

Using algorithms to solve problems in urban transport optimization Case study: Prishtina
Sallauka Astrit, LikajRame, Gashi Blendi 77

VEHICLE ENGINES. APPLICATION OF FUELS TYPES. EFFICIENCY

Energy analysis of two-cylinder steam turbine from nuclear power plant
Mrzljak Vedran, Prpić-Oršić Jasna, Baressi Šegota Sandi, Medica-Viola Vedran 81

Extension of geometry and investigation of deformation on crossed helical gears to increase load capacity and performance

Linda Becker, Christian Kirchhoff, Peter Tenberge, Dietmar Vill
Ruhr-University Bochum Germany
Linda.Becker@rub.de, Christian.Kirchhoff@rub.de, peter.tenberge@rub.de, dietmar.vill@rub.de

Abstract: *Crossed helical gear units are used in many applications. They range from actuators and power take-offs to household appliances and functions in automotive engineering and production processes. The design is often based on a material combination of steel-worm and plastic-wheel. Based on the research on high efficient plastic materials, they already replace a large number of steel applications. In order to improve the load capacity and performance of crossed helical gears, they must be understood in detail. This article deals with a new calculation method to design optimized flank geometries and to investigate them with regard to their properties in gear mesh. In addition, the deformation and the load distribution in the gear mesh will be examined in more detail. The observation is made in the normal section. In this section, all relevant influences on the performance of the gearing can be analyzed. The pressure and deformation are verified with the help of an FEM-simulations.*

Keywords*: CROSSED HELICAL GEARS, PLASTIC GEARS, FEM-SIMULATION*

1. Introduction

The multitude of applications of crossed helical gear units requires quickly adaptable and optimally designed gearings. Crossed helical gears are found in actuators and auxiliary drives as well as they are increasingly used in automation processes. The high gear ratio in a small space is a great advantage, like it is in worm gears. The development of highly efficient and resilient plastic materials makes it possible to replace more gear applications with steel wheels by plastic wheels. The material behavior of plastic is different than steel. A number of influencing factors have to be taken into account. This paper describes the approach in a research project in which a new calculation method for designing and calculating the loads on crossed helical gears was developed. To investigate the meshing behavior and load distribution of crossed helical gears, it is necessary to know the exact geometry.

Niemann and Winter [1] calculate the geometry of a crossed helical gear using a counterpart rack. The rack rolls on the two pitch circles of the individual gears. The gears, considered in this article, consists of a worm and a helical gear. For this reason, the terms worm and wheel are used in the following text. Niemann and Winter [1] calculate the meshing, pressures, sliding paths etc. only at the screw point. Boehme [2] has extended the approach. He defines a counterpart rack from two known gears. The rack is a thin counterpart rack in space. Boehme calculates the variables along the entire path of contact. His approach allows changes for axis distance and changes in the axis crossing angle of 90°. VDI 2736-3 [3] provides a simple procedure for the initial evaluation of the load-carrying capacity. In order to be able to take all necessary influences into account, the investigations must be carried out in more detail.

The calculations in this article are also based on the gear geometries derived with the help of a counterpart rack arranged in space. The geometry of the worm and the wheel is generated by applying the law of gearing. Pressures and sliding paths can be calculated in the entire contact path. The distribution of load on the individual teeth has an influence on the running behavior and load-carrying capacity of a gear. The more tooth flanks are in contact, the less load each individual tooth has to bear. The load distribution on the tooth flanks depends on the stiffness of the plastic material and the deformation of the teeth. To verify the calculation, these correlations are analyzed with the help of FEM-simulations.

2. Calculation process

A crossed helical gear consists of two cylindrical gears. The axes of these two gears cross at a shaft angle Σ and have the center distance a.

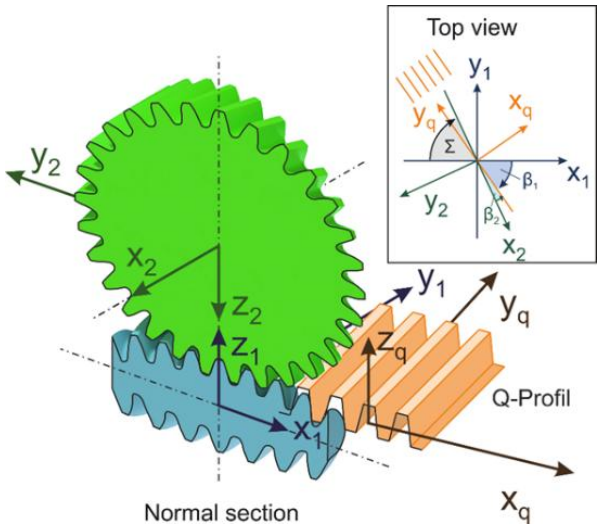


Fig. 1 *Coordinate systems of the crossed helical gear (normal section) and Q-profile*

For further investigations, it is necessary to determine some basic parameters of the gear pair to be designed: the numbers of teeth z_1, z_2, the normal modulus m_n and the centre distance a, the pressure angle in the normal section α_n, the shaft angle Σ and the two helix angles β_1 and β_2. From these parameters, the remaining parameters can be calculated. The reference profile is selected according to standard with DIN 867 [4].

The parameters are defined in individual coordinate systems. The right-hand coordinate system of wheel 1 (system 1) and wheel 2 (system 2) are shown in Fig. 1. For the analysis in the gear meshing, both wheels must be considered in one system. This is done by a global coordinate system X, Y, Z, which corresponds to the system of wheel 1. The counterpart rack has a local coordinate system q, which is also shown in Fig. 1. A fourth order polynomial (equation 1) forms the rack profile. This will be called Q-profile in the further cause of article. The individual coefficients q_0 to q_4 can be chosen arbitrarily. The pitch is considered in the coefficient q_0. q_1 considers the normal pressure angle and influences the gradient of the flank line. q_2, as well as q_3 allow various modifications to the profile for optimum design of the gears. In this article, for the involute form only q_0 and q_1 are used.

$$y_q(u) = q_0 + q_1 \cdot u + q_2 \cdot u^2 + q_3 \cdot u^3 + q_4 \cdot u^4 \qquad (1)$$

$$z_q(u) = u \cdot mm \qquad (2)$$

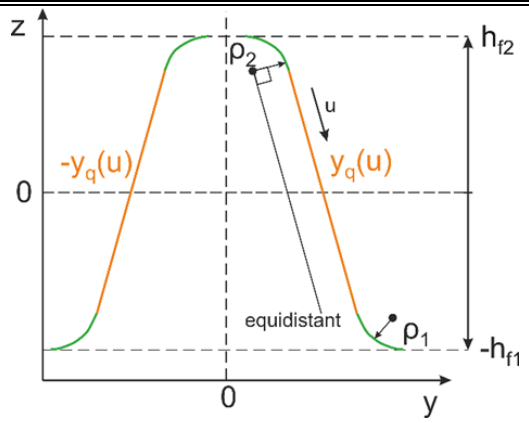


Fig. 2 *Profile of the counterpart rack of an involute flank with q_0 and q_1; the fourth order polynomial from equation 1 is shown in orange*

The parameter u describes the flank course of the Q-profile, which is initially limited by the dedendums h_{f1} and h_{f2}. It is assumed that the tip diameters result from the diameter of the material cylinders during the manufacturing process. For plastic wheels, the type of manufacturing process determines the tip circle. The rounding on the Q-profile are only required to create the tooth root fillets of the two wheels. The transition between the tip fillet of the Q-profile and the flank line is tangential and smooth. Mirroring a flank creates a whole tooth, so the whole counterpart rack can be generated. Fig. 1 shows the counterpart rack, the rack profile is shown in Fig. 2. To describe the complete Q-Profile, tangent and normal vectors at the Q profile have to be determined. These become particularly important when considering the velocities in meshing and the Hertzian theory. For the transformation of the tangent vectors into the transverse sections of the wheels, the helix angles β_1 and β_2 are required. The Q-profile, including the vectors associated with, are transformed in the coordinate systems of wheel 1 or 2.

The path of contact results from the points of contact with the Q-profile. The observation is made in the transverse section of the worm or the wheel. For each point on the path of contact, there is one point of contact on the rack and one on the flank. The rack moves translationally along the profile reference line. The gear rotates with angular velocity $\omega_{1,2}$ around its own axis of rotation. A profile point P on the rack meets the wheel point S at the pitch point E. The z-coordinate of the point on the rack corresponds to the z-coordinate of the pitch point. For the y-coordinate, the law of gearing is considered. The parameters from equation 3 depend on the variable u, which describes the flank course.

$$y_{e1}(u) = (r_{01} - z_{p1}(u)) \cdot \left(\frac{z'_{p1}(u)}{y'_{p1}(u)}\right) \qquad (3)$$

With the aid of a known point E, a point S on the flank is determined. Both gears mesh with each other, if each mesh with the counterpart rack.

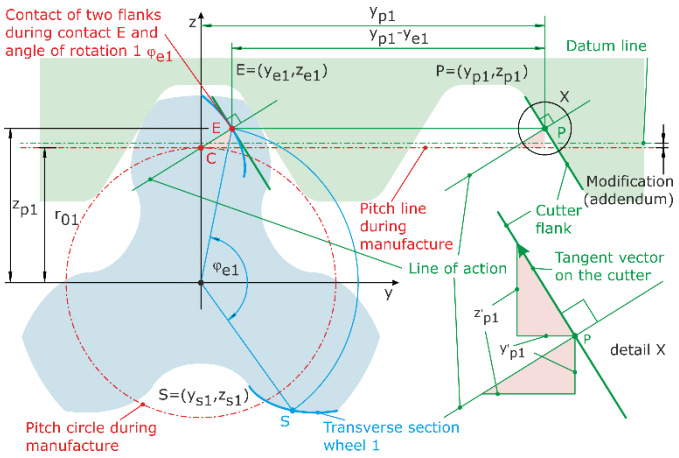


Fig. 3 *Deriving the gear geometry from the counterpart rack and the gear law*

The rack can be used in different angular positions. This enables variable shaft angles according to Boehme [2]. The path of contact is limited by the two tip diameters. The start of meshing A results from the cross point of the path of contact with the tip diameter of gear 2, the end of meshing E results from the cross point with the tip diameter of gear 1.

The path of contact is derived from the two transverse sections. In each transverse section, there exists a pitch point $E_{1,2}$. From these, the pitch point ES of the crossed helical gear is obtained. From the coordinates of the contact points in each contact position, the line of contact is obtained. Graphically, the pitch points are determined by finding the point of intersection of the path of contact with the X, Z plane, or the Y, Z plane. This results in a pitch point in each transverse section. The total contact ratio ε_γ results from the transverse contact ratio ε_α and the overlap ratio ε_β under consideration of the overlap angles φ_α and φ_β and the number of teeth z_1.

$$\varepsilon_\gamma = \frac{\varphi_\alpha + \varphi_\beta}{360°} \cdot z_1 \qquad (4)$$

To ensure that the gears created can be used in practice without problems, they are examined for meshing interference.

The equivalent radii of curvature for arbitrary curves are calculated using Bronstein [5]. To describe the tooth surfaces in three dimensions, the parameters u and v are being used. The parameter v describes the flank in the width direction, the parameter u describes the flank surface in the height direction. A shaft angle of 90° between the mesh lines can cause them to coincide with the principal curvature directions and lead to problems in the numerical evaluation. To prevent this, a transformation of the mesh lines u, v by the angles τ_g and τ_h, to the lines g and h is applied.

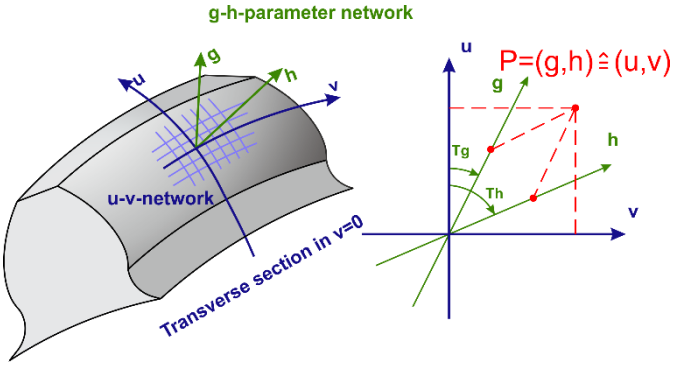


Fig. 4 *Parameter network for describing the tooth surface*

The principal curvatures are calculated using Bronstein [5]. With the corresponding formulas, curvatures on curved surfaces can be determined in general. With the help of an extension [6], the principal curvature directions are determined to match the previously determined principal curvatures. It is possible that a principal curvature radii runs towards infinity. To exclude singularities in calculation the reciprocal of the radii is used. This procedure is also particularly suitable for calculating modified flank shapes. There are no restrictions with regard to geometry. To determine the angle between the two principal curvature directions, both wheel flanks are brought together at the contact points. This is important to find the position and orientation of the two semiaxes of the contact ellipse.

The calculation program analyze the Hertzian pressure along the entire path of contact. The Hertzian theory is carried out according to known methods [7]. Instead of the rolling cylinders, two ellipsoids in contact are considered for a general view. The necessary tooth normal force is determined from the torque balance about the x_1 axis.

Plastic has a different material behavior than steel. The temperature dependence of the E-modulus as well as the stiffness behavior have a significant influence. A material parameter considers the influence of the plastic gear. The load distribution on the tooth flanks in tooth meshing changes due to the load-dependent deformation of the plastic wheel. To calculate the deformations, the steel worm is considered as a rigid element. Plastic is the more stressed and deformed material. The gears will fail on the plastic wheel.

In his work, Pech [7] derived the deformation of a plastic gear based on a bending beam. He uses a non-linear material model and describes the shape of the beam with the help of the tooth tip and height, as well as the normal module of the gear. The total deformation of the plastic gear is determined from the tooth bending and the surface deformation according to Hertz. The following figure shows the equations and correlations of Pech graphically.

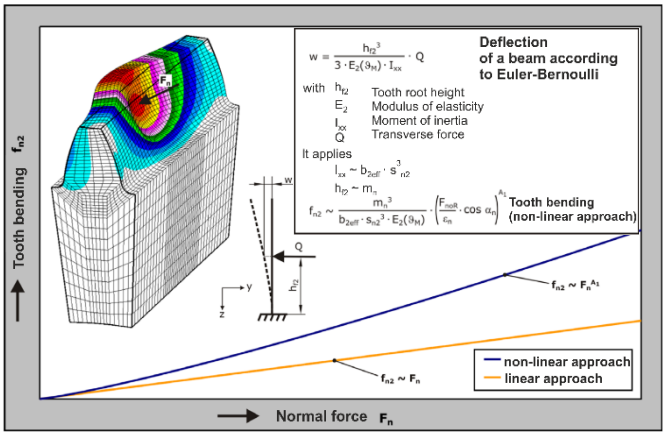


Fig. 5 *Total deformation of a gear flank with the approach of Pech [7]*

The procedure according to Pech is integrated in the new calculation. Now it is possible to determine the total deformations λ_{zus} depending on the load F_n at each meshing position. The parameter $\kappa u \cdot F_n$ describes the load distribution depended on the teeth in contact. At the end, the total deformation is a combination of the bending deformation λ_{pechF} and the Hertz surface deformation δ_{HF}. A curve of tooth deformation in the form of a 3rd order polynomial is assumed. This is consistent with the data according to Pech. The course and the assignment is done with the parameter $f_{R2}(u)^3$.

$$\lambda_{pechF}(\kappa u, u) = f_{R2}(u)^3 \cdot A_0 \cdot \frac{(m_n)^3}{b_{2eff} \cdot (s_{n2})^3 \cdot E_{2\vartheta}} \cdot (\kappa u \cdot F_n \cdot \cos(\alpha_n))^{A_1} \quad (5)$$

$$\lambda_{zus}(\kappa u, u) = \lambda_{pech}(\kappa u, u) + \delta_{HF}(\kappa u, u) \quad (6)$$

This allows further information to be derived from the extended path of contact. The load distribution in the contact area can be determined with the help of the deformation from the plastic gear. The calculation for distributing the load among the meshing tooth flanks in detail is being further refined in current research work.

The velocities and efficiencies at the pitch point are determined analogously to Boehme [2]. It is possible to calculate them at any position of the contact line. With the help of the velocities at the flank, the lubrication of crossed helical gears can also be studied in more detail in subsequent research topics. To be able to calculate the sliding paths (worm and wheel), it is important to know the orientation of the contact ellipse. The orientation is considered relative to a horizontal line through the pitch point. The sliding path is an indication for wear and can be calculated with the contact time and the contact ellipse. It is determined how the flank of a wheel moves as a function of the running parameter u through the contact ellipse. The contact time is determined with the help of the tangential velocity and the path through the contact ellipse.

3. Simulation

The contact points of crossed helical gears of all meshing tooth flanks are located in the normal section plane. Therefore, to analyse tooth deformation, it is useful to determine the 2D tooth contours of both gears in this plane.

Fig. 6 shows a worm and the normal section plane (gray) through the z-axis, which is orthogonal to the tooth flanks. The transverse section geometry (orange) is also shown below.

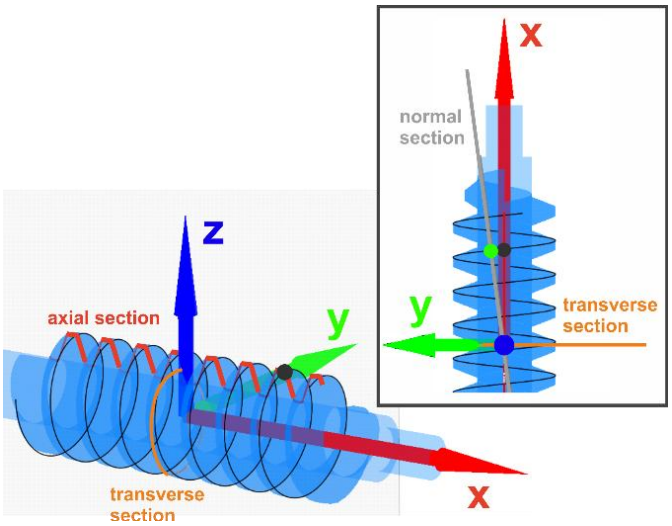


Fig. 6 *Worm with screw helix of an axial section point*

At first, for crossed helical gears with a helix angle of $\beta > 45°$, it is useful to determine the axial section geometry from the transverse section contour. In the further course, this is done for the worm. For this purpose, the helix function for an arbitrary tooth flank point P is used. In Fig. 6, the point P and the respective helix function are shown in black. With the curve parameter t, the helix describes the screwing of a flank point around the x-axis. Here, t_{tot} is the total number of revolutions over the wheel width b. The radius r and the angle φ are calculated in the x-plane ($x = x_P$) of the point P.

$$\mathrm{Helix}(t, x_P, y_P, z_P) = \begin{pmatrix} b \cdot \frac{t}{t_{tot}} + x_P \\ r(y_P, z_P) \cdot \cos(2\pi \cdot t + \varphi(y_P, z_P)) \\ r(y_P, z_P) \cdot \sin(2\pi \cdot t + \varphi(y_P, z_P)) \end{pmatrix} \quad (7)$$

$$r(y_P, z_P) = \sqrt{{y_P}^2 + {z_P}^2} \quad (8)$$

$$\varphi(y_P, z_P) = \arctan2(y_P, z_P) \quad (9)$$

To calculate the axial section contour, the curve parameter t is determined, when the y-component results in 0. In this way for each point in the transverse section, an axial section point is directly defined.

The normal section profile can also be determined with the helix function in a similar way to the axial section profile. For crossed helical gears according to Boehme [2], the normal section plane does not necessarily have to include the z-axis. In this case, the point M in this section (x_M, y_M, z_M) describes the shortest distance orthogonal to the z-axis. By transforming the helix, the normal section is located in the xz-plane. The coordinate transformation can be described mathematically with equation 10.

$$\mathrm{Helix}_n(t, x_P, y_P, z_P) = \begin{pmatrix} \cos(\beta - 90°) & -\sin(\beta - 90°) & 0 \\ \sin(\beta - 90°) & \cos(\beta - 90°) & 0 \\ 0 & 0 & 1 \end{pmatrix} \cdot \left(\mathrm{Helix}(t, x_P, y_P, z_P) - \begin{pmatrix} x_M \\ y_M \\ z_M \end{pmatrix} \right) \quad (10)$$

The contour in the normal section results from the transformed helix and the condition y = 0. The numerical root-finding algorithm provides the curve parameter t of the desired point in the normal section. Fig. 7 shows the axial section point in black. From this point a normal section point results, shown in green. Performing the described procedure for all points (of the axial section profile) results in the green contour in the normal section.

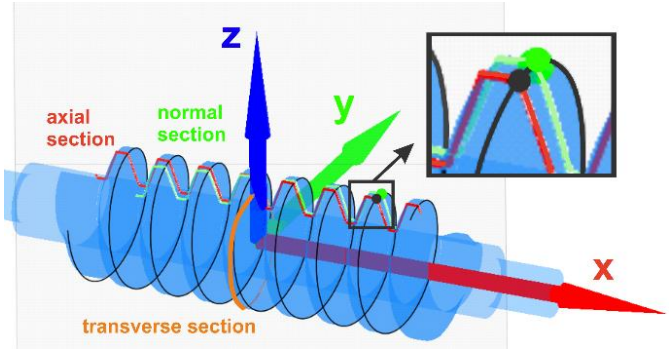


Fig. 7 *Determining the normal section contour from the axial section*

With the tooth stiffness model it is possible to determine the deformation of points on the tooth flank in the normal section. This enables the calculation of the actual overlap and the load distribution. To validate this model, an FE-routine in the normal section geometry of the gears was set up. Nodes are defined on the contour lines. By screwing them along the helix functions, the 3D-mesh of the gears is generated.

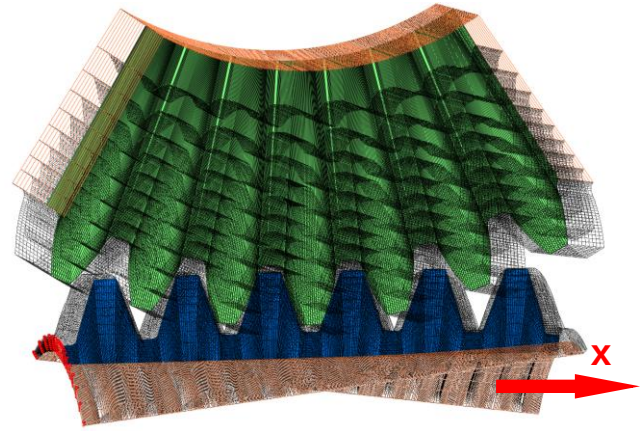


Fig. 8 *FE-mesh generation from the normal section profiles*

By generating the flanks from the normal section, only the relevant parts of the gears (that can come into contact) are meshed. This context is shown in Fig. 8 as well as the mesh that is refined in the area of the tooth contacts. The constraints are drawn in orange. The crossed helical gear is constrained in all degrees of freedom. Only at the worm, axial displacement in the x-direction is allowed. The axial force resulting from the input torque is introduced at the worm (red). The advantage of this FE-model results in the deformations and occurring stresses which are calculated directly at the nodes in the normal section.

4. Results and discussion

To prove the calculation, a reference gear pair was calculated. Pech [7] and Boehme [2] use the following gear-geometry:

Table 1: *Basic data of the reference gear pair [7] and [2]*

	worm	wheel
Center distance	30 mm	
Normal module	1,25 mm	
Normal pressure angle	20°	
Axis crossing angle	90°	
Helix angle	82,493°	7,507°
Number of teeth	1	40
Tip diameter	12,068 mm	52,932 mm
Root diameter	6,443 mm	47,307 mm
Profile shift factor	0	0
Face width	32 mm	10 mm

In the following table, the calculation results from different methods are compared. Boehme [2] compared his results with those of Pech [7]. VDI 2736-3 [3] is generally used as a basic design guideline.

Table 2: *Comparison of the calculation results to the reference gearing*

	New method	Boehme [2]	VDI 2736-3 [3]
Total contact ratio	1.8367	1.8369	1.8369
Tooth normal force	212.835 N	216.93 N	215.86 N
Hertzian pressure	110.79 N/mm^2	110.83 N/mm^2	110.12 N/mm^2
Efficiency	54.55 %	54.32 %	54.54 %
Sliding velocity	0.758 m/s	0.769 m/s	0.758 m/s
Sliding path wheel 2	35.46 mm	38.81 mm	-
Hertzian deformation	62.35 µm	-	-
Total deformation	109.58 µm	-	-

The parameter show good agreements in the results. VDI 2736-3 calculates the parameter at the screw point. To compare the values at the screw point, the results from the calculation according to Boehme and the new method are also given at this point. However, the values can be determined at any point on the contact line. With the help of the new method, it is also possible to obtain a good result regarding the total deformation with simple equations. This is an important basis for the investigation of the load distribution in the tooth mesh.

5. Conclusion

In this research work, the calculations on crossed helical gears were extended. The load distribution in the multiple engagement was examined depending on the existing load and the stiffness of the plastic material. The tooth deformation was taking into account with the load distribution. The simplifications assumed in the calculation provide good agreement in both approaches. A counterpart rack profile is defined using the fourth-order polynomial. The geometries of the two wheels are derived with one side of the rack in each case. By meshing with the rack, both wheels also mesh with each other. It is possible to consider shaft angles deviating from 90°. In addition to crossed helical gears, the calculation can also be used for spur gears. This new calculation process for crossed helical gears forms the basis for new improved, designed and optimized gears of various application areas. It shows great potential for improvements. The calculation values always assume the highest load on the gear unit. The potential for improvement is far from exhausted and will be further investigated in this ongoing study, also like the study of the load distribution in the tooth engagement in detail. New flank geometries and modifications for crossed helical gears are being developed to improve the gears and make them more efficient.

6. References

1. G. Niemann, H. Winter, *Maschinenelemente Band 1-3*, In: Springer-Verlag [1960]
2. C. Boehme.: *Berechnungsverfahren zur Erweiterung der Anwendungsgrenzen und der Optimierung von Schraubradgetrieben*, Ruhr-Universität Bochum [2020]
3. Verein Deutscher Ingenieure, VDI 2736: *Thermoplastische Zahnräder* Blatt 1-4., Berlin: [Beuth-Verlag 2014/2016]
4. Deutsche Industrie Norm, DIN 867: *Bezugsprofile für Evolventenverzahnungen an Stirnrädern (Zylinderrädern),* Beuth Verlag, Berlin, [1986]
5. Bronstein, I. N., Semendjajew K. A., *Taschenbuch der Mathematik*, B.G. Teuber Verlagsgesellschaft [1991]
6. Massachusetts Institute of Technology 3.4 Principal curvatures Link: http://web.mit.edu/hyperbook/Patrikalakis-Maekawa-Cho/node30.html [13.05.22]
7. M. Pech, *Tragfähigkeit und Zahnverformung von Schraubradgetrieben der Werkstoffpaarung Stahl/Kunststoff*, Bochum [2011]

Acoustic emission method of diagnostic of elevating rudder covering in places of lightning strikes impact

Leonid Vinogradov[1], Muharbij Banov[2], Alekseij Nasibulin[3]
Riga Technical University Institute of Civil Aviation, Riga, Latvija[1], Riga Technical University Institute of Civil Aviation, Riga, Latvija[2]
Latvian Council of Science, Riga, Latvija[3]
E-mail: leonids.vinogradovs@rtu.lv, muharbij@inbox.lv, aleksejs.nasibulin @mail.ru.

Abstract: *Acoustic emission (AE) is the process of emission of mechanical waves by materials caused by dynamic local restructuring of its internal structure under the influence of stresses of any kind. The source of AE is plastic deformation, the formation and growth of cracks, the outflow of a working fluid (liquid or gas) through holes. The AE method, unlike other methods of non-destructive testing (NDT), is passive, i.e. using the physical field of emission generated by the defects themselves. The acoustic emission (AE) method is based on the registration and analysis of acoustic waves arising in the process of plastic deformation and fracture (crack growth) of diagnostic objects. It makes possible to determine the places where the structure of the material changes when lightning strikes the covering of the elevating rudder for the composite laminate from which the elevating rudder of the RRJ aircraft is made.*
KEYWORDS: *acoustic emission; diagnostics, elevating rudder; composite laminate; lightning stroke.*

Introduction

The acoustic emission (AE) method is based on the registration and analysis of acoustic waves arising in the process of plastic deformation and fracture (crack growth) of diagnostic objects. It makes possible to determine the places where the structure of the material changes when lightning strikes the covering of the elevating rudder for the composite laminate from which the elevating rudder of the RRJ aircraft is made.

When llightning acts on the elevating rudder, the covering of which is made of two panels of 7-layer carbon composite, it becomes necessary to diagnose the material in places close to the visual destruction of the covering of the elevating rudder. A potential change in the structure of the layers of the composite material can occupy much larger areas than the zones of visual surface damage to the composite covering.[1]

The object of diagnostic

The object of diagnostic is the RRJ aircraft elevating rudder made of composite materials, which is a three-component honeycomb core construction of two 7-layer panels and a honeycomb core.[2]
The elevating rudder passed certified tests for lightning stroke in accordance with the program before the trials.
The value of the rupture load of the elevating rudder after lightning stroke was determined, which made up to 110% of the rupture load as a result of the trials.

The appearance of the elevating rudder after static crushing tests is shown in Fig.1.



Fig.1.*The elevating ruder after lightning strikes impact by the end of crushing tests.*

The zones of lightning impact on the elevating rudder in the area of the root and end parts are shown in Fig. 2, from which it can be seen that there is one in the root part, and two places of lightning impact in the end part.



a)The root part of elevating rudder.



b) The end part of elevating rudder.

Fig.2*. The zones of lightning impact on the elevating rudder.*

Device for Elevating rudder Diagnostics by Acoustic Emission Method.

For the diagnostic was used a portable two-channel acoustic emission device POCKET AE-2 under the control of the AEWin package to which piezoelectric converter were connected. [5]

Device settings during diagnostics are shown in the Table below.

Threshold	HFF	LPF	Preamplifiers	Sampling frequency
30 dB	5 kHz	1000 kHz	inside 26 dB	2 MSPS

Tab.1. Conduction of diagnostics by the AE method is shown in the photo Fig.3.



Fig.3. *The diagnostic of the elevating rudder's part by AE method.*

Piezo sensors attachment on the construction of the skin of the elevating rudder is shown in Fig.4.Triple reservation of AE measurements was carried out (three independent sensors and measuring devices) to strengthen reliability of diagnostics.

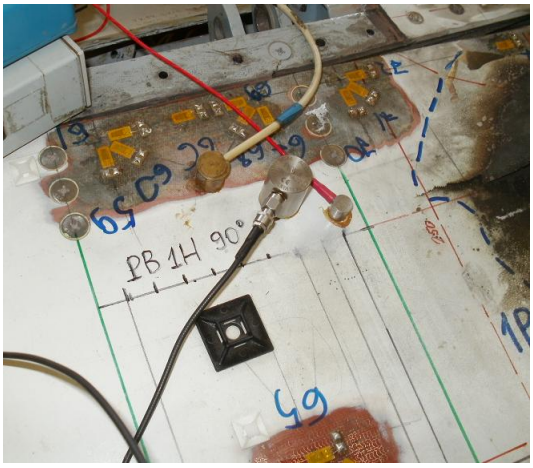
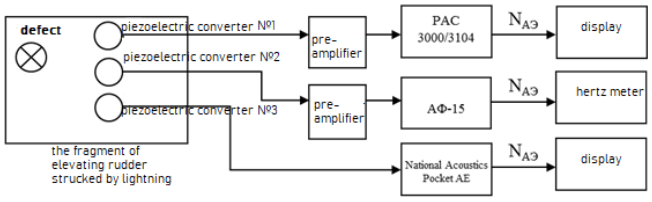


Fig.4. *Piezo sensors attachment on the construction of the skin of the elevating rudder.*

The block diagram of acoustic emission measurements for the elevating rudder's notch zones, from where the triple reservation of the acoustic signal measurement can be seen, is shown in Fig.5.



1,5 смBlock diagram of acoustic emission measurements for elevating rudder's notch zones.

The results of diagnostics of the elevating rudder covering in places affected by lightning.

The object of research was the root and end parts of the elevating rudder after lightning strikes, on which acoustic sensors were glued. In the places of diagnostics (impact by lightning), the object was locally heated up to 80°C. At the same time, the probe scanned the area from the center of lightning impact to the periphery. As a result, two zones of emission variation were observed: a weak one along the periphery and a strong one closer to the center. The attached Figs. 6 - 8 show the damage zones in zones PB1, PB2 and PB3: blue - hammering, red - intensive crushing (acoustic emission method) and green - initial damage (acoustic emission method).[6]

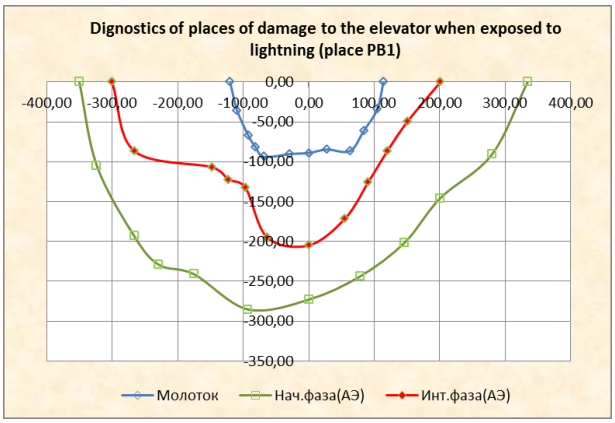


Fig.6. *Diagnostics of PB1 zones in the root part of the elevating rudder. Blue - hammering, red - intensive crushing (acoustic emission method) and green - initial damage (acoustic emission method).*

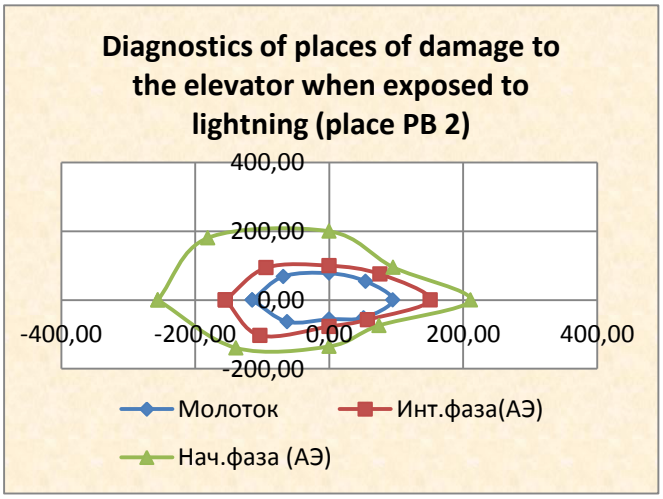


Fig.7. *Diagnostics of PB2 zones in the root part of the elevating rudder. Blue - hammering, red - intensive crushing (acoustic emission method) and green - initial damage (acoustic emission method).*

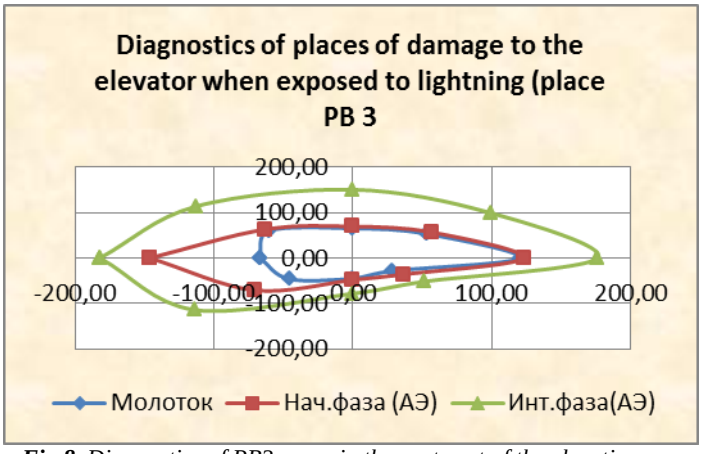


Fig.8. *Diagnostics of PB3 zones in the root part of the elevating rudder. Blue - hammering, red - intensive crushing (acoustic emission method) and green - initial damage (acoustic emission method).*

On Fig.9. Zones of diagnostics of the elevating rudder PB1 are applied the object of diagnostics (the root part of the elevating rudder): central unpainted - material delamination by taping; middle orange - intensive phase of AE and extreme blue - initioal phase of AE.

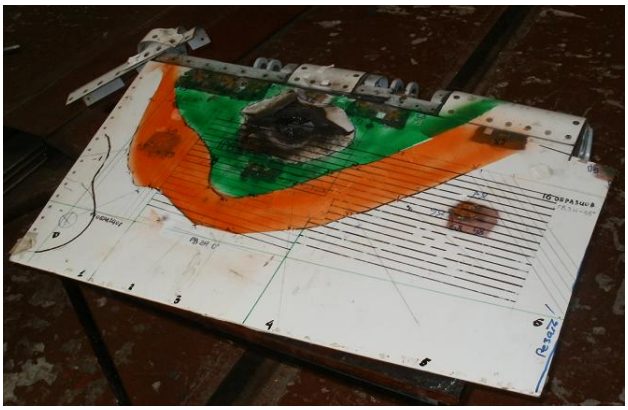


Fig.9. *Zones of diagnostic of the elevating rudder.*

The following results were obtained investigating the covering of the elevating rudder in places affected by lightning by acoustic emission method:

- ✓ the diagnostic of changes in the structure of the composite material of the elevating rudder in places affected by lightning PB1, PB2 and PB3 was conducted;
- ✓ the zones of change in the structure of the composite material near the places of lightning impact were determined;
- ✓ the zone of a strong change in the structure of the material was found by manually tapping the covering directly near the destruction zone and is an ellipse for the PB1 zone with dimensions of 100x200 mm
- ✓ the zone of intense and initial changes in the structure of the composite was determined by the acoustic emission method (intense - 350x500 mm);
- ✓ it is necessary to conduct strength tests of the samples of the elevating rudder covering in the zones PB1, PB2 and PB3 and compare the obtained characteristics with the characteristics of samples from undamaged covering to confirm the diagnostic results. [3;4]

Conclusion.

The diagnostics of the elevating rudder covering zones near the places of lightning impact was performed by the acoustic emission method. The zones of intensive and initial changes in the strength characteristics of the elevating rudder covering in places affected by lightning were determined. The zone of a strong change in the structure of the material was found by manually tapping the covering directly near the destruction zone and is an ellipse for the PB1 zone with dimensions of 100x200 mm. The zone of intense and initial changes in the structure of the composite was determined by the acoustic emission method (intense - 350x500 mm).

There is a good agreement of zones of change in the strength characteristics of the elevating rudder in the area of lightning impact, obtained by acoustic emission methods and strength tests of samples.

References:

1. Коллакот Р. Диагностика повреждений. – М.: «Мир», 1989.
2. Дробот Ю.Б., Грешников В.А., Бачегов В.Н. Акустическое контактное течеискание// Москва, «Машиностроение» 1989
3. Сазонов А.А., Мисейко А.Н. Выявление язвенной коррозии на промысловых трубопроводах методом акустической эмиссии // Тезисы доклада 3ей Международной конференции «Диагностика трубопроводов». – М., 2001.
4. Britton C. F. Methods and equipment for measurements and control in the field of corrosion. – Copenhagen, 1974.
5. РД 03-131-97. Правила организации и проведения акустико-эмиссионного контроля сосудов, аппаратов, котлов и технологических трубопроводов.
6. Иванов В.И., Быков С.П., Рябов А.Н. О критериях оценки степени опасности дефекта по параметрам акустической эмиссии. – Дефектоскопия, 1985, №2, с.62- 68.

Application of hardfacing arc methods in Bulgarian ship repair SME

Yordan Denev
Technical university of Varna
e-mail: y.denev@tu-varna.bg

Abstract: *The paper deal with methods for hardfacing used in small and medium sized ship repair enterprise. The difference between welding and hardfacing are explained. In first part of the paper are analyzed disadvantages and advantages of arc hardfacing welding methods, materials and consumables in hardfacing. After that are described two case studies from ship repair industry. In ship repair SME with restricted resource some of hardfacing methods are not applicable. In this paper are described hardfacing methods which are applicable in this type of ship repair yard.*
Key words: HARDFACING, SHIP REPAIR, SMALL AND MEDIUM ENTERPRISES, SHIELTED METAL, ARC WELDING

1. Introduction.

Small and medium sized enterprises(SME) are the backbone of Europe industry. Their workplace are about 90% of all in the European Union. In Bulgaria SMEs in ship design, shipbuilding and ship repairing are more than 30[10]. SMEs are subjected to different constrains. Some of them can be divided into two categories: technological constrains and functionality constrains. Technological constrains impact to normal functionality of SME shipyard and they can be connected with geometrical limited(length, breath, depth of building facilities), crane lifting capacity and etc. Functionality constrains are connected with limited access to financing, limited personal number, limited personal skills and capabilities.

In ship repair industry in some cases are necessary different detail or elements form ship hull, machine and mechanisms to be hardfacied. This method is used when wearing of details and elements is not so big and their functions are not so important. Hardfacing is process where on surface is applied metal to fill wear part of the detail is. This process is applied in rebuilding, design and fabrication of details in all heavy industries and partly in ship repair industry. The difference between welding and hardfacing process is that in welding the two parts are connected together while in hardfacing process has rebuilding the details dimensions. In hardfacing process all welding methods are applicable but take into account production equipment and restrictions of SMEs mainly are used arc welding methods.

Hardfacing is similar like welding process but not at all. In some cases, this process required special equipment and material. Hardfacing can be done with powder spraying while this method is not applicable for welding.

2. Arc hardfacing methods

The arc methods for hardfacing can be divided into several types: shielded metal arc welding, submerged arc welding, flux core arc welding electric arc and plasma arc welding[1].

2.1. Shielded metal arc welding

This method is mostly used in all area of heavy industry. It has some advantages:

- simply for operation- it is not necessary special equipment and devices;
- easy for transportation;
- possibilities for operation in different position;
- it is applicable for all types of steel;
- it can be used for hardfacing of different material thickness and wear;

Disadvantages of the method are:

- low hardfacing speed;
- low coefficient of efficiency;
- height impute temperature;

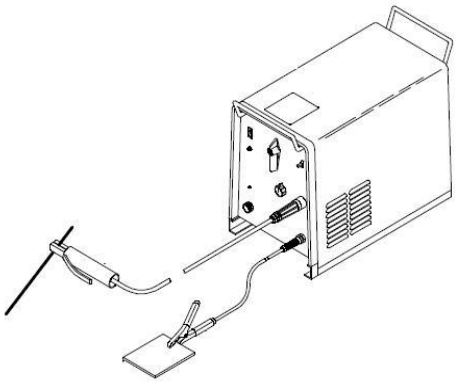


Fig.1*. Shielded metal arc welding scheme[6]*

2.2. Submerged arc welding process

Submerged arc welding process has some advantages:

- easy for automatization- in modern manufacturer this method is fully amtomatizated;
- heighter hardfacing speed than shielded metal arc welding;
- easy for operation- it isn't require special skills;
- it can be semi mechanized method;
- heighter coefficient of efficiency

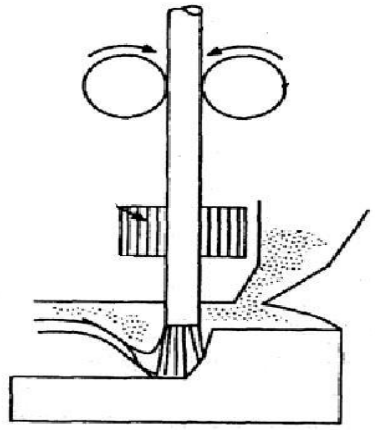


Fig.2*. Submerged arc hardfacing [4]*

Disadvantages are:

- height impute temperature;
- expensive equipment and consumables

2.3 Flux cored arc welding

Advantages of flux cored arc welding are:

- height hardfacing speed;
- possibilities for hardfacing wide range of wears;
- Easy to operate;

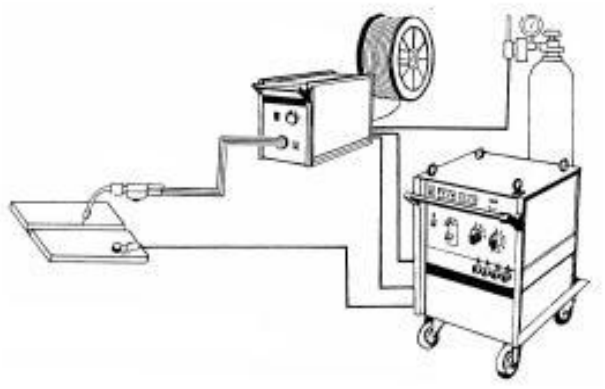


***Fig.3**. Gas shielded metal arc welding [8]*

Disadvantages of this method are:
- in a lot of manufacturers machines and equipment for this method are mechanization. This didn't allow hardfacing in different position in the space;
- expensive equipment and consumables in comparing with shelted metal arc welding process;

2.4. Plasma arc welding(hardfacing)

Advantages of this method are:
- suitable for automatization;
- night melting point materials can be used;
- precise control over thickness and shape;

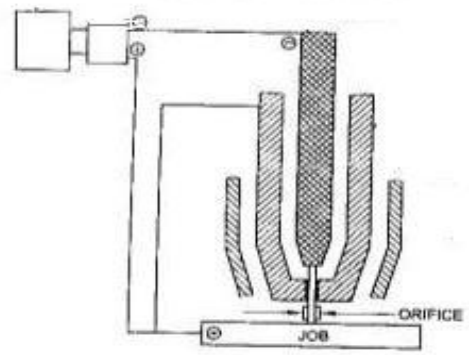


***Fig.4**.Plasma arc welding [5]*

Disadvantages:
- limited mobility;
- height cost for equipment;

Important characteristic in hardfacing is dilution. The dilution is the relation between area of welding metal in rebuilding layer and all welding area, fig. 5. The mathematical equation is:

$$D = \frac{B}{A+B} * 100, \%$$

Where: B- rebuilding metal, A- hardfaced metal

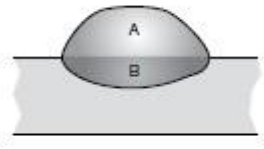


***Fig.5**. Dilution calculations [9]*

Different hardfacing methods has different dilution degree. In table1 are shown dilution degree of different hardfacing methods. Maximum degree has submerged arc welding and minimum gas tungsten arc welding. The maximum dilution degree of submerged arc welding is due to automatic operation.

In dilution process important is to be controlled. According [9] there are some factors:
- Right welding procedure;
- Welding sequence;
- Correct polarity;
- Welding position
- Welding technique;

***Table 1.** Dilution degree in different welding methods*

	Welding method	Abbreviation	Type	Dilution, %
1	Shielded metal arcd welding	SMAW	manual	15-30
2	Gas tungstun arc welding	TIG	manual/ automatic	15
3	Submerged arc welding	SAW	automatic	30-50
4	Gas shielded metal arc welding	MIG/ MAG	semi-automatic / automatic	15-35

In a lot of cases resistance and durability of hardfaced layers depend on pattern type. There are different pattern types. On fig. 6 are shown more used types in ship repair industry.

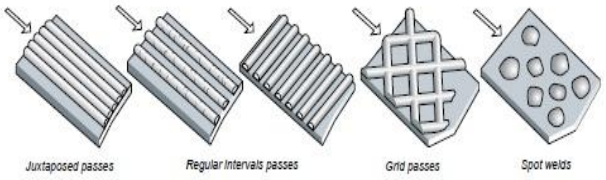


***Fig.6.** Pattern types used in hardfacing [9]*

3. Materials used in hardfacing process

Selection of material for hardfacing depends on chemical composion of basic metal. In hardfacing like in welding has two rules:
- Rm1≈Rm2;
- Chem1≈ Chem2

where: Rm1- tensile strength of basic metal; Rm2- tensile strength of hardfacing metal; Chem1- chemical composion of basic metal; Chem2- chemical composion of hardfaced metal;

Mechanical characteristic of hardfaced metal depended on filler metal. Different types of hardfacing electrodes for different mechanical characteristics of hardfaced area are shown on fig.7.

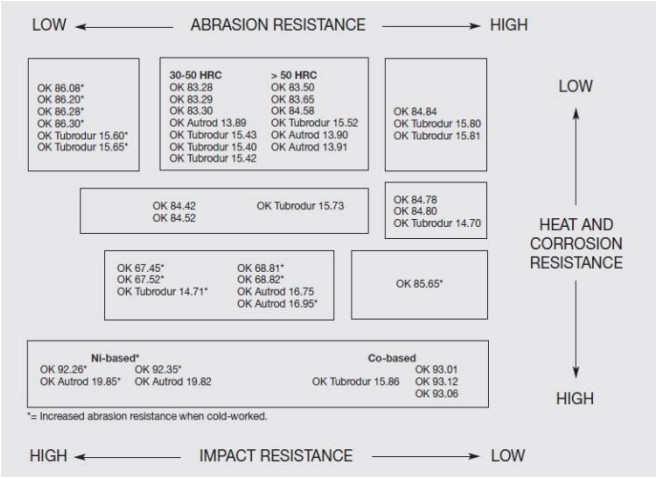


***Fig.7.** Types of hardfacing electrodes [3]*

Hardfacing weld metal ca be divided into several categories [3]:
- Iron based;
  - Martensitic and austenite alloys;
  - Carbide rick alloys;
- Non iron based;
  - Cobalt alloys;
  - Nickel alloys;

- Martensitic;
  - Good metal to metal resistance;
  - Good impact resistance;
- Austenitic;
  - Excellent impact resistance;
  - Good build up alloys;
  - Fair abrasion resistance;
- Carbide rich;
  - Excellent abrasion resistance;
  - Good heat treatment;
  - Poor impact resistance;
- Cobalt and nickel based;

All of this metal categories have proper mechanical, chemical and resistance characteristics. Selection of them for industry depends form applications and field of element working environment.
In ship repair industry hardfacing in mainly used for details jointed on abrasion and friction impacts. In this case hardfacing electrodes should be selected with height abrasion resistance from fig.7.
According [7] authors widely described materials, processes and consumables for hardfacing process. They described the problem from view point of hardfacing is to improve and extend life of different parts and components.

4. Hardafing in ship repair SME.

In SME take into account technological and functionality constrains it has a production limitations. Some of these limitations are done by lack of personal skills form one side and impossibilities of SME to adequate financing from other. Lack of financing leads to limitations of production equipment, personal skills and consumables. In this case is good practice SMEs to use some of hardfacing methods mentioned in point two. These methods didn't require special equipment and personal skill. These methods are shielded metal arc hardfacing and flux cored arc hardfacing.
In paragraph 2 are mentioned advantages and disadvantages of every one of possibility arc hardfacing method in SME. Shielded metal arc welding is most applicable in hardfacing process because it use welding equipment and machines but different type of electrodes. In cases when we have deep wearing of ship hull and equipment elements for example anchor chain hawse pipe we should to used hardfacing with shielted metal arc method we just need to take hardfaced electrodes or welding electrodes and to do it. The pattern used in this case is juxtaposed passes perpendicularly of wear.



Fig.8. Hardfaced area of anchor chain hawse pipe[2]

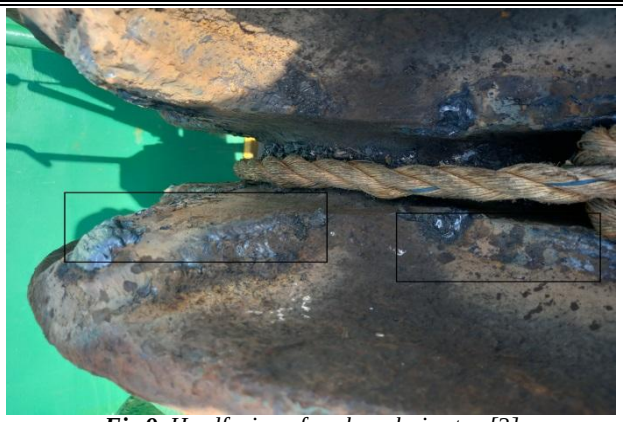


Fig.9. *Hardfacing of anchor chain star [2]*

The same hardfacing process with plasma arc welding will take 2-3 time more time because the workers should to done additional operations like dismounting, transportation to workshop, hardfacing and mounting again. If we have a lot of operations, it will be better to fabricated new element or construction but it is related with higher cost.
On fig.8 and fig.9 with black fields are marked hardfaced area of anchor chain hawse pipe and anchor chain star. They are impacted to height abrasion and friction action. In this case hardfacing operations are done with electrodes for welding de=3.25mm.

5. Conclusion

From described advantages and disadvantages of arc hardfacing methods in SME take into account restricted production facilities, personal skill and lack of financing not all of methods are applicable. Most applicable are shielded metal arc welding and flux cored arc welding.
Hardfacing process in applicable for all metals and their alloys used in shipbuilding, ship repairing and heavy production industries.
Hardfacing is reconstruction method reduced final cost of details or components of mechanical systems compared with new building.
At this method the operator can to select filler material for reconstructed of wear part of details or components depends on working medium. By selecting of proper filler material is possible to achieve abrasive resistance, impact resistance and heat and corrosion resistance. Last two characteristics are very important for details and components from shipping and ship repair industry.
Future work of the topic will be oriented to analyze of technological characteristics of welding electrodes used in hardfacing.

6. References

1. Afrox Product Reference Manual, Hardfacing, section 12
2. Authors own picture archive
3. ESAB, Repair and maintenance welding handbook, second edition
4. Gowlthaman, K., Saiqanesh, J., Rejamanikam, C., Determination of submerged arc welding process parameters using Taguchi method and regression analysis, 2007, Indian Journal of Engineering and Material Science, p. 177-183;.
5. Indian Railways Centre for Advanced Maintenance technology, Maharajpur, Gwalior, Handbook on Welding Techniques, CAMTECH/ E/ 14-15/ Welding/1.0
6. Miller Electric Mfg. LLC, Guidelines for shelted metal arc welding(SMAW), 2018, USA;
7. Pradeep,G., Ramesh, A., Durga Prasad, B., A review of hardfacing processes and materials, 2010, International Journal of Engineering Sciencye and Technology, Vol. 2(11),pp. 6507-6510;
8. Weldability, An introduction to MIG welding, WWS Group;
9. Welding Alloys Group, Fundamentals of hardfacing, 2018,
10. МИ, Регистър на МСП, РБ, Министерство на икономиката, [Онлайн.

Perspectives of the auto world during the pandemic – international and national view

Nataša Tomić-Petrović

University of Belgrade, Faculty of Transport and Traffic Engineering, Belgrade, Serbia,

e-mail: natasa@sf.bg.ac.rs

***Abstract**: We live in a time of the Covid pandemic, when losses are being noticed in the car industry. Experts state that stabilization of the market is not expected before 2023. Data from the European Automobile Manufacturers Association (ACEA) showed that for the first time in 2021, hybrid electric cars were equalized with "diesels" on the European Union market. Last year, 1.901.239 new hybrid electric vehicles were registered on the common market. In April 2021, our capital Belgrade was awarded for the best Urban Mobility Plan. Our city has increased the safety of traffic participants, given priority to pedestrians and cyclists, reduced emissions and improved energy efficiency, while expanding pedestrian zones. The National Association of Autonomous and Electric Vehicles has launched a project aimed at increasing environmentally friendly traffic in Serbia. Eco 2 line of electric buses works in Belgrade from January 2022. And in Serbia, parts for Audi, Porsche and BMW will be produced in the "Motherson" factory, which was opened at the end of November 2021.*
KEY WORDS: *AUTO INDUSTRY, "TESLA", URBAN MOBILITY, SERBIA, PANDEMIC*

1. INTRODUCTION

The first car magazine was published in the United States in 1895 under the title "The Horseless Age", which clearly showed that the old mode of transportation became old-fashioned.

"Lancia"'s 115 years and memories of more than a century of famous Italian elegance remain. The Lancia brand was founded in Torino on November 27th 1906 by Vincenzo Lancia and Claudio Fogolin, car enthusiasts employed by Fiat. Although there are no new models in "Lancia" today, their first car was produced in 1908. And that was the "Lancia" model with 12 hp. The fame of the brand grew, they went through the First World War, followed by the models "Lambda", "Augusta", and after the Second World War in 1950, "Lancia" presented the model "Aurelia", the first car in the world with a V6 engine. By the way, "Ipsilon" is the longest up-to-date and the best-selling "Lancia"'s model in history, with more than three million cars sold.

Today we live in a time of the Covid pandemic, when losses are being noticed in the car industry. [see: 5] Experts state that stabilization of the market is not expected before 2023. In China, production has been slowed down since the beginning of the pandemic, and this continued in 2021, and the production of semiconductors for cars and technical devices are bearing the brunt. The digital age [see: 3] and pandemic are rapidly changing our lives.

Data from the European Automobile Manufacturers Association (ACEA) showed that for the first time in 2021, hybrid electric cars were equalized with "diesels" on the European Union market.[1] Sales of the gasoline using cars in the EU fell by 17.1% last year, and of all new cars registered in the EU, hybrid vehicles made 19.6%, electric vehicles on batteries 9.1%, and plug-in hybrids for 8%.

2. THE CASE OF SERBIA

In April, 50 years ago, the production of "Stojadin" i.e. "Zastava 101" began, which was presented at the fair in Belgrade in April 1971 and it was produced until November 2008. 1.045.458 cars left the factory in Kragujevac, what makes it the best-selling "Zastava" model in the history. In the 12th of April 2022, the production of Fiat 500 L continued, after the return of workers from the paid leave. At the "Fiat-Chrysler Automobile Serbia" factory, cars will be produced in two shifts, and up to 200 cars will come off the lane in one shift. The specific management plan for the car factory in Kragujevac is still unknown and in July 2021 it was announced that company "Siemens" intends to make the city of Kragujevac the center for train production in Europe.

In April 2021, our capital Belgrade was awarded for the best Urban Mobility Plan.[2] Belgrade is the winner of this year's the European Sustainable Urban Mobility Planning (SUMP) Award, given by the European Commission and launched in 2012. Our city has increased the safety of traffic participants, given priority to pedestrians and cyclists, reduced emissions and improved energy efficiency, while expanding pedestrian zones.

The National Association of Autonomous and Electric Vehicles[3] has launched a project aimed at increasing environmentally friendly traffic [see: 1] in Serbia. Eco 2 line of electric buses works in Belgrade from January 2022. But due to the introduction of this line, one bicycle path in the city disappeared.

It is planned that the construction of the subway in our capital starts from the 1st of November 2021. The first line has been announced in 2028, and the second in 2030. At the same time, works on the BG train are under way. [see: 4]

And in Serbia, parts for Audi, Porsche and BMW will be produced in the "Motherson" factory, which was opened at the end of November 2021.

And after several months of testing and evaluation of cars that are present on the Serbian market since the beginning of 2021, in April 2022, the commission announced the results and the car of the year in Serbia in 2022 is "Toyota Jaris Cross". At the same time, due to the high level of safety, availability on the market, favorable vehicle maintenance conditions and despite the extraordinary circumstances of the pandemic, "Volkswagen ID.4" was rightly crowned with title of the electric car of the year in Serbia in 2022.

A school example of the evolution of the model is the new "Peugeot 308" on whose instrument panel is the flag of the French Republic. It is a sophisticated vehicle equipped with radars and sensors. It is considered to be the most aggressive "lion" so far, because the car knows how to brake itself, everything works on the button. The quality of all functions is the highest, but still, if the driver is taller /185 cm/, there is no room left behind him for an adult passenger, what is the most serious shortcoming. Due to the lack of cars, every model that arrives in Serbia is sold.

[1] Last year, 1.901.239 new hybrid electric vehicles were registered on the common market.

[2] Previous winners of this award were the cities of Brussels, Manchester, Malmö, Bremen and others.

[3] This non-profit professional organization is a regional partner for urban mobility of the European Institute of Innovation and Technology and in April 2021. It launched the "E-retrofit" project. The "Fiat 500 L" was chosen as a model vehicle.

3. NEWS FROM THE AUTOMOTIVE INDUSTRY IN THE WORLD

It is interesting that the German "Volkswagen" (VW) became the main partner in the project of "greening" the traffic system on the Greek island of Astypalaia[4], in the Southeastern Aegean. [see: 2] The German giant supplies the island with 1,000 electric vehicles of various types and purposes, so as to replace 1,500 vehicles powered by fossil fuels. Vehicle charging stations and a system of renewable electricity - generators for solar and wind power - will also be provided. Unfortunately, "Volkswagen" has to compensate 8.5 million of its customers in the EU who before 2015 bought diesel vehicles of that company with a built-in eco-decoy what was an industrial scandal. It was announced that in 2017 it was acknowledged that more than 600,000 vehicles sold on the American market were equipped with special cheating software, so the official control of harmful gas emissions showed 40% lower values than those achieved in regular traffic. VW has also joined a growing group of manufacturers developing autonomous multi-purpose electric vehicles. VW has presented a concept of robotaxi called "onepod", which has large glass surfaces and drives itself while passengers have an undisturbed view on the surroundings.

And in Croatia, the company "Rimac cars" (innovator is Mate Rimac, and he founded the company in 2009) presented a new vehicle. It is the first Croatian production car, called "Nevera" /after an unexpected and strong Mediterranean storm that "runs" on the Adriatic Sea/. This remarkable car has even 1,914 horsepower and can develop a top speed of 412 kilometers per hour. This hypercar is expected to go on sale. And during July 2021, this Croatian company[5] became the majority owner of "Bugatti", a well-known French sports car manufacturer, which has so far operated within the "Volkswagen" group.

According to the research, Chinese consumers are more willing to accept alternative powertrains than European or American customers. At the beginning of 2021, the Chinese phone manufacturer "Xiaomi" informed the public that "Xiaomi" plans to start the production of electric cars in the year 2024. However, the electric model "Mask Myth 9" with three rows of seats for six passengers and a system for biometric driver recognition was presented at the salon in the Chinese metropolis of Guangzhou. With one charge of lithium-ion batteries, the range is up to 520 km, and it is announced that a version with a range of 650 km will appear in 2023. In January 2022, sales of electric cars increased by 132% compared to January last year. Although the price of raw materials, such as lithium, is rising.

And the Romanian manufacturer "Dacia" made a hit with the electric car "Spring"[6]. This car is increasingly in demand, it is the cheapest electric car in Europe, and its sales in Serbia should start in 2022. 7,.000 Dacia Springs have already been ordered from Germany.

In Malaga, a 100% electric driverless bus has appeared in Spain, which travels six times a day from the port to the center of Malaga, in the south of Spain. This was initiated by the company "Avansa".

The American company Ford Motor has to withdraw 617.000 vehicles due to the problems with the roof racks of vehicles, after an investigation on the problem during 2020. In April 2021, after the investigation, the National Traffic Safety Agency asked "Ford" to withdraw the vehicles, i.e. when there were 11 cases of tearing off the roof racks on the "SUV Explorer" vehicles. This withdrawal referred to models produced in 2016 and 2019.

"Toyota" has presented the new crossover "bZ4X", the first model in the new series of battery electric vehicles (BEV), and the name of the series "bZ" is an abbreviation of "beyond Zero". The advantages of this new electric SUV vehicle are thanks to the use of the battery[7] as an integral part of the chassis, under the vehicle floor, which is spacious and comfortable. This vehicle will also offer advanced technological functions, including a solar panel on the roof, to help charge the battery while driving or at rest. However, the American plan is that half of the cars will be zero-emission.

From Korea, they presented a super modern SUV with advanced technology, "Hyundai Tuson Hybrid", which is the fourth generation of "Tuson" which reaches a maximum speed of 193 km/h. And finally, the "Hyundai jonic electric"[8], a Korean electric car, which confirmed the practicality of everyday city driving.

The Bavarians have introduced the "BMW 14" - the premiere of the new generation of "BMW drive" command system that focuses on the functionality of the touch screen. This model is a combination of sporty energy typical for BMW and a range that brings peace on long journeys with the elegance of design, spaciousness and practicality of the four-door model. Produced in the Munich plant, it is a fully electric and the range with full batteries is between 510 and 590 km, depending on the version.

"Tesla" is the most famous company that produces electric cars, and one of the new companies is the Chinese "NIO" electric car company, which announced the ET7 model, an electric sedan with autonomous driving technology, as well as a new luxury electric crossover EC6. Despite the pandemic that reigns, "Renault" has confirmed its leading position on the European electric car market.

. And when we speak about safety the German giant Daimler AG, which owns Mercedes-Benz, has registered an interesting patent, which deflates tires at high speed in the case of emergency. When the standard braking system fails, the driver could be able to activate an additional function and thus stop the vehicle. This patent includes a central (control) unit and an air release mechanism, and is primarily intended for electric /hybrid models, although it could also be used by cars with internal combustion engines. Daimler AG has focused on electrified models, as they do not use brake cables and hydraulic systems, but drive-by-wire technology. The deflated tire adheres more to the ground and creates more friction, which contributes to stopping the vehicle. But if you blow out too much air it can fall off the rim. Because of that German engineers designed a pressure balancing valve to solve the problem. We will see when this technology will come to life in four-wheelers, and there are many candidates. The models from the EQ family are primarily considered.

Ab aeterno it was dreamt of extending the age of human existence on all meridians. It was dreamt of moving into outer space, and the possibility of salvation was sought in the event of overpopulation on the Planet Earth and other dangers. Attempts were also made to develop ideas about the means of penetration into space (Tsiolkovski KE 1857-1935). Belief in science was almost unlimited.

[4] This island has an area of 97 square kilometers and is an exemplary model of an island with "climate-neutral mobility". This is a unique example in this part of the world, because all commercial and service vehicles will be powered by electricity.

[5] It will own a share of 55% in Bugatti, and produces electric powertrains and batteries for the world's major carmakers, as well as small series of exclusive electric sports cars, such as "Nevera".

[6] "Spring" is 3.73 meters long and with a single battery charge (27.4 kWh) provides a range of up to 230 kilometers. It is powered by an electric motor with 44 hp.

[7] With a fully charged battery, the expected range is more than 450 kilometers, depending on the version.

[8] Unlike most electric cars, the e-motor is at the front, as in classic models.

And today… ..in connection to space exploration, at the beginning of December 2021, several space missions were organized from various parts of our planet. Launch of "Falcon 9"[9] from the Space Center in Cape Canaveral. "Currently, the golden age of human spaceflight" is considered by experts from NASA, and new astronaut flights to the Moon are planned for 2025 at the latest. The mission of a Chinese solar-powered space robot rover landed on the moon three years ago to explore the dark side of this celestial body and it continues**.**

4. CONCLUSION

We need a green planet. It is significant that Japan has also increased its target rate for reducing carbon emissions to 46% by 2030, from 2013 levels. E-cars are much more [ally friendly. It is believed that soon there will be more chargers for e-cars in the world than classic petrol stations. Electric car sales in China increased for 132% in a year.

And after several months of testing and evaluation of cars that are present on the Serbian market since the beginning of 2021, in April 2022, the commission announced the results and the car of the year in Serbia in 2022 is "Toyota Jaris Cross". At the same time, due to the high level of safety, availability on the market, favorable vehicle maintenance conditions and despite the extraordinary circumstances of the pandemic, "Volkswagen ID.4" was rightly crowned with title of the electric car of the year in Serbia in 2022.

The turmoil in the world, especially the crisis and the war in Ukraine have led to many changes, "Audi", for example, has stopped production in certain locations. Despite the announcements on the closure, from the Russian factories the plants of "Stelantis" and "Micubishi" were still working at the end of March 2022. The transport of goods[10] also suffered losses. Some firms have a problem maintaining the liquidity. Anyway the electric car market has experienced rapid growth and evolution.

With hope that the war in Ukraine will end soon, we shall continue to hope and save our Planet for the next generations…

Concordia civium, murus urbium – (Harmony of citizens is the rampart of the cities).

[9] The task of "Falcon 9" is to place NASA's powerful X-ray device in Earth orbit, which should detect and explore black holes and neutron stars.

[10] About 10,000 companies are operating in the transport sector, of which 1,700 in the international sector.

REFERENCES

1. Black W, 2010, Sustainable Transportation: Problems and Solutions, The Guilford Press, New York.
2. Tomić-Petrović, N. (2018).”Vehicles for the future – dilemmas and perspectives”, *International Scientific Journal Trans&motoauto World*, published by Scientific technical Union of Mechanical Engineering, year III, issue 4/2018, pp. 155-157.
3. Tomić-Petrović, N. (2019). “New vehicles as our reality”,“Trans motoauto world“, Year IV, issue 2/2019, p. 44-46.
4. Prof. dr Nataša Tomić-Petrović, “The Future of Moto Auto World “, *XXVIII International Scientific Conference trans&MOTOAUTO'20*, 22. 06 - 25.06.2020 – Varna, Bulgaria, Conference Proceedings, p. 19-20 (ISSN 1313-5031 (Print), ISSN 2535-0307 (Online).
5. Prof. dr Nataša Tomić- Petrović, ”Right to Health in the Times of Pandemic (The Case of Serbia)“, Juridical Current Journal, Year XXIV, No. 1 (84), 2021, p. 37-41.

Practical UML subset for railway engineers to support formal modeling

Gábor Lukács*, Tamás Bartha
Budapest University of Technology and Economics
lukacs.gabor@edu.bme.hu

Abstract: *The acceptance and popularity of formal modeling is increasing in the development of safety-critical railway interlocking systems, because it allows the specification of the system's functionality using mathematically rigorous rules. The goal of the research described here is to introduce a simple, easy-to-learn, and useful UML (Unified Modeling Language) subset that supports railway engineers in developing the functionality of system elements at the system planning level. The selection of this UML subset is based on our practical experience. We examine the properties and limitations of this subset through a case study using the Yakindu Statechart Tools. The components specified with the proposed UML subset can be easily transformed into timed automata that we studied using the UPPAAL framework. In the paper, we also present the UPPAAL model for the case study. We are currently working on the implementation of a transformation using the UML subset presented in this paper, which makes it possible to generate formal models from Yakindu to UPPAAL in an automated way.*
Keywords*: RAILWAY, FUNCTIONAL SPECIFICATION, UNIFIED MODELLING LANGUAGE, TIMED AUTOMATON*

1. Introduction

The use of Model-Based Systems Engineering (MBSE) is gaining popularity in the development of transport applications [1]. This field is also preferred by railway engineers due to the advantages and power of modeling. In practical applications, formalisms such as e.g. the Unified Modeling Language (UML) are widespread [2]. A number of workbenches have already been prepared to support the use of UML during the system development lifecycle (without claiming completeness: Enterprise Architect [3], Yakindu Statechart Tools [4], etc.).

Railway transport is a traditionally safety-critical engineering field. In the current practice of railway system development, the level of expected safety is determined by the necessary risk reduction [5]. Functional safety aims at preventing the unacceptable risk of physical injury or damage to the health of people caused by the erroneous operation of a system, with the proper implementation of one or more safety functions [6]. The specification of the correct functionality of the system is a core concept of safety, the implementation of which is the responsibility of the domain engineers.

One way to meet the requirements of safety-critical applications is through the application of formal methods [7]. Formal modeling provides an opportunity to precisely specify the functionality of systems using logical-mathematical rules. Even though formal methods are claimed (several pieces of research support this claim) to help avoid specification errors, domain engineers are reluctant to use them in the system design/development activities. The reason: their application often requires significant additional expertise, since they are abstract, computer science-based methods. Consequently, railway engineers can often only acquire these skills after years of hard work.

The research described in this paper aims to present a simple case study demonstrating the practical application of a methodology that supports railway engineers in the construction and verification of formal specifications. The proposed specification-verification environment aims to decrease the need for a mathematical/computer science background/knowledge at the system development level. The application of the proposed framework supports the creation of correct, complete, consistent, and verifiable functional specifications of a given component. In summary, this approach leads to a significant improvement in quality and distributes the development costs more evenly among the related lifecycle phases.

In this paper, first, we give an overview of the background related to our research goal (in Section 2). Thereafter in Section 3, we present a practical UML subset that supports railway engineers in developing the functionality of system components at the system planning level. In Section 4, we describe a simplified case study through which it is presented how can use the given UML subset in practice to specify the functionality of a component. As part of our case study, we show one possible way of how the specified component can easily be transformed into timed automata that we studied using the UPPAAL framework. At the end of the paper, we put the results into a broader context (Section 5) and give a conclusion (Section 6).

2. Related work

The Gamma Statechart Composition Framework (GSCF) is an integrated toolset to support the design, verification and validation, and code generation for component-based reactive systems [8]. GSCF provides a modeling language and framework for the hierarchical decomposition of statechart components in an object-oriented way. The framework is currently integrated with 3rd party modeling tool (Yakindu Statechart Tools) and model checker (UPPAAL) to support formal verification of the constructed models. GSCF automatically generates an implementation of an individual component. This environment also allows back-annotation and test generation. The main difference between the GSCF and our proposed framework is that the former targets software engineers as end-users, whereas we aim to support railway engineers with our specification-verification environment. The objectives, processes, and tools used in both frameworks are similar. However, our methodology does not deal with code generation, because it is not intended to support that level of abstraction. Both frameworks hide the inherent complexity of using formal methods by offering a high-level user interface.

The research goal of the thesis by D. Darvas [9] was to analyze the applicability of formal methods in the domain of industrial control systems and propose a specification-verification environment. The main challenges of the chosen domain were performance and usability. The author proposes the application of model checking to support the software development of industrial control systems. The described platform supports domain engineers by hiding the formal details, the computer science-based mathematical background. The case studies of this work are related to the European Organization for Nuclear Research (CERN). In connection with our research, the following results of the thesis are relevant: formal specification for programmable logic controller (PLC) modules and model checking of critical PLC programs. Our research goal connects very closely to this thesis with differences in the domain and abstraction level.

The paper of Y. Y. Nazaruddin et al. [10] presents an application of a formal methods-based model checking for safety verification of a railway interlocking system. The proposed model checking techniques are implemented on a timed automaton of the considered interlocking system. The safety behavioral specification is expressed as Computation Tree Logic (CTL) formulas. The UPPAAL tool is used to perform the model checking. The distinction between this study and our research is that we performed modeling and model checking at the component design level, while the study [10] implemented it at the system level.

Paper [11] is a very recent survey that gives an overview related to formal specification and verification of smart mass transit railway interlocking systems. This survey also refers to our research

work [12], in which we give an overview of the proposed framework with a case study. Paper [12] places the proposed framework in the development process and the described case study shows the application of the methodology step by step.

3. Methodology

In this section, we outline the overall methodology we propose in our other paper [12]. The main steps to be performed by railway engineers are as follows (note, that the main steps of the process comply with the best practice based on [6]):

1. inputs of the process: requirements from the stakeholders (mainly in natural language), system requirements specification, architecture design, and the distribution of system requirements to components;
2. specification of each component: interfaces, functionality (behavior), configurations (parametrics), and the rest of the requirements;
3. formal verification: the transformation of the requirements defined in step 2 into temporal logic (CTL) formulas [7], the transformation of the component defined in step 2 into formal models (timed automata) [7];
4. outputs of the process: formally verified component specification.

As the overall methodology was already introduced in the paper [12], in this paper, we focus on step 2 more in detail. However, the case study presented later (in Section 4) covers the whole process, so it demonstrates the approach outlined in the list above in its entirety.

The proposed methodology provides a specification environment for designing the functionality of each component of the system. This specification environment builds on four pillars related to a component: requirements, interfaces, configuration, and behavior (step 2 above). Many existing solutions can be used to describe these artifacts. Our approach uses structured natural language for specifying the requirements, UML component diagrams [13] and a tabular description form for the interface definitions, a specific tabular method for defining the configuration elements, and UML state machines [13] for describing the behavioral aspects of a component. We found that railway system engineers can easily create the specifications given in step 2 by using only a subset of the UML diagrams (see Fig. 1 and Fig. 2). These subsets are shown in Fig. 1 (UML component diagram) and Fig. 2 (UML statechart). In both figures, the red parts are not used in the proposed methodology described above.

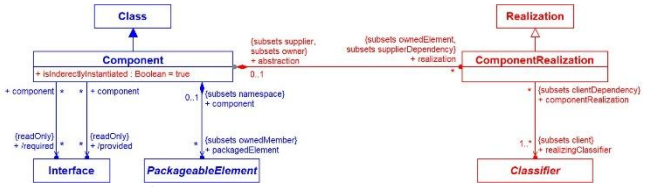


Fig. 1 Subset of UML component diagram based on [13]

A significant part of the discarded UML subset marked in red in Fig. 1 and 2 can be easily replaced with the retained UML subset marked in blue. The selected, blue-marked subset allows to express the same information much simpler and more concisely as the omitted, red-marked subset, which helps with the clarity and portability of the specification.

Another example of such simplification is that we do not use a "terminate" pseudostate in our statechart subset shown in Fig. 2, because we used the precondition, that components cannot be created, and terminated at any time during the software lifecycle (that is all components are eternal in this approach). This approach is based on the assumption that we have an embedded software that starts to "run" after the power supply is switched on, and continues to work until the power supply is switched off.

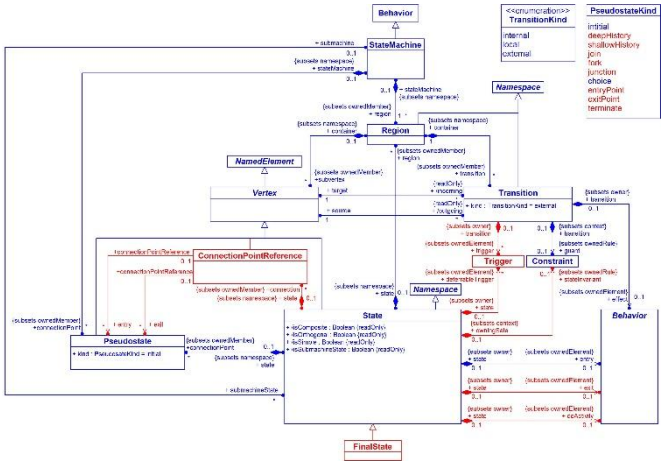


Fig. 2 *Subset of UML statechart based on [13]*

4. Case study

In this section, we describe a case study about a simple component – namely detection point – using the methodology described in Section 3.

The purpose of the detection point is to detect a railway vehicle's presence within its scope. The functionality of the detection point is described simply: If the train is over the detection point it is 'occupied', and when the train is not over the detection point it is 'free'. These are functional requirements of the detection point in a high level of abstraction. We note, that railway engineers can significantly supplement this behavior during the specification of a system based on the experiences gained so far and domain-specific knowledge. So the described functionality above can be complemented by the several interactions with end-users (operators) and designers during the development process. In this paper, we do not write about these processes, thus the case study can be discussed in a very simple way.

As described in the previous paragraph, the functionality of the detection point at a high level of abstraction can be specified by the following two functional requirements:

A. If a train is within the scope of the detection point, it provides an 'occupied' signal.

B. If a train is not within the scope of the detection point, it provides a 'free' signal.

Based on described functionality in the previous paragraph, the interface specification of the detection point can be specified with a combination of Fig. 3 and Table 1.

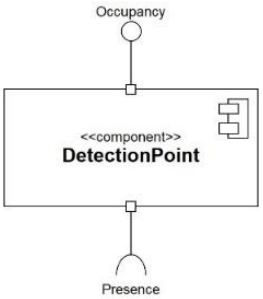


Fig. 3 *Interfaces of detection point (UML component diagram)*

Table 1 *Interface specification of detection point*

Identifier	Type	Codomain	Initial value	Brief description
Presence	Input	[free | occupied]	occupied	Presence input.
Occupancy	Output	[free | occupied]	occupied	Occupancy output.

Based on the interface specification (Fig 3. and Table 1) and the functional requirements (A and B), a possible implementation of the detection point in Yakindu (version 3.5.9) is shown in Table 2 and Fig 4. Note that for the sake of simplicity, the case study is not equipped with parameters (e.g., time), i.e., there is no given configuration specification. This means that the set of configuration elements in this case study is empty, i.e. from the point of view of modeling in Yakindu it is an empty set.

Table 2 *System definition implemented in Yakindu*

```
@CycleBased(100)      // 100 ms long cycle
@ChildFirstExecution

interface:
// External interfaces of detection point - Input variables
var in_presence_p : boolean = true            // Input - Presence
// External interfaces of detection point - Output variables
var out_occupancy : boolean = true            // Output - Occupancy
```

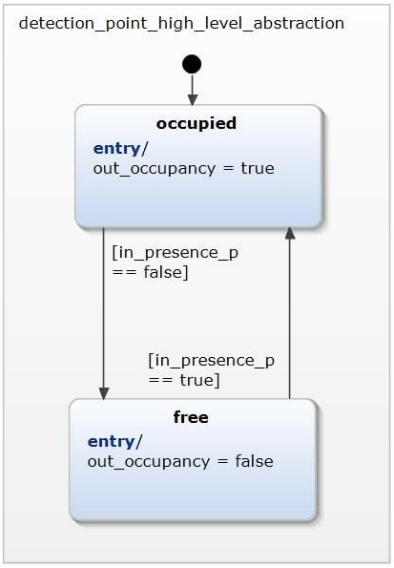


Fig. 4 *Statechart of detection point implemented in Yakindu*

Starting from the Yakindu model of the detection point described above, we also constructed the UPPAAL model of this component. For this, we used the UPPAAL version 4.2.24.

Before the UPPAAL model of the detection point could be called ready for simulation and model checking, it needed certain additional features. Three things were necessary to implement for the UPPAAL model of the detection point to make it suitable for simulation and model checking: time handling (by the automaton called 'tick'), execution control (by the automation called 'runcontrol'), and input function (by the automaton called 'inputgeneration', when applicable). The supplementary automata are included in the system declaration part of the UPPAAL model (see Table 3). Accordingly, the UPPAAL model of the detection point consists of four automata, of which the functionality of the detection point (see Fig 4) is realized by the automaton 'presencehandling' (see Table 4 and Fig. 8).

Table 3 *System declarations in UPPAAL*

```
// Automata
tick = TC();                    // Automaton - Cycle generator
runcontrol = RC();              // Automaton - Run control
inputgenerator = INPGEN();      // Automaton - Input generator
presencehandling = PH();        // Automaton - Presence handling

system tick, runcontrol, inputgenerator, presencehandling;
```

Table 4 declares the interface variables of the detection point ('in_presence_p' as input and 'out_occupancy' as output variable). The other variables in Table 4 support simulation and model checking (see the details in the description of each automaton).

Table 4 *Declarations in UPPAAL*

```
// External interfaces of detection point - Input variables
bool in_presence_p = true;          // Input - Presence
// External interfaces of detection point - Output variables
bool out_occupancy = true;          // Output - Occupancy

// Channels and variables for simulation
chan CYCLE;              // Tick, start new cycle (1 tick == 100 ms)
bool ISRUN = false;      // Tick ran (true: ran, false: did not run)

// Run control, permissions within a tick
broadcast chan ALLOWEDRUN;    // Running permissions of functions
int PERMISSION = 0;           // Running permissions of functions:
// 0: not used, initial
// 1: INPUTGENERATOR is allowed to run
// 2: PRESENCEHANDLING is allowed to run
```

The automaton called 'tick' consists of two states (Fig. 5). The 'start' state is a committed state, so there is no time delay in this state. In the 'run' state the component performs its functions. When the 'tick' automaton transits from the 'start' to the 'run' state, a new cycle begins ('CYCLE!'). A cycle lasts 100 ms (Table 5). The cycle length is represented by the invariant of the 'run' state, i.e. 't<=1'. When the component has finished running, the automaton goes from the 'run' to the 'start' state. The 'tick and 'runcontrol' (see Fig. 6) automata are interleaving in terms of control. The 'tick' automaton gives run permission to the 'runcontrol' using channel 'CYCLE'. The 'runcontrol' automaton indicates to the 'tick' automaton when it has finished running using the variable 'ISRUN'. When the cycle ends, the clock variable 't' will reset, and the variable 'ISRUN' will return to false.

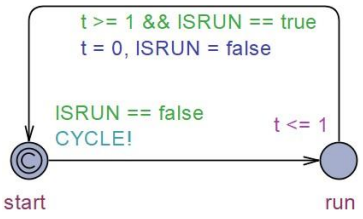


Fig. 5 *Automaton 'tick' for time handling*

Table 5 *Declarations of automaton timehandling*

```
// Clock variable
clock t;      // Length of a tick/cycle (in 100 ms units)
```

The automaton called 'runcontrol' is responsible for execution of the component's functions in the correct sequence (see Fig. 6).

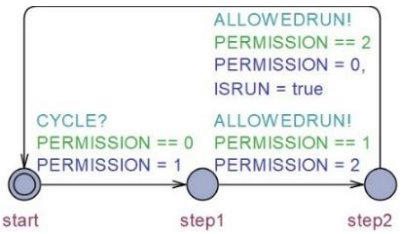


Fig. 6 *Automaton for execution control*

Each of the automatons belonging to the detection point functions has a unique identifier ('PERMISSION'). In this case study, identifier 1 is the automaton 'inputgenerator' and identifier 2 is 'presencehandling'. The order of execution matches the numeric order of identifiers: first 'inputgenerator' then 'presencehandling'. Each automaton receives its run permission via the broadcast channel 'ALLOWEDRUN', and they use the variable 'PERMISSION' to examine if it is their turn.

One possible input function of the detection point implemented in UPPAAL is shown in Fig. 7. The parameters and declarations of this automaton are described in Table 6. Depending on our modeling purposes – but not necessarily in all cases – we may need an input function for each component. This function can be specified in several forms. In our case study, we constructed an input function for the presence inputs of the component detection point that covers all possible input combinations. The created function is shown in Table 6. Each cycle begins with the detection point object reading its input. The input to be read is always randomly selected (see Fig. 7, 'inp:int[0,1]') from the set of specified input combinations. The automata perform their task depending on the detected input and current state. (Note that in this case study the detection point does not have parameters and timers.)

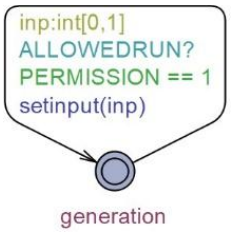


Fig. 7 *Automaton for input generation*

Table 6 *Declarations of automaton input generator*

```
// Input generator function
int setinput(int inp){
if (inp == 0) {in_presence_p = false;}
else if (inp == 1) {in_presence_p = true;}
return 0;
}
```

The presence handling function implemented in UPPAAL is shown in Fig. 8. This automaton is constructed based on the state machine shown in Fig. 4. The variables are named equally in the Yakindu and UPPAAL models, so the "transformation" can easily to trace.

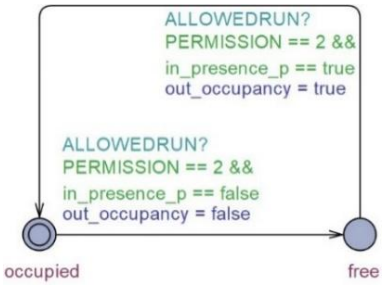


Fig. 8 *Automaton to presence handling.*

So far so, with the activities performed in the previous paragraph, we have constructed a formal model of the detection point in the form of a timed automaton from the specification of the railway engineering domain. At this point, only another input is missing to verify the model, which we would like to do in this case study with model checking: specifying requirements 'A' and 'B' by CTL formulas. The formalized requirements and the results of the model checking are shown in Table 7.

5. Results and discussion

Our research focuses on a formal modeling-based methodology to support railway engineers during the development lifecycle. The proposed environment builds on a UML subset for specification and model checking for verification. In this paper, we summarized the main steps of the proposed methodology, described the UML subset, and presented the steps of the process in a case study from the UML specification of a component to the model checking. The Yakindu Statechart Tools and UPPAAL framework were selected and used for the presented case study. We have found that the transformation between the two tools can be ensured according to simple rules for the defined UML subset, which provides a good opportunity to automate part of the process.

Table 7 *Results of model checking*

Req.	CTL formulas	Result of model checking
A	in_presence_p == true --> out_occupancy == true	Property is satisfied.
B	in_presence_p == false --> out_occupancy == false	Property is satisfied.

We worked together with domain engineers during the development of the described case study. Our conclusion is that one possible small subset of UML statecharts and UPPAAL automata could be easily mastered by railway engineers. For this reason, domain engineers did not refuse to use formal methods in this way. We found that the main difficulty for the domain engineers is to prepare the requirement specification. The problem is that they do not deal with the formalize-ability aspects of the requirements during the preparation of specifications. To solve this issue, we began to develop an intermediate domain language in this field of the railway.

6. Conclusion

In this paper, we presented the applicability of a formal modeling-based methodology through a case study. The proposed process we have performed provides a specification-verification environment for railway engineers. This framework facilitates the construction of high-quality functional specifications during the development compared to traditional development. We found that the proposed UML subset could be applicable in the railway-specific domain to support formal modeling and model checking already in the early stages of the lifecycle. During the transformation from the Yankidu to the UPPAAL, we found that a part of the proposed process can be well automated. We are currently working on the implementation of this transformation tool.

7. References

1. P. Micouin, *Model Based Systems Engineering: Fundamentals and Methods* (2014)
2. R. Bernhard, *Modeling with UML* (2016)
3. G. Blokdyk, *Sparx Systems Enterprise Architect* (2021)
4. A. Marron, et al., *Embedding Scenario-based Modeling in Statecharts*, MoDELS (2018)
5. CENELCE EN 50129, *Railway applications – Communication, signalling and processing systems – Safety related electronic systems for signalling* (2018)
6. CENELEC EN 50126, *Railway Applications – The Specification and Demonstration of Reliability, Availability, Maintainability and Safety (RAMS) – Part 2: Systems Approach to Safety* (2017)
7. J. Wang, W. Tepfenhart, *Formal Methods in Computer Science* (2019)
8. V. Molnár, B. Graics, A. Vörös, I. et al., *The Gamma Statechart Composition Framework: Design, Verification and Code Generation for Component-Based Reactive Systems*, ICSEC, pp.1-4. (2018)
9. D. Darvas, *Practice-Oriented Formal Methods to Support the Software Development of Industrial Control Systems* (2016)
10. Y. Y. Nazaruddin, T. A. Tamba, K. Pradityo, et al., *Safety Verification of a Train Interlocking Timed Automaton Model*, IFAC, Vol. **52**, Issue 15, pp. 331-335 (2019)
11. L. Kadakolmath, U. D. Ramu, A Survey on Formal Specification and Verification of Smart Mass Transit Railway Interlocking System, IJSSE, **11**(6): 671-682 (2021)
12. G. Lukács, T. Bartha, *Construction of formal models and verifying property specifications through an example of railway interlocking systems*, Pollack Periodica, **14**(2):39-50 (2019)
13. C. Bock, et al., *Unified Modeling Language 2.5.1* (2017)

Unaccompanied combined transport with rail legs in Romania

Nicolae Mugurel Tănăsuică
CFR Marfa – National Company of Freight Railway Transport, Bucharest, Romania
mugurel_tanasuica@yahoo.com

Abstract: *The paper deals with the development of the unaccompanied combined transport (UCT), in Romania. Firstly, it presents statistics and performs a quantitative analysis, depicting a sharp decline of the UCT after 1990, its low weight in the total freight transport volumes and the main characteristics of the domestic traffic which has had a higher weight than in the neighbouring countries and is almost completely connected with the Port of Constanta. The qualitative analysis indicates a great weight of the empty boxes (generating higher costs and prices), the disappearance of several type of services during the time and the fact that the Port of Constanta has not become a real engine for UCT yet. The paper identifies as reasons for these evolutions the changes in the economy, the cancelation of the support measures implemented before 1990, the route competition, the competition with other ports at the Black Sea, the constraints for the transit through the Bosphorus Strait and the lack of practical support measures. It is interesting that the policies and the strategies before and after 1990 are practically identical, but the measures implemented before 1990 are not compliant with the European legislation. Secondly, the paper performs a comparison between the UCT with rail legs and the road transport. The analysis depicts several structural, technical, and operational issues (poor status of the railway infrastructure and container terminals, the charges for the use infrastructure that are higher in the railway case and the investments in the roads) making UCT not attractive on the market. On the other hand, the calculations based on the method used in the Marco Polo Programme, respectively using the EcoTransit application indicate lower external costs and important savings in CO_2 and other polluting gases. Thirdly, the paper deals with the possible support measures, emphasizing that the measures implemented in Austria could be models for the Romanian authorities. European legislation related to the state aids also needs revisions, so that it would not embarrass the transport policies. The main conclusion is that UCT could develop only if subsidies and other appropriate support measured would be implemented.*

Keywords: COMBINED TRANSPORT, TRAFFIC VOLUME, PRODUCTION SCHEME, PRODUCTION COST, EXTERNAL COST, POLLUTION, SUPPORT MEASURES

1. Introduction

For decades, the combined transport was defined as a door-to-door service performed by at least two transport modes [1]. This meaning is kept in the "European Agreement on Important International Combined Transport Lines and Related Installations' (AGTC)" and in the "Convention for the Unification of Certain Rules for International Carriage by Air", originally signed in 1929 in Warsaw and last time amended in Montreal, in 1999. However, in the seventies from previous century, this concept has been replaced by multimodal transport [2].

Today, in Europe, we also deal with a special form of multimodal transport, respectively the intermodal transport having the characteristic that the loads are not divided when they are transferred from one mode of transport to another one [3]. It is interested that in America, this term is used as a synonymous for multimodal transport [4].

Moreover, the intermodal transport also has a particular form of implementation, for which the name of combined transport is given. In this new approach, the combined transport is defined as "intermodal transport where the major part of the European journey is by rail, inland waterways or sea and any initial and/or final legs carried out by road are as short as possible" [3].

The general definition practically does not impose any constraint for loads or for the length of the different legs. From this perspective, even if the combined transport is seen as a solution for shifting the traffic from roads to other less polluting transport modes, it does not help the efforts to implement the transport policies having this aim. Therefore, the 'Council Directive 92/106/EEC of 7 December 1992 on the establishment of common rules for certain types of combined transport of goods between Member States' comes with the following provisions [5]:

1.The subjects for the combined transport must be "the lorry, trailer, semi-trailer, with or without tractor unit, swap body or container of 20 feet or more" [5];

2.The road legs are limited:

- "between the point where the goods are loaded and the nearest suitable rail loading station for the initial leg, and between the nearest suitable rail unloading station and the point where the goods are unloaded for the final leg, or;
- within a radius not exceeding 150 km as the crow flies from the inland waterway port or seaport of loading or unloading. [5]"

3.The carriage on rail, inland waterway or sea "exceeds 100 km as the crow flies" [5].

When the subject of carriage is a container, a swap body or a semitrailer (identified in accordance with the international standards ISO6346 and EN13044), we talk about unaccompanied combined transport (UCT) [6]. The paper deals with the development of the unaccompanied combined transport (UCT), in Romania.

2. Development of the UCT in Romania

Table no.1 depicts the main moments in the development of the UCT services in Romania.

Table no. 1: Moments in development of UCT in Romania [7]

Year	Event
1955	Start of containerisation in Romania Setup of the railway units specialised in trucking and handling intermodal units
1958	Entry into force of a Domestic Freight Tariff, including "General conditions for carriage of the containers"
1969	First transports of large containers with length of 10'
1970	Start of operations in the first container terminal, București Basarab Run of the first train carrying large containers of 10', between București Basarab and Brașov
1972	Introduction of the course of "Multimodal transports" in the study programme dedicated to the students enrolled at the specialization "Railway remote Control and Transport technology" (today, "Transport engineering") of the faculty of Transports from the Polytechnic Institute of Bucharest (today POLITEHNICA University of Bucharest)
1973	Start of operations in the first modern container terminal, 16 Februarie 1933 (today Bucureștii Noi)
1974	Adoption of a strategy for the development of Romania stipulating the following ideas: "a rational weight will be given to any transport mode, the aim being to use in the most efficient way the inland waterways and railways in order to avoid the pollution" [8]
1975	Publication of regulation regarding the large containers by the Romanian Naval Register
1978	Adoption of a strategy for the development of Romania stipulating: "it is necessary to use in the most efficient way all the means and to optimise the transport, respectively to implement on a large scale the modern technologies,

Year	Event
	especially the palletisation and the containerisation".
1986	Publication of the "Guidelines for the combined transport through the ECM units"
1993	Ratification by Romania of the European Agreement on Important International Combined Transport Lines and Related Installations (AGTC)
1999	Issuing of the Government Ordinance no. 33 from 30th of August 1999 establishing rules in the combined transport of the goods, approved through the Law no. 401 / 2002
2000	Issuing of the Government Decision no. 193 / 2002 approving the Guidelines for application of the Government Ordinance no. 33 from 30th of August 1999 establishing rules in the combined transport of the goods
2001	Issuing of the Government Decision no. 1003 from the 4th of October 2001 approving the "Strategy for the development of the railway system in Romania, in the period 2001 – 2010", including a section dedicated to the intermodal transport
2003	Start of operations in Constanţa South Container Terminal (CSCT), in the Port of Constanta
2007	Launch of the Operational Sectoral programme TRANSPORT, stipulating the promotion of the intermodal transport and the modernisation of some terminals
2009	Star of operations in Rail Port Arad (at Curtici)
2011	Approval of the "Strategy for intermodal transport in Romania 2020" through the Order of the Minister of transports no. 457 from 20th of June 2011 – never implemented
2020	Approval of the "Strategy for the development of the railway infrastructure 2021-2025", containing an annex related to the intermodal transport

It is interesting to remark that the strategies in 1974 and 1978 include principles that are practically identical with those ones defined in the European white papers published in 2001 and 2011, respectively in European documents adopted during the las decade.

Regarding the first container terminal built in Romania (16 Februarie 1933, today Bucureștii Noi), this one was designed by Romanian engineers, without the help of foreign consultants, with a configuration which be considered actual even today.

3. Trends and evolutions

The UCT in Romania knew its golden period between 1970 and 1989. The strategies mentioned in the table no.1 were implemented through investments in container terminals, rolling stock and other equipment, staff formation and specialization, adoption of specific operational regulations, as well as through strong support measures. In the centralized economy at that time, the transport tasks were being allocated with priority to the railway system and to the inland waterways through the national transport plans. At the same time, bans were imposed to the road transport, which was limited at short distances of no more than 100 km [9]. Practically, taking into account the average distances recorded in that period, this one was employed only for pick-up and delivery services from / to clients not served by railways.

The traffic volumes recorded in this period were impressive. According to the data available on website of the Organisation for Economic Co-operation and Development (OECD), Romanian Railways carried more containers than the railways in the two German states taken together (figure no. 1). In terms of tonnes, the performances in Romania are quite similar with those in the two Germanies (figure no. 2).

A monography published at the e 65th celebration of the Bucharest Regional Railway Branch confirms these facts. It indicates that, in 1983, the volume of the goods dispatched in containers from this branch reached to 900000 tonnes [10].

In 1989, 29 container terminals were being operational, and 19 others were being under construction. According to the plans in force at that time, at least one terminal should have had to be developed in every country department.

On the other hand, in the same year the performance of the combined transport in the total railway performance measured in tonnes carried on railways reach only to 3.3% (10.103 million tonnes from 306.302 million tonnes) [11,12].

After 1989, a very sharp decline occurred, as indicated in the figures no. 3 and 4. Today, the traffic volumes measured in TEU and tonnes represent only 12,57%, respective 21.4% from the volumes recorded in 1989.The main reasons for this evolution are the structural changes in the national economy generating the disappearance of the national transport plans, bankruptcy and closure of most of the traditional clients, the liberalisation followed by a development of the road transport and the lack of any support measure [11, 12].

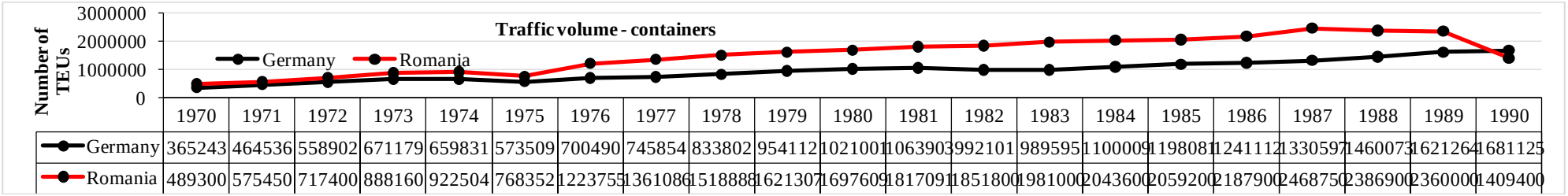
Negative effects had the bankruptcy of the former units of the Romanian Railways. specialised in trucking and terminal operating. In the reforming process of the Romanian Railways, they were transferred, in 1998, to the newly created national freight operator as a subsidiary, then they were privatised in 2002, but this process did not help them to survive. Thus, UCT lost important resources, specialised staff and knowledge, which could be replaced with difficulty.

Statistics depict the UCT characteristics in Romania [13]. Thus:

1. In comparison with other countries, such as Poland, the UCT has not developed during the last two decades. The values of the traffic volume measured in TEU has kept relatively constant. A decrease could be observed in the period of the financial and economic crisis started in 2008, but a recovery has occurred later.
2. UCT in Romania is performed using almost exclusively ISO containers. The numbers of swap bodies and semitrailers carried on railways could be neglected. This fact is generated by the fact that the road carriers in Romania have not invested in swap bodies or in specific semitrailers, cranable and compliant with the UIC standards for carriage on rail wagons. However, during the last decade, some foreign companies have organised freight transport in cranable semitrailers to and from a terminal connected to the main border station between Romania and Hungary (Curtici). This traffic is served in Romania by the railways only on the border line, on 8 km, while the respective customers have preferred for the rest of the Romanian territory only the pure road carriage. This happens due to the poor status of the railway infrastructure, generating higher transit times and costs than in the case of the roads.
3. UCT keeps a low weight in the total performance of the railways, both in terms of tonnes and tonnes - kilometres (fig. no. 5). An increase could be observed in the last years in the case of the performances measured in tonnes - kilometres, due to the routing through Romania of the containers from Turkey to the Western countries or vice versa by the subsidiaries in Romania and Bulgaria of two traditional operators from other countries.
4. In Romania, the traffic flows served by the UCT are unbalanced. The empty intermodal transport units (fig. no. 6) have a very high weight in the total performances of the UCT, even if this weight has known a small decrease in the last years. It varies between 30 – 40%, in comparison with Germany, where only 20 - 25% from the TEUs are empty. This characteristic could be explained through two aspects:

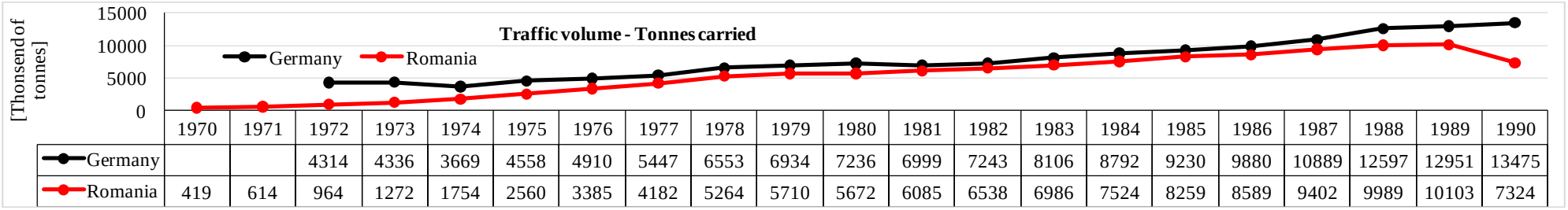
a) The demand characteristics. The transport intermediaries claim that they have encountered difficulties in finding goods which could stuff the intermodal transport units on the return trips. Impossibility to operate the intermodal transport units in the load – load system imposes to the transport providers to increase the charges invoiced to their customers at levels allowing them to cover the costs of the empty run of the units, too. Consequently, UCT becomes more expensive than other solutions.

b) The fact that the intermodal transport units belong to the shipping companies or to the European intermodal transport operators, having their own optimisation solutions in connection with them. Consequently, the units are not repositioned in Romania, so that they could be operated in the load – load system.



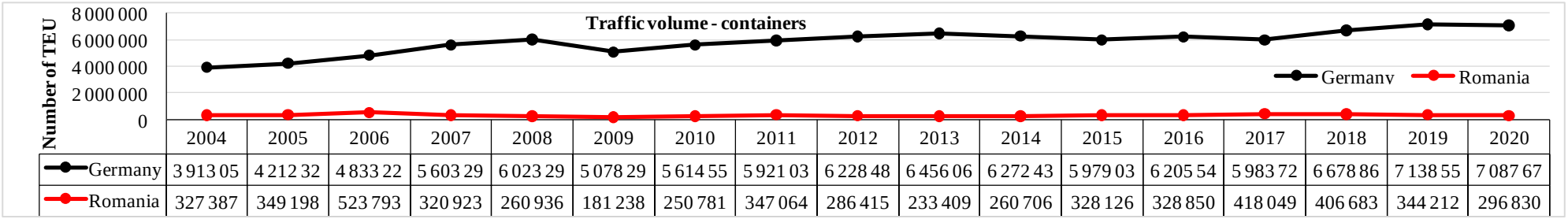
	1970	1971	1972	1973	1974	1975	1976	1977	1978	1979	1980	1981	1982	1983	1984	1985	1986	1987	1988	1989	1990
Germany	365243	464536	558902	671179	659831	573509	700490	745854	833802	954112	1021001	1063903	992101	989595	1100009	1198081	1241112	1330597	1460073	1621264	1681125
Romania	489300	575450	717400	888160	922504	768352	1223755	1361086	1518888	1621307	1697609	1817091	1851800	1981000	2043600	2059200	2187900	2468750	2386900	2360000	1409400

Fig. no. 1: Traffic volumes measured in TEU, in the period 1970 – 1990 [11]



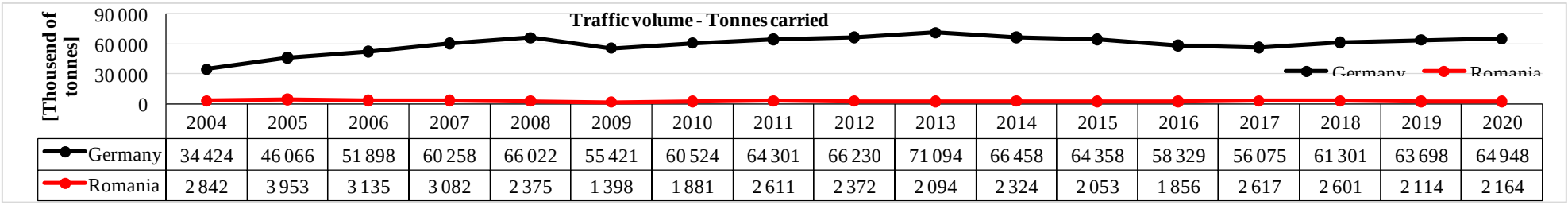
	1970	1971	1972	1973	1974	1975	1976	1977	1978	1979	1980	1981	1982	1983	1984	1985	1986	1987	1988	1989	1990
Germany			4314	4336	3669	4558	4910	5447	6553	6934	7236	6999	7243	8106	8792	9230	9880	10889	12597	12951	13475
Romania	419	614	964	1272	1754	2560	3385	4182	5264	5710	5672	6085	6538	6986	7524	8259	8589	9402	9989	10103	7324

Fig. no. 2: Traffic volumes measured in thousands of tonnes, in the period 1970 – 1990 [11]



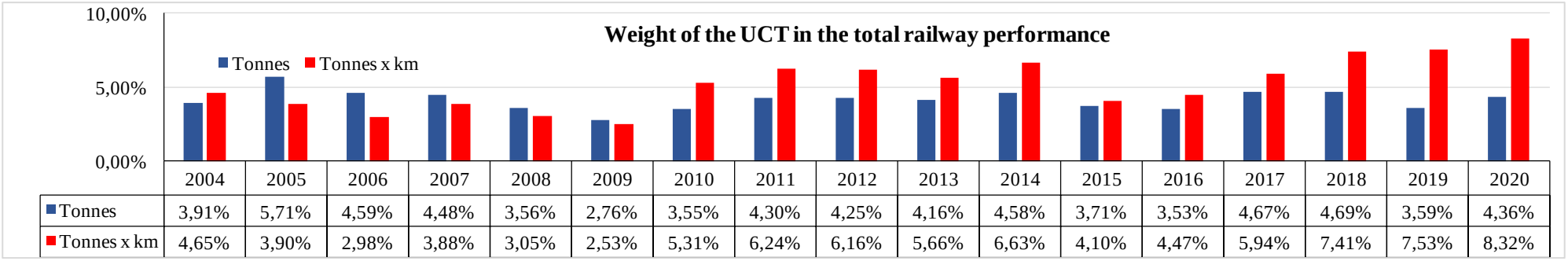
	2004	2005	2006	2007	2008	2009	2010	2011	2012	2013	2014	2015	2016	2017	2018	2019	2020
Germany	3 913 05	4 212 32	4 833 22	5 603 29	6 023 29	5 078 29	5 614 55	5 921 03	6 228 48	6 456 06	6 272 43	5 979 03	6 205 54	5 983 72	6 678 86	7 138 55	7 087 67
Romania	327 387	349 198	523 793	320 923	260 936	181 238	250 781	347 064	286 415	233 409	260 706	328 126	328 850	418 049	406 683	344 212	296 830

Fig. no. 3: Traffic volumes measured in TEU, in the period 2004 – 2020 [13]



	2004	2005	2006	2007	2008	2009	2010	2011	2012	2013	2014	2015	2016	2017	2018	2019	2020
Germany	34 424	46 066	51 898	60 258	66 022	55 421	60 524	64 301	66 230	71 094	66 458	64 358	58 329	56 075	61 301	63 698	64 948
Romania	2 842	3 953	3 135	3 082	2 375	1 398	1 881	2 611	2 372	2 094	2 324	2 053	1 856	2 617	2 601	2 114	2 164

Fig. no. 4: Traffic volumes measured in tonnes, in the period 2004 – 2020 [13]



	2004	2005	2006	2007	2008	2009	2010	2011	2012	2013	2014	2015	2016	2017	2018	2019	2020
Tonnes	3,91%	5,71%	4,59%	4,48%	3,56%	2,76%	3,55%	4,30%	4,25%	4,16%	4,58%	3,71%	3,53%	4,67%	4,69%	3,59%	4,36%
Tonnes x km	4,65%	3,90%	2,98%	3,88%	3,05%	2,53%	5,31%	6,24%	6,16%	5,66%	6,63%	4,10%	4,47%	5,94%	7,41%	7,53%	8,32%

Fig. no. 5: Weight of the UCT in the total railway freight traffic in Romania, between 2004 and 2020 [13]

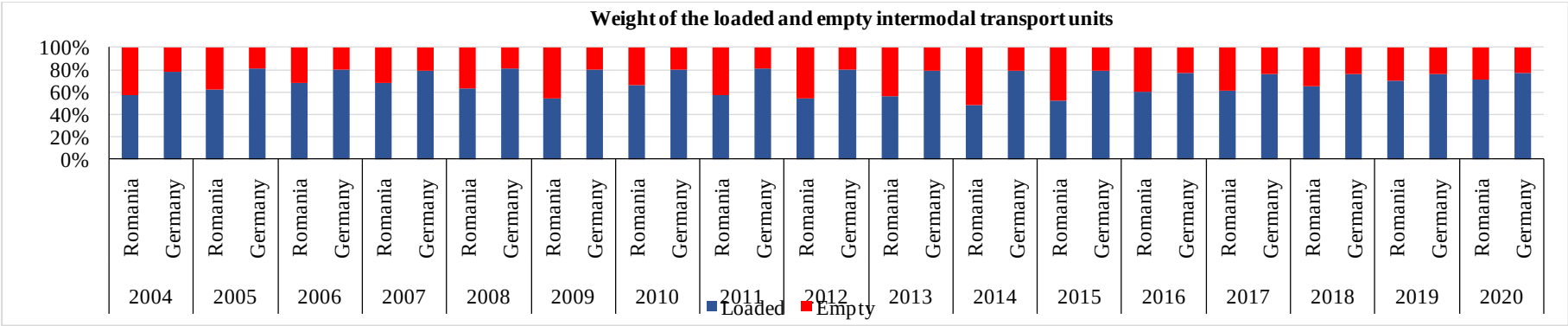


Fig. no. 6: Weight of the loaded and empty ITU in Romania in comparison with Germany, between 2004 and 2020 [13]

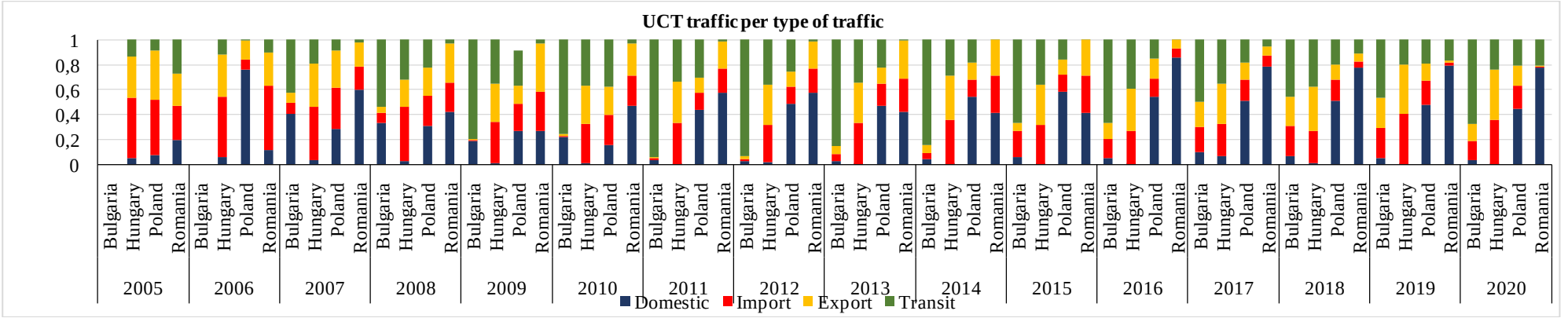


Fig. no. 7: Weight of the UCT in the total railway performance in Romania, between 2004 and 2020 [13]

5. An interesting evolution could be observed in the case of the volumes recorded in the different traffic types. Between 2004 and 2020, the weight of the international traffic has significantly decreased, the TEUs of import and export volumes becoming practically neglectable, both in terms of volumes and weight in the total traffic volume. The transit seems to become more important due to the subsidiaries in Romania and Bulgaria of two traditional railway operators in other countries, which rerouted intermodal transport units from or to Turkey on the Romanian railway network. On the other hand, the domestic traffic has known an important increase in its weight, becoming from far dominant.

6. UCT in Romania differentiates from the similar services in the neighbouring countries, in which the international traffic looks more important than the domestic one. Moreover, in Bulgaria, the highest weight is recorded in the case of the transit traffic. This difference could be explained through the fact that the railway routes through Romania between Western countries and Turkey, respectively between China and Europe are longer than on the competing routes through Serbia, respectively Belarus and Poland. Compared with the other Balkan route, the Romanian route is characterised by a longer Diesel leg, too. In this context, we should observe that no regular or experimental train has passed through Romania from or to China.

7. The statistical records corroborated with the traffic flows published in the General Master Plan of Transport [13, 14] lead to the conclusion that almost the entire domestic traffic is connected with the Port of Constanta. On the other hands, the port mainly serves the foreign trade of Romania, due to its geographical position. From this perspective, we could assert that the domestic traffic is, in fact, international. The transport of intermodal transport units is registered in domestic rail traffic, between railway stations located on the national territory, but the goods inside them go or come from abroad.

In the case of the Port of Constanta, we should also observe that the container traffic volume knew its maximal value in 2007, respectively 1.4 million TEU. It has decreased during the economical crises and has not recovered later. In 2020, only 643025 TEU passed through the port. For comparison, the number of boxes handled in the Port of Gdansk increased from 512000 TEU in 2010 to 1924000 TEU in 2020.

A breakdown taking into account the transport means used for the container transport to and from the port of Constanța is presented in table no. 2.

Table no. 2: Breakdown of the container traffic volumes, in TEU, through the Port of Constnața [7]

Year	TEU	Rail	Road	Sea	Inland waterways
2007	1411414	14.70%	14.80%	69%	1.60%
2009	594303	18.33%	51.14%	29.03%	1.50%
2019	666036	Not available			0,26%
2020	643725				0,19%

In these circumstances, it is obviously that the Port of Constanța has not become a real engine for the UCT with rail legs in Romania. Its poor performances in container traffic could be explained by [7]:

1. Development of container terminals in the Ukrainian and Russian ports at the Black Sea and the competition with these ports.

2. The preferences observed in the case of many great shipping companies to establish hubs in the Mediterranean ports and to serve the ports at the Black Sea (including Port of Constanța) only with feeder ships, carrying containers mostly for or from the local market (pick-up and delivery services);

3. The size constraints imposed by the Turkish Straits for the passage of the ships. Practically, ultra-large-container ships (ULCS) having lengths of 400 m and carriage capacities of more than 20000 TEU are not allowed on Bosphorus Strait. The biggest portcontainer ships which have called on the Port of Constanța have not overcame a length of 300 m in length and a capacity of approximatively 9000 TEU. Consequently, we could talk about problems of economy of scale in the case of the ports located at the Black Sea in comparison with other European ports.

Looking at the rail services dedicated in Romania to the intermodal transport units, specific features could be also revealed:

1. In domestic traffic, the trains have in composition only wagons loaded with ISO containers and are commissioned by one single client [7, 13, 15];

2. Trains serving more clients could be observed only in international traffic [15];

3. The most important clients of the container trains use their own facilities for loading or unloading the boxes to and from the wagons. In such cases, transhipment and road legs miss. A good example is the main Romania car manufacturer (SC Automobile Dacia SA) [15].

4. In the last decade, the services have been performed between [15]:

- Private sidings to terminals or vice versa;
- Public sidings in a station to terminals or vice versa;
- Terminals to terminals.

5. The services are organised mainly as the shuttles and the Y-shuttle trains (shuttles with antennas). From this perspective, an evident regress regarding the implementation of different production systems could be remarked in the comparison with the container rail transport in 1989 (table no. 3).

4. Competition with other type of services

Taking into account the geographical position and conditions, in Romania, both competition and cooperation between the different transport modes are possible. From this perspective, the container carriage on rails could not be competed by the solutions involving the sea transport. On the other hands, for different traffic relations and customers, alternative solutions to the UCT with rail legs are possible on roads and inland waterways.

Regarding the road transport, statistical data differentiating the pure container road carriage and the road legs related to the UCT solutions are not available. However, as the table no. 4 shows, in the case of the unitised loads, the customers have changed their preferences opting for container rail carriage more than for road services. Roads still remains the main competitor for UCT through the conventional services recording much higher volumes than the total ones related to the railway transport [13].

At the same time, the container river transport on Danube has always been a weak competitor (table no. 4). Its traffic volumes knew a constant increase till 2011 and a sharp decline after this year [13]. In the best year for the inland waterways, three companies provided services on the Danube [15]:

- Mainrom, between Constanta and Giurgiu and serving mainly the Bucharest area;
- Bulgarian River Shipping Company, between Constanta and the Bulgarian ports at the Danube, respectively Belgrade;
- Helogistics Holding GMBH, between Constanta and Budapest [16].

The decline of the container river transport has been generated by the bankruptcy of the Mainrom Company (effect of the financial–economic crisis started in 2008 and competition with land services) and the cancellation of the Helogistics services only after one year from their start, due to the low demand and poor navigation conditions [16].

5. Issues in the UCT development

In comparison with the unimodal solutions (supposing only a simple carriage between the sites of the consignor and the consignee), UCT supposes the following processes and operations:

1. Road carriage on the initial leg, between the consignor and the combined transport terminal;

2. Transhipment between the road vehicles and the railway wagons, done directly or after handling and temporary storage;

3. Rail carriage to another terminal;

4. Transhipment between the railway wagons and the road vehicles, done directly or after handling and temporary storage;

Table no. 3: Production systems used in Romania [7]

Description according to the Intermodal Transport Association (EIA)		Description according to the DIOMIS project commissioned by the International Union of Railways (UIC)		1989	2011	2017	2020
Liner production systems	Shuttle	Direct trains O/D lanes	Shuttle	YES	YES	YES	YES
			Y-shuttle train (train with antennas)	YES	YES	YES	YES
	Triangular service		No DIOMIS equivalent	NO	NO	NO	NO
	Conventional liner service	Less-than-trainload O/D lanes	Liner train	YES	YES	NO	NO
			Group train	YES	NO	NO	NO
	Collection and distribution service		No DIOMIS equivalent	-		-	-
Network production systems	Hub-and-spokes		Turntable production system	YES	NO	NO	NO
	Gateway network		No DIOMIS equivalent	YES	YES	YES	YES
	No EIA equivalent		Gateway production system – HUPAC model	NU	NO	NO	NO
	Shuttle network		Hub-and-spokes - Intercontainer – Interfrigo model	YES	YES	NO	NO
			Mainhub / Megahub production system	NO	NO	NO	NO
No EIA equivalent			Mixed intermodal/conventional production system	DA	NO	NO	NO

Table no.4: Container traffic volumes specific to the roads, railways and inland waterways [13]

Transport mode	Unit of measure	2007	2008	2009	2010	2011	2012	2013	2014	2015	2016	2017	2018	2019	2020
Road	Thousend tonnes	18443	20425	19989	14084	1414	1129	2021	1012	1479	781	784	381	639	563
Rail		3082	2375	1398	1881	2611	2372	2094	2324	2053	1856	2617	2601	2114	2164
IWW		124	128	142	182	146	59	5	9	3	80	60	3	8	2
Road	Million tonnes - km	2253	1747	1262	918	356	337	349	307	484	197	251	125	188	142
Rail		612	465	280	657	919	830	733	813	561	605	818	969	1002	1022
IWW		52	50	44	54	54	26	4	5	2	21	15	2	4	2
Rail	TEU	320923	260936	181238	250781	347064	286415	233409	260706	328126	328850	418049	406683	344212	296830
IWW		9927	11555	11721	12579	16129	6739	1155	3114	1380	6664	4839	1266	1821	1242

5. Road carriage, on the last leg, between the last terminal and the consignee.

Consequently, UCT with rail legs must cope with:

1. Structural issues generated by the specific UCT operations:

a) Possible supplementary durations making the overall transit times higher than in the case of the road transport:
- Transit times related to the initial and final road legs (1 – 3 hours);
- Standstill times in terminals for the intermodal transport units;
- Duration of the handling and transhipment between the rail and road systems in terminals;
- Transit times on railway legs higher than in the case of the road transport, due to longer distances, regulations and infrastructure status;

b) Planning and scheduling of the different operations, as well as the allocations of the necessary resources, generating additional costs;

c) Resources having specific costs:
- Specialised staff (crane operators, etc);
- Specific equipment (reach stackers, rail-mounted gantry cranes, etc);
- Power or the Diesel fuel consumed by the specific equipment;

2. Technical and operational issues in connection with the rail legs of the UCT:

a) Shuntings for composing or decomposing the train sets when the useful length of the tracks in terminals are lower than the train lengths;

b) Shuntings for transfer of wagons or train sets between the terminals and the railway stations serving them;

c) Procedures imposed by the railway safety regulations in the dispatching station, in transit stations or in the arrival station of an intermodal train (technical and commercial checks, brake tests, etc.);

d) Locomotive change if the traction system changes;

e) Administrative procedures imposed by the railway legislation and regulations;

f) Limits imposed by the clearance profile to the size of the assembly formed by every wagon and the containers loaded on it;

g) Possible decisions of the infrastructure managers that could generate delays in the train circulation, affecting in a negative manner the punctuality.

In addition to these factors, in Romania, negative effects occur due to the poor infrastructure status, consequence of the lack of investments for modernization during the last 30 years and of the important delays in overhaul [14]s. Despite the fact that the train lengths and gross tonnages could be considered satisfactory, the rail infrastructure comes with limitations for the technical speed (even on modernized lines), a very low commercial speed and a clearance profile for the intermodal consignments under the requirements of the European regulations and customer expectations. Table no. 5 presents a comparison between the situation on the Romanian rail network to the trains and the standards stipulated in the European

Table no. 5: Railway and intermodal parameters in Romania versus the international standards [7]

Parameter		Unit of measure	Target		Actual value in Romania
			Moderni-sed lines	New lines	
Vehicle loading gauge	AGTC	-	UIC B	UIC C	UIC B
	Intermodal	-	P/C 70 – P/C 400		P/C 45 – P/C 375
Speed		[Km/h]	Minimal 120		85 - 90 Commercial speed 18 km/h
Authorised mass per axle	v≤100 km/h	[t/axle]	22.5	22.5	20,5
	v≤120 km/h		20	20	
Authorised mass per linear meter		[t/m]	8	8	7,2
Minimum useful siding length = maximal train length		[m]	750	750	500-700 m
Train weight		[t]	Minimal 1500 t		1400 - 3000

Agreement on Important International Combined Transport Lines and Related Installations (AGTC) or required by the customers.

Investments have been made and modernization works have been performed only on the different sections of the railway line included on the actual Orient / East - Med Corridor / Pan European Corridor IV. These works are not finished even if, according to forecasts from 2011, they would have had to be finalized for several years [7]. At the same time, they have always embarrassed the rail traffic, coming with limitation of the line transport capacity and producing important delays for the trains and consignments. Therefore, the combined transport operators and the direct customers seem to prefer to organize UCT solutions with road transport on very long distances, to and from the Romanian – Hungarian border and rail legs including only a section of 8 km in Romania and on longer segments abroad.

Regarding the other railway lines composing the Romanian railway network, no modernization work has been performed up to now and they have continuously deteriorated. The main effects are:

- Poor quality of the railway carriage and UCT;
- Unpredictability in delivery of the intermodal transport units;
- Poor utilisation of the resources, due to the longer turnround cycles for wagons and locomotives and the long period in the same service for the staff;
- Increase of the transport costs on the railway legs.

At the same time, despite the fact that 29 land terminals were being operational in 1989, only 4 of these could be used today. In the period after 1989, the continuous and sharp decline of the UCT made difficult decisions for their modernization. Later, the Sectoral Operational Programme TRANSPORT 2007 – 2013 made available some funds for modernisation of terminals, but no project developed.

All these issues have happened simultaneously with huge investments in the modernization of the roads and construction of highways, increasing the attractivity of the road transport.

Moreover, the policy for charging the infrastructure use has proved totally favorable to the road transport. For more than one decade, the standard toll for heavy lorries has been kept at the level of 1210 euro / year and lorry [17]. If a lorry runs 1100000 km / year [18], this value is equivalent with 0.01 euro / km. This Romanian toll is 41 times lower than the toll applied on the Austrian roads (on the highways in Austria, the tolls are even much higher) [19]. At the same time, the normal charge for the rail infrastructure use is higher in Romania than in Austria [19].

A comparison between the tolls and the charges for the rail infrastructure use indicate the following values:

- In the case of a 40’ container carried on roads on 250 km, 0.01 euro/km x 250 km = 2.5 €/ container;
- in the case of a 40’ container, carried alone on a railway wagon included in the composition of a train with 35 wagons loaded everyone with a 40’ container and running on on 250 km:
  - before 2018, [(15 lei / train-km : 4.95 lei/€) x 250 km] : 35 containers / train = 21.64 € / container;
  - Since 2018, 0.3 x 21.64 = 6.5 euro / container.

However, during the last 15 years, private companies invested in the development of the Rail Port Arad, a terminal connected to the border station Curtici, respectively in the development of three smaller intermodal facilities in Ploiesti and in the area of Bucharest.

6. UCT benefits

Benefits will be presented in the case of services between the Bucharest area are and the Port of Constanta. Calculations are done using the Marco Polo methodology, for the external costs [20], respectively the EcoTransIT software tool (compliant with the European Standard EN 16258:2012), for the quantities of pollutants avoided [21]. They are based on the following assumptions:

- For intermodal transport units:
  - Container type: 40’ container (Universal) ;
  - Container gross weight: 28 t / container;
  - Container tare: 4 t / container;
- For the UCT with rail legs:
  - Railway relationship: Titan terminal (served by Bucuresti Sud railway station) – Constanta South Container Terminal (served by Constanta FerryBoat station);
  - Load on wagon: 1 40’ container / wagon;
  - Train composition: 35 wagons / train
  - Distance on the road leg around Bucharest: 50 km;
  - Load on a road vehicle: 1 40’ container / vehicle;
- For pure door-to-door road transport:
  - Distance: 275 km;
  - Load on a road vehicle: 1 40’ container / vehicle.

Consequently:

- Table no. 6 presents the calculations and the savings in external costs generated;
- Table no. 7 depicts the quantities of pollutants avoided when using the UCT.

7. Support measures

A simple check on the website of the European Commission in the area of the state aids reveals a lot of decisions approving subsidies for combined transport in different countries and different periods [22]. Moreover, the financial support has come, many times, with additional measures facilitating the UCT development. From this perspective, Austria seems to be a good example and model. Therefore, table no. 8 presents the possible support measures, comparing the situation in Romania with that one in Austria [7, 23], .

Practically, in Romania, no aid measure has sustain the development of the UCT. This fact happens, even if some legal provisions have allowed such actions. Firstly, the Government Ordinance no. 88 / 1999 stipulate that the government is allowed to subsidize the purchasing of equipment for combined transport (vehicles, handling equipment, intermodal transport units and computer systems). Unfortunately, after the accession of Romania at the European Union, such measures could be implemented only after their approval by the European Commission. Secondly, ‘Council Directive 92/106/EEC of 7 December 1992 on the establishment of common rules for certain types of combined transport of goods between Member States’, as it was amended after the accession of Romania and Bulgaria to the European Union, allows the exemption from the payment of the vehicle taxes if such vehicles would be used in combined transport. Unfortunately, the Romanian Fiscal Code does not contain provisions in this way.

In this context, special comments need the European regulations. Firstly, we should observe that Austria provides an example in which measures supporting the accompanied combined

Table no. 6: Savings in external costs generated by the run of a container train between the Titan terminal and Constanta South Container Terminal (located in the Port of Constanta)

Traffic data		**External costs - road transport**			**External costs – Unaccompanied combined transport**										**Savings**	
					Road leg			**Diesel traction**			**Electrical traction**			**TOTAL**		
Container number	**Net tonnes / container**	**km**	**Unit cost in euro / 1000 tkm**	**Euro / train**	**km**	**Unit cost in euro / 1000 tkm**	**Euro / tren**	**km**	**Unit cost in euro / 1000 tkm**	**Euro / train**	**km**	**Unit cost in euro / 1000 tkm**	**Euro / train**	**Euro / train**	**Euro / train**	**Euro / container**
35	24	275	42.40	9794.40	50	42.4	1780,80	9.27	18.7	145.61	219.7	6.7	1236.70	3163.11	**6631.29**	**189.47**

Table no. 7: Quantities of pollutants avoided by the run of a container train between the Titan terminal and Constanta South Container Terminal

Pollutant			Road	UCT			Quantities of pollutant avoided
				Road leg	Rail leg	Total	
GHG emissions (calculated as CO2 equivalents)	Well-to-tank	tonnes	1	0,31	0,95	1,26	-0,26
	Tank-to-wheel		6	1,29	0,05	1,34	4,66
	Well-to-wheel		7	1,6	1	2,6	4,4
Carbon dioxide (CO2)	Well-to-tank	tonnes	1	0,33	0,85	1,18	-0,18
	Tank-to-wheel		6	1,27	0,05	1,32	4,68
	Well-to-wheel		7	1,6	0,9	2,5	4,5
Sulfur dioxide (SO2)	Well-to-tank	Kg	2,96	0,5916	2,8997	3,4913	-0,5313
	Tank-to-wheel		0,04	0,0084	0,0003	0,0087	0,0313
	Well-to-wheel		3	0,6	2,9	3,5	-0,5
Nitrogen oxides (NOx)	Well-to-tank	Kg	3	0,3	1,2	1,5	1,5
	Tank-to-wheel		16	3,7	0,8	4,5	11,5
	Well-to-wheel		19	4	2	6	13
Non-methane hydrocarbon (NMHC)	Well-to-tank	Kg	1,7	0,44	0,04	0,48	1,22
	Tank-to-wheel		0,3	0,06	0,06	0,12	0,18
	Well-to-wheel		2	0,5	0,1	0,6	1,4
Particulate matter (PM10)	Well-to-tank	Kg	0,1	0,03	0,21	0,24	-0,14
	Tank-to-wheel		0,3	0,06	0,03	0,09	0,21
	Well-to-wheel		0,4	0,09	0,24	0,33	0,07

Table no. 8: Support measures – comparison between the situation in Austria and Romania

<table>
<tr><th>Measure type</th><th colspan="6">Austria [23]</th><th colspan="2">Romania [7]</th></tr>
<tr><td rowspan="4">Financial support</td><td colspan="6" rowspan="2">Aids for terminal construction and modernisation [23]</td><td>Sectoral Operational Programme TRANSPORT 2007 – 2013</td><td>No fund spent, No terminal built or modernised</td></tr>
<tr><td>Operational Programme Great Infrastructure</td><td>No fund spent up to now</td></tr>
<tr><td colspan="6">Aids for purchasing equipment used in combined traffic [23]</td><td colspan="2">NO</td></tr>
<tr><td colspan="6">Aids for feasibility studies[23]</td><td colspan="2">NO</td></tr>
<tr><td colspan="6">Direct subsidies (grants) [23]
<table><tr><th>Traffic type</th><th>Type of intermodal unit</th><th>Gross weight</th><th>30–100 km</th><th>101–250 km</th><th>>250 km</th></tr><tr><td rowspan="8">Domestic</td><td rowspan="2">GC20, WAB 20, WAB 25</td><td>Up to 25 t</td><td>19</td><td>29.80</td><td>36.20</td></tr><tr><td>> 25 t</td><td>12.50</td><td>19.50</td><td>23.70</td></tr><tr><td rowspan="2">GC 30, WAB 30</td><td>Up to 25 t</td><td>26.60</td><td>38.30</td><td>44.40</td></tr><tr><td>> 25 t</td><td>19</td><td>29.50</td><td>37.20</td></tr><tr><td rowspan="2">GC 40, SAN 70, WAB 40</td><td>Up to 25 t</td><td>36.10</td><td>49.80</td><td>55.80</td></tr><tr><td>> 25 t</td><td>22.70</td><td>35.30</td><td>45.10</td></tr><tr><td rowspan="8">Import - export</td><td rowspan="2">GC20, WAB 20, WAB 25</td><td>Up to 25 t</td><td>16.20</td><td>25.80</td><td>31.40</td></tr><tr><td>> 25 t</td><td>10.70</td><td>16.80</td><td>20.50</td></tr><tr><td rowspan="2">GC 30, WAB 30</td><td>Up to 25 t</td><td>22.90</td><td>33.10</td><td>38.40</td></tr><tr><td>> 25 t</td><td>16.30</td><td>25.50</td><td>32.20</td></tr><tr><td rowspan="2">GC 40, SAN 70, WAB 40</td><td>Up to 25 t</td><td>31.10</td><td>43.10</td><td>48.30</td></tr><tr><td>> 25 t</td><td>19.50</td><td>30.40</td><td>39.00</td></tr><tr><td rowspan="8">Transit</td><td rowspan="2">GC20, WAB 20, WAB 25</td><td>Up to 25 t</td><td>9.50</td><td>16.40</td><td>18.70</td></tr><tr><td>> 25 t</td><td>6.50</td><td>10.50</td><td>12.00</td></tr><tr><td rowspan="2">GC 30, WAB 30</td><td>Up to 25 t</td><td>14.30</td><td>21.00</td><td>22.90</td></tr><tr><td>> 25 t</td><td>10.00</td><td>16.00</td><td>19.00</td></tr><tr><td rowspan="2">GC 40, SAN 70, WAB 40</td><td>Up to 25 t</td><td>19.50</td><td>27.40</td><td>28.70</td></tr><tr><td>> 25 t</td><td>11.90</td><td>16.10</td><td>23.00</td></tr></table></td><td colspan="2">NO</td></tr>
<tr><td rowspan="2">Fiscal support</td><td colspan="6">Excempting from the payment of the tax for road vehicles that are used exclusively on the initial and final leg [23]</td><td colspan="2">NO</td></tr>
<tr><td colspan="6">Reimburstment of 15 % from the montly tax for road vehicles, for every transport in Ro-La trains or if it is a part of a combined transport with semitrailers [23]</td><td colspan="2">NO</td></tr>
<tr><td rowspan="2">Bans</td><td colspan="6">Bans for road vehicles overcoming 3,5 t [23]:
• Every Saturday, in the time interval 15:00 – 24:00
• on every Sunday and in holydays in the time interval 00:00 – 22:00
• In the period 6th of July – 31st August,on every Saturday and on the 3rd of October in the time interval 7:00 şi 15:00
• In the period 4th January – 14th of March, on the highways A12 Inner and A13 Brenner
• during the night, for vehicles overcoming 7.5 tonnes, in the time interval 22:00 - 05:00</td><td colspan="2" rowspan="2">Only on a limited number of road sectors and in specific periods from the year</td></tr>
<tr><td colspan="6">• Temporary bans for heavy vehicles on the Brenner corridor, for reasons related to the high air pollution</td></tr>
<tr><td>Other measures</td><td colspan="6">Very high tolls taking into account the pollution standards. Special tolls for certain highways, including during the nights [23]</td><td colspan="2">NO</td></tr>
</table>

	Drastic limitation of the number of transit permits for vehicles registered in countrias that are not members of the European Union [23]	NO

Table no. 9: Comments in connection with the „Community guidelines on State aid for railway undertakings" (2008/C 184/07) [25]

Provisions in the Communication from the Commission „Community guidelines on State aid for railway undertakings" (2008/C 184/07)	**Comments**
"102. As regards aid for rail infrastructure use, the eligible costs are the additional costs for infrastructure use paid by rail transport but not by a more polluting competing transport mode."	• The definition are not clear and could generate different interpretations: – In the restrictive approach, only the charge for the use of the infrastructure; – In the largest approach, the total cost of rail transport. This approach underlies on the fact that the rail transport must comply with rules more severe that in the road system and that it is not possible without specific operations (train circulation according to schedules / trainpaths, commercial and technical checks in the dispatching station, on route and in the destination station, test brakes, etc.). • The Commission practice has been, since 2012, to include in the eligible costs only the infrastructure use charge and the fees related to the terminals.
"103. As regards aid for reducing external costs, the eligible costs are the part of the external costs which rail transport makes it possible to avoid compared with competing transport modes."	• The study of the different decisions adopted by the European Commission in connection with the state intensions to grant aids for different forms of combined transport or railway transport reveal the fact that different methodologies had been used. For example, Austria and France presented calculations based on methodologies developed in these countries, while Italy and Romania employed the Marco Polo methodology. At the same time, no methodology has become a standard. There are only recommendations. Different methodologies could lead to different results. • The definition does not indicate anything in connection with the methodology for calculating the external costs. As different methodologies have been used, with possible different results, there is a risk to generate different interpretations and decisions for similar conditions and situations.
„107. The Commission considers that there is a presumption of necessity and proportionality of the aid when the intensity of the aid stays below the following values: (a)for aid for rail infrastructure use, 30 % of the total cost of rail transport, up to 100 % of the eligible costs; (b)for aid for reducing external costs, 30 % of the total cost of rail transport, up to 50 % of the eligible costs";	• Based on the study of the different decisions adopted by the European Commission in connection with the state intensions to grant aids for different forms of combined transport or railway transport, it could be asserted that these aid intensities could not be sufficient. For instance, in the case of the decisions regarding the single wagonload traffic and the combined transport in Austria, the figures presented in a clear manner in these documents revels higher differences between the cost of the rail-based solutions and road carriage (even if Austrian request complied with the standard intensities). At the same time, the Commission admitted that the total costs specific to the Alpine Rolling Motorway and to the Ro-La trains in Romania could be covered with aids having intensities of more that 30% from the total costs. • The customers will choose the rail or UCT services only these services will bring real benefits to them. Real benefits mainly mean for customers charges / prices lower than the prices specific to the road transport . Other benefits such as shorter transit times could interesting in specific circumstances. From this perspective, the provisions at point 107 do not comply with the customers' behaviour and could not help the development of the UCT.
"108. For aid above these thresholds, Member States must demonstrate the need and proportionality of the measures in question."	• The study of the different decisions adopted by the European Commission depict the fact that this provision prolonged the assessment procedures. • The Romanian experience in connection with the Ro-La trains proves that supplementary explanations are necessary and that arguing could represent real challenges in the relation with the Commission staff.

transport (prohibition of lorries carrying certain type of goods on the Brenner corridor) had to be removed following an infringement procedure started by the European Commission. In the Commission's opinion, the Austrian brake the European rules regarding the liberalisation of the transport and the competition [24]. Secondly, we must remark that the "Community guidelines on State aid for railway undertakings" contain provisions embarrassing the adoption of support measures. Comments on this topic are presented in the table no. 9. All these facts lead to the idea that the European regulation in the area of state aids, liberalisation and competition in the transport sector could create real barriers in the implementation of the policies and strategies aiming to shift the traffic from roads to other less polluting solutions.

8. Conclusions

UCT has a real tradition in Romania. Despite remarkable achievements before 1989, such services are employed at a very low level on the transport market, due to structural, technical and operational issues. Particularly, the poor status of the railway infrastructure and terminals corroborated with the long transit times specific to them have determined the customers to prefer the road transport.

At the same time, the UCT comes with real benefits for the society and iis seen, in the official strategies and programmes, as a solution for shifting the traffic from roads and for sustainable development. It could develop and reach to the performances in the past only through intelligent measures increasing its attractivity.

Based on the Austrian experience, the UCT development is possible through:

- Investments in the railway infrastructure;
- Development and modernisation of the terminals;
- Direct grants (subsidies) for operations;
- Financial support for acquisition of specific equipment (specialised wagons, trucks, containers, swap bodies, computer systems, etc.);
- Fiscal measures, such as excepting from the payment or reducing the different taxes and charges;
- Real changes in the principles and policies regarding the charging for the use of the rail infrastructure, respectively for the use of roads;
- Bans for heavy road vehicles;
- Severe limitations in the number of the transit permits for heavy road vehicles registered in countries that are not members of the European Union;
- Internalization of the external costs.

Last but least, the European legislation in the areas of transport liberalisation, competition and state aids needs important revisions.

9. References

1. ***, Internet website of the Comité Maritime International, https://comitemaritime.org/publications-documents/cmi-yearbook/, visited on the 15th of March 2022;
2. ***, Internet website of the United Nations, https://treaties.un.org/pages/ViewDetails.aspx?src=TREATY&mtdsg_no=XI-E-1&chapter=11&clang=_en, visited on the 15th of March 202;
3. ***,"Terminology on combined transport", Economic Commission for Europe of the United Nations (UN/ECE), Geneva, (2001);
4. ***, "Transportation expressions", Bureau of Transportation Statistics, Washington DC, (1996);
5. ***, Internet website of the European Commission, https://eur-lex.europa.eu/legal-content/EN/TXT/?uri=celex:31992L0106, visited on the 1st of March 2022;
6. ***, Internet website of the International Union of Railways, https://uic.org/freight/combined-transport/, visited on the 1st of March 2022;
7. TĂNĂSUICĂ N.M., "Quo vadis transporturile multimodale", Conference of Railway Rolling Stock, Club Feroviar, Bucharest, 19 May 2021 (2021)**;**
8. SBORA T., TĂNASE G., ŞERBAN D., *" Econmia, organizarea ;I planificarea transporturilor*", Editura Didactică și Pedagogică, Bucharest (1979);
9. ***, „Sectoral Operational Programme Transport 2007 – 2013. Final version". Ministerul Transporturilor şi Infrastructurii, Bucharest (2007).
10. ***, „Mărturii și împliniri 1919-1984", Regionala C.F. București, Bucharest (1984);
11. ***, Internet website of the Organisation for Economic Co-operation and Development (OECD), https://data.oecd.org/transport/container-transport.htm, visited on the 15th of March 2022;
12. FISTUNG D., MIROIU R., POPESCU T., „Transportul feroviar în România, de la apariție și până în prezent", în Noua Enciclopedie a României. Cunoașterea enciclopedică a României – Caiet de lucru 4 – Transporturi, Centrul dde Informare și Documentare Economică, National Economical Research Institute „Costin C. Kiriţescu" belonging to the Romanian Academy, Bucharest, (2019);
13. ***, Internet website of the Eurostat, https://ec.europa.eu/eurostat/web/transport/data/database, visited on the 1st of March 2022;
14. ***, Internet website of the Ministry of transports and Infrastructure in Romania, http://www.mt.gov.ro/web14/strategia-in-transporturi/master-plan-general-transport/documente-master-plan1/613-documente-master-plan-general-de-transport, visited on the 1st of March 2022;
15. TĂNĂSUICĂ N.M., "Transportul unităților de transport intermodal pe căile ferate din România", Conference organized by Club Feroviar with the theme „Tasks of the railway transport in the development of competitive logistical solutions", Constanța, 5 – 6 April 2011 (2011);
16. ***, website of the Helogistics company, . www.helogistics.at/index.php?pid=138lang=2&nid=12, visited on the 9 martie 2011;
17. ***, Internet website of the National Highway and Road Infrastructure (CNAIR), http://www.cnadnr.ro/, visited on the 15th of March 2022;
18. ***, Internet website of theNational Union of Road Hauliers in Romania, https://www.untrr.ro/ro/, visited on the 1st March 2022;
19. ***, Internet website of the ASFINAG, https://www.asfinag.at/, visited on the 1st of March 2022;
20. BRONS M., CHRISTIDIS P. „External cost calculator for Marco Polo freight transport project proposals", European Commission - Joint Research Centre, Louxemburg (2011);
21. ***, Internet websie of the EcoTransIT project, https://www.ecotransit.org/en/emissioncalculator/, visited on the 1st April 2022;
22. ***, Internet website of the Europpean Commission (state aids cases), https://ec.europa.eu/competition/elojade/isef/index.cfm, visited on the 1st of March 2022;
23. ***, Internet website of the Federal Ministry of Climat Action, Energy, Mobility, innovation and Technology of Austria, https://www.bmk.gv.at/public.html, visited on the 15st March 2022;
24. ***, Internet website of the European Commission, https://ec.europa.eu/commission/presscorner/detail/en/CJE_03_50, visited on the 15th of March 2022;
25. ***, Internet website of the European Commission https://eur-lex.europa.eu/legal-content/EN/TXT/?uri=celex%3A52008XC0722%2804%29, visited on the 15st of March 2022.

Comparative Analysis of Methods for Defining the Speed of the Vehicle in Vehicle-Pedestrian Collisions

Zovak Goran[1], Kučinić Tomislav[2], Cindrić Josip[3], Velić Želimir[2]
Centre for Vehicles of Croatia[1]
Faculty of Traffic and Transport Sciences[2] – University of Zagreb, Croatia
Mobile Expert[3] – company for vehicle evaluation
goran.zovak@cvh.hr, tomislav.kucinic@fpz.unizg.hr, josip.cindric@mobile-ekspert.net, zelimir.velic@fpz.unizig.hr

Abstract: *Pedestrians are the most vulnerable road users and traffic accidents involving pedestrians are the most complex type of traffic accident to analyse. The paper describes the kinematics of traffic accidents involving pedestrians and presents statistical data on pedestrian traffic accidents. The main element which needs to be calculated regarding a pedestrian collision is the impact speed of the vehicle involved in the collision. This paper aims to present various models of vehicle impact speed calculation. As a part of this paper, several crash tests were conducted using a pedestrian dummy to determine the reliability of the models. Additionally, the PC-Crash simulation software was also used to calculate the impact speed of the vehicle.*
Keywords*: PEDESTRIAN COLLISION, TRAFFIC ACCIDENTS, CRASH TEST, PC-CRASH, PEDESTRIAN*

1. Introduction

Traffic accidents are one of the leading causes of death in the world. If we analyse the number of fatalities in traffic accidents, 20% of them are pedestrians. As pedestrians are the most vulnerable traffic users, a significant portion of pedestrian accidents results in injury or death.

Determining the impact speed of a vehicle in a vehicle-pedestrian collision is one of the most important elements in the analysis of this type of traffic accident. Accurate and precise speed estimation is crucial for court and administrative procedures, but also for understanding and successfully reconstructing the event. When analysing a traffic accident, it is necessary to determine the exact cause of the accident in order to prevent and take action aimed at reducing the number of pedestrian fatalities.

The paper presents various types of vehicle-pedestrian collisions: frontal collision, lateral striking collision and running over. The paper also analyses several different methods for calculating vehicle impact speed in vehicle-pedestrian collisions. These methods were used in realistic crash tests of pedestrian collisions.

Traffic accident simulation software is used in addition to the classic methods for determining vehicle speed and their relevance is demonstrated in the paper. Contrary to the classic methods, software tools take into consideration all relevant parameters and incorporate modules for the visualisation of conducted simulations, thereby enabling a visual presentation of pedestrian's movements from the moment of impact until stopping.

2. Statistical number of pedestrian casualties

Pedestrians are among the most vulnerable groups of road users. In the period from 2010 to 2018, in the European Union there were 280,000 severely injured pedestrians and 51,000 pedestrian fatalities. The number of pedestrian fatalities has decreased by 2.6% on average each year from 2010 to 2018. In 2019, the EU registered 5,180 pedestrian deaths which account for 21% of fatalities in traffic accidents [1]. In 2019, 297 people were killed in traffic accidents in the Republic of Croatia, with pedestrians accounting for 26.2% of the fatalities. In 2020, there were 237 fatalities, with pedestrians accounting for 16%. [2] On average, 20% of all fatalities in traffic each year are pedestrians.

3. Pedestrian collision

Analysis of traffic accidents involving pedestrians requires a special approach due to the complex dynamics of pedestrian's movements before, at the time of and after the impact. The main classification of vehicle-pedestrian collision is shown in Chart 1 below and is divided into frontal collision, lateral striking and running over. The specified classification of vehicle-pedestrian collisions was defined during the 1970s and remains unchanged to this day. [4]

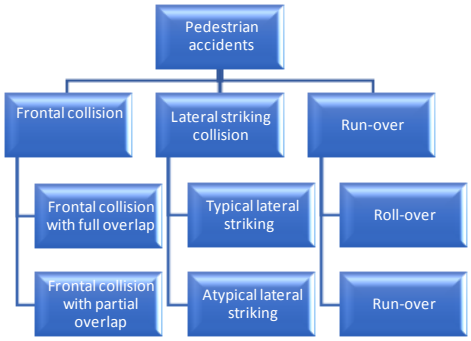


Chart 1 *Pedestrian accidents classification*

Frontal collision is a collision between the front part of the vehicle and the pedestrian's body that fully or partially overlaps with the outline of the vehicle and is sub-divided into full frontal collision and partial frontal collision. A full frontal vehicle-pedestrian collision is a collision where the body of the pedestrian fully overlaps with the outline of the vehicle and at the moment of impact partially or fully takes over the speed of the vehicle. [3].

Partial frontal pedestrian collision is a collision between the front part of the vehicle with the pedestrian where the body partially overlaps with the outline of the front part of the vehicle. Partial frontal exit collision is when the pedestrian is exiting the outline of the front part of the vehicle at the moment of impact. Partial frontal entry collision is when the pedestrian is moving towards the vehicle's trajectory and partially enters the outline of the front part of the vehicle [5].

Lateral striking is a type of accident in which the pedestrian comes into contact with the side of the vehicle. Scientific papers divide lateral striking impact into typical and atypical. In a typical lateral striking, the pedestrian's body comes into contact with the side of the vehicle which is behind the vehicle's front part. In the case of a typical lateral striking, the vector of the pedestrian's centre of gravity is directed forward and sideways, with possible rotation around the central vertical axis. In the atypical lateral striking, the pedestrian comes into contact with the protruding parts of the vehicle or parts that have detached from the vehicle due to contact with the pedestrian, such as side mirrors or rooftop cargo [6].

The last category of vehicle-pedestrian collisions is run-over. Run-over accidents are categorised as run-over and run-over by

wheel [3]. Run-over is described as a traffic accident in which the pedestrian comes into contact with the vehicle's undercarriage. Run-over by the wheel is a run-over in which at least one wheel runs over a part of the pedestrian's body. In addition to the above categories, the run-over can be classified as simple and complex with respect to the position of the pedestrian's body immediately before the run-over. In a simple run-over, the pedestrian was already laying on the road before the collision, which was not caused by the previous contact with the vehicle than ran over the pedestrian. In a complex run-over, the pedestrian is struck down by the vehicle and is then run over as he is laying on the road [3], [5], [7].

4. Methods for calculating vehicle impact speed

In order to determine the cause of a traffic accident involving a pedestrian, the key fact that needs to be determined is the vehicle speed at the moment of contact with the pedestrian. Several different models for determining vehicle speed are used depending on the type of pedestrian collision. Methods for calculating vehicle impact speed can be classified as methods that apply to all types of collisions and methods that apply only to pedestrian accidents. The most commonly used methods that apply to pedestrian collisions and that will be further discussed in this paper are the calculation of speed based on skid marks, pedestrian throw distance, vehicle damage, throw distance of windshield fragments and determination of speed using data from the EDR (Event Data Recorder). A proper scene investigation and analysis of documented traces have to be conducted in order to apply any of the above methods.

4.1. Calculation of vehicle speed based on skid marks

One of the simplest methods for calculating speed in a collision, including collisions involving pedestrians, relies on vehicle skid marks. This method can be applied if the skid marks have been documented and if the exact location of impact is known. In most cases, pedestrian collisions are caused by the driver's delayed reaction. As a result, the vehicle forcibly brakes, leaving skid marks on the pavement. These marks are the result of the force generated by the vehicle's braking system which is through tyres transferred to the pavement. Visible traces must be reliably measured during the scene investigation and marked on the situation plan in order to determine the speed of the vehicle at the start of skid marks. The skid marks alone are not sufficient for determining vehicle speed. In order to accurately estimate the speed of the vehicle at the start of skid marks, it is necessary to determine the deceleration of the vehicle at such braking. To accurately estimate the speed based on resulting skid marks, the vehicle's braking coefficient and the coefficient of friction at the time of the accident in question must be determined. The speed is calculated based on the length of the mark caused by hard braking using the following equation [8]:

$$V = \sqrt{2 \cdot a \cdot S} \qquad [1]$$

where "V" is the speed of the vehicle at the start of skid marks expressed as [m/s], "a" is the deceleration of the vehicle expressed as [m/s^2] and "S" is the length of skid marks expressed as [m]. In order to estimate the speed of the vehicle on impact with the pedestrian based on the documented skid marks, it is essential to accurately and unambiguously determine the location where the vehicle struck the pedestrian. The authors of papers examining the calculation of vehicle speed based on documented skid marks specify that with modern vehicles equipped with the anti-lock braking system (ABS), the hard braking marks are usually visible only when using photo filters or infrared spectroscopy [9]. The model for calculating vehicle speed from skid marks needs to be expanded with the equation for calculating speed loss when two objects collide, taking into account their respective masses. The model for calculating impact speed is [10]:

$$v_n = \frac{m_v + m_p}{m_v} \cdot \sqrt{2 \cdot a \cdot S} \qquad [2]$$

where, in relation to the main equation, the loss of speed is calculated relative to the vehicle mass m_v and the pedestrian's mass m_p.

4.2. Calculation of vehicle speed based on pedestrian throw distance

The method for defining speed based on pedestrian throw distance is based on the premise that we know the location of the primary contact between the vehicle and the pedestrian, i.e. place where the vehicle struck the pedestrian, as well as the final location where the pedestrian stopped after sliding on the road. The total pedestrian throw distance is defined based on the distance between these two locations, and is used to approximate the vehicle's impact speed using the following equation:

$$v_{\mathrm{n}} = 12 \cdot \sqrt{S_{odpj}} \qquad [3]$$

In the above equation, V_n is the car impact speed expressed as [km/h], and S_{odpj} is the pedestrian throw distance expressed as [m]. It must be noted that the above equation can be applied if the following conditions are met: the braking of the vehicle at the moment of impact resulted in deceleration greater than 3 m/s2, the accident was a full frontal pedestrian collision and the results may vary ±10 %. With partial braking or braking resulting in smaller deceleration, the contact between the pedestrian's body and the vehicle is longer, the carrying phase is longer, which may lead to greater deviations in the results, making them unreliable. The specified equation was devised during the tests conducted by the Institute for Motor Vehicles at Technische Universität in Berlin, based on the simulations of collisions with a dummy, 175cm high and weighing 75kg. The tests were also corroborated by the analyses of real-life accidents. [8] Based on the previous tests, Kramer established that the functional dependence between the average throw distance of an adult and the impact speed of a car can be analytically shown using the following quadratic function:

$$S_{odpj} = -0.348 + 0.28 \cdot V_n + 0.062 \cdot V_n^2 \qquad [4]$$

The throw distance of children is generally around 20% greater than the throw distance of adults. If deceleration is taken into account, the equation is as follows:

$$S_{odpj} = 0.0178 \cdot a \cdot V_n + 0.0271 \cdot \frac{V_n^2}{a} \qquad [5]$$

The impact speed can be derived from the following:

$$V_n = \sqrt{0.1 \cdot a^4 + 37 \cdot a \cdot S_{odpj}} - 0.33 \cdot a^2 \pm 3.6 \qquad [6]$$

In order to efficiently apply the above equations in defining vehicle impact speed, the following conditions must be met:

- Full collision with the pedestrian (full frontal collision)
- The collision was caused by a car
- The collision is in the braking path
- Vehicle deceleration is greater than 3 m/s2
- In the case of smaller children that are struck by a vehicle with greater impact speed, the throw distance is shorter

The above equations for calculating vehicle speed based on the pedestrian throw distance are used when the accident is a full frontal collision. In the case of partial overlap with the vehicle, when less than the half of the width of the pedestrian's body is impacted by the front left or right part of the vehicle, the distance

from the location of impact and the pedestrian's final location can be calculated using the following equation:

$$V_n = 10 \cdot S_{odb} \quad [7]$$

4.3. Determining speed based on vehicle damage

The vehicle impact speed can be determined based on the position and the intensity of damage to the vehicle [11]–[14]. Determining the vehicle impact speed based on initial contact of the pedestrian's head on the parts of the vehicle body.

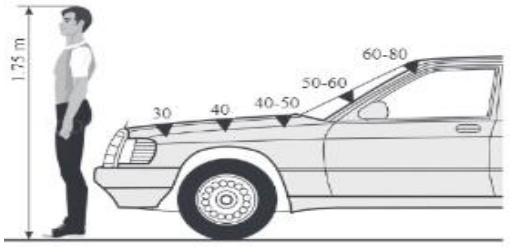


Figure 1 *Determining impact speed based on initial contact of the pedestrian's head on the vehicle* [14]

Figure 1 shows points on the vehicle where the pedestrian's head made initial contact with the vehicle body. The points are marked by the speed in km/h, used to evaluate the impact speed. The damage to the vehicle is compared to the vehicle's earlier image and the initial contact between the pedestrian's head and the vehicle's body is determined. The approximate vehicle speed is determined based on this comparison. The downside to this method of determining vehicle impact speed is that the speed cannot be estimated accurately and unambiguously, but only the minimum and maximum speed at which the collision could have occurred can be determined. The pedestrian's height and position at the moment of collision, as well as the structure of the front part of the vehicle, affect the accurate estimation of the speed of the vehicle.

4.4. Determining speed based on windshield fragment throw distance

An approximation of the car's impact speed in cases when we know both the location of impact and the windshield fragment throw distance S_{odks}, i.e. the distance where approximately 20 glass fragments, 5-10 mm in diameter, are found. The glass dissipation size R is not included in the calculation. With the average windshield height (H=1.2 m), the car impact speed can be estimated relative to the distance S_{odks}, according to the chart shown in Figure 2.

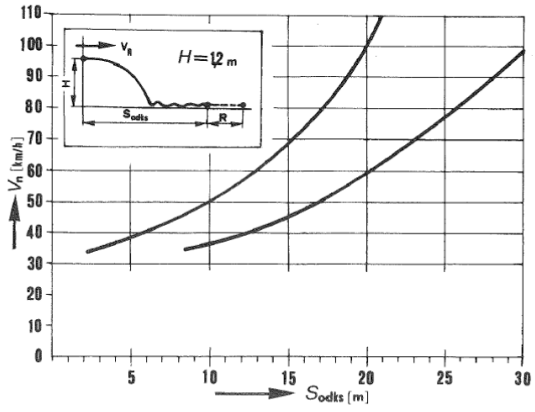


Figure 2 *Impact speed relative to the windshield fragment throw distance* [8]

Thus, according to the above chart:
vn= 40 km/h, from 5.8 to 12.5 m
vn= 60 km/h, from 13 to 20 m
vn= 80 km/h, from 17 to 25 m
vn= 90 km/h, from 19 to 29 m, from the location of impact.

Based on the experimental results, we can estimate what the speed of the car was when the breaking of the windshield or headlight lens occurred. Ten fragments distributed over a surface area of 1 m^2 are considered the point when the glass fragments first fell to the ground.

If we know the distance between the position of the vehicle at the moment when the glass breaking occurred and the position where the glass fragments on the pavement begin, we can estimate the vehicle speed at the moment of glass breaking by using the following equations:

- For a windshield flush with the front part of the vehicle:
$$V_n = 2.75 + 1.65 \cdot S_{odks} \quad [8]$$
- For a windshield behind the vehicle hood:
$$V_n = \sqrt{20 \cdot S_{odks}} \quad [9]$$
- For headlight lenses:
$$V_n = 2 + 1.7 \cdot S_{odks} \quad [10]$$

4.5. Determining the speed using the Event Data Recorder (EDR)

It is not uncommon that the traces at the scene of a pedestrian accident are not properly documented or visible, or that the pedestrian throw distance is unknown. Conducting a quality analysis of vehicle-pedestrian collisions lacking input data for vehicle speed calculation can be difficult. This is one of the many reasons why the event data recorder (EDR) was introduced. The event data recorder is a chip installed in the airbag control module. All new cars are equipped with an airbag control module, but not necessary with an EDR. The tendency is to install an EDR that would record the vehicle dynamics in as many cars as possible [15].

The EDR continuously records the vehicle's dynamics, condition of individual vehicle systems and at sudden changes in speed or deceleration (characteristic of a collision), detects a collision through the sensors installed on the vehicle and records data from approximately 5 seconds before to 250 ms -2 seconds after the collision. The length of recorded data depends on the generation of the EDR, with newer devices recording more data. The data recorded in the EDR during a collision represent new input data that can be applied to calculate the impact speed. In some accidents, the impact speed can be estimated solely based on the data recorded by the EDR as the device records the vehicle speed [10].

In order to conduct an accurate analysis of an accident, the data stored in the EDR cannot be the only source of information but should be incorporated with other data collected during or after the scene investigation, thereby contributing to a more accurate analysis of the accident. [15]

The use of the EDR in vehicle-pedestrian collisions becomes problematic when the vehicle is not equipped with active pedestrian protection systems. As a result of a significant difference between the pedestrian and vehicle masses, there is no significant change in the vehicle speed and consequently, the EDR fails to recognize a collision. In newer vehicles with installed active pedestrian protection systems, the EDR records data that can be used in the pedestrian collision analysis [16]. In less complex cases, the impact speed can be deducted from the EDR data. However, in more complex accidents the EDR data must be loaded into simulation software to accurately determine the vehicle's impact speed.

4.6. Calculating speed using PC-Crash simulation software

The software packages designed for pedestrian accident analysis enable the visualisation of the pedestrian's movement

from the moment of primary contact with the vehicle up until his final ground impact. The option of creating a simulation of the collision and conducting a comparative analysis of vehicle damage and pedestrian injury make such software a highly efficient tool for clarifying the circumstances of such an accident.

In a 3D simulation of the vehicle-pedestrian collision, the vehicle is regarded as a single rigid body, whereas the pedestrian's body is shown using the Multibody simulation model, i.e. as a system of interconnected bodies that provides a realistic view of such an accident and adequately demonstrates pedestrian's movements. The pedestrian is modelled as a system consisting of 16 elements connected by joints, and each of its positions can be defined along the x, y and z axes. This kind of imaging makes it possible to precisely determine the pedestrian's movement or position at the moment of impact [3], [17], [18].

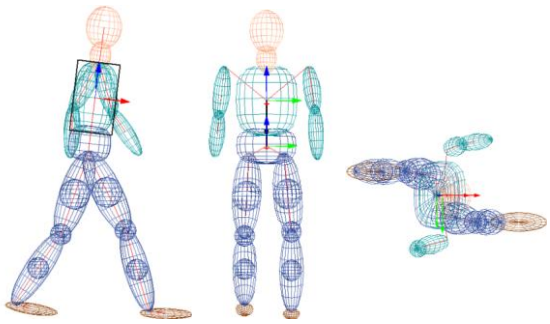


***Figure 3**. Illustration of the Multibody system in PC-Crash*

Figure 3 shows an illustration of a walking multibody in PC-Crash simulation software. Depending on the pedestrian's body type and position at the moment of impact, the simulation software adjusts the multibody to fully mimic the pedestrian involved in the accident.

In order to make a simulation of a vehicle-pedestrian collision, the first thing that needs to be determined is the exact location of the impact. Determining the pedestrian's exact position and speed vector on impact is also essential. PC-Crash will calculate the impact speed based on the throw distance, provided that as much known data as possible is loaded into the software.

5. Comparative analysis of the methods for calculating vehicle impact speed

In order to compare the methods for defining the vehicle impact speed in a vehicle-pedestrian collision described in the previous section, we will use the data obtained from the crash tests conducted by the Institute of Traffic-Technical Expertise of the Faculty of Transport and Traffic Sciences. A total of three crash tests were conducted, simulating a collision with a dummy. The tests included a collision between a Renault Traffic commercial van and a child dummy and two collisions between a Hyundai Accent and an adult dummy at different impact speeds. The crash tests were carried out under test conditions, where all input parameters and test results were known. Regardless of that fact, we will examine the applicability and relevance of individual methods in defining vehicle speed.

Crash test 1 involved a collision between a Renault Traffic commercial van and a child dummy at an impact speed of 54 km/h. The dummy throw distance was 29.20 m. It was rainy and the surface was therefore slippery. The dummy was wearing a baseball hat that after the collision was found 7.30 m away from the impact location. It can be thus concluded that the theory that a hat falls within a radius of 1.0 m from the impact location cannot be applied in this example and that in a real-life collision its application would lead to false conclusions. The collision with the dummy left significant deformations on the vehicle, as shown in Figure 4. Damaged front bumper, dented hood and cracked right headlight and turn signal light are also visible. The intensity and height of the dent on the hood can be linked to the impact of the dummy head. Given the position of the damage and the fact that the vehicle is a commercial van, the impact speed cannot be estimated based on the pedestrian head-on-vehicle contact.

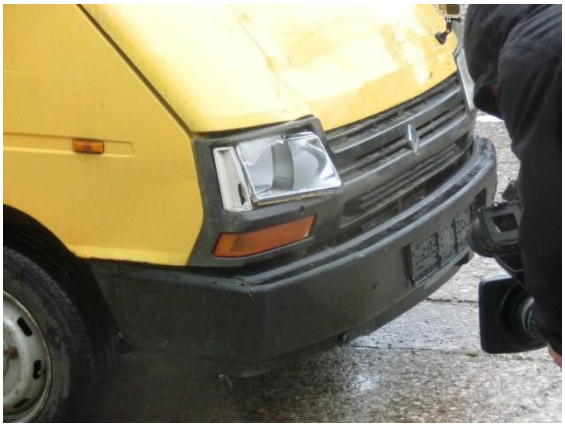


***Figure 4.** Damage to the commercial vehicle*

As there is no record in the investigation report that the vehicle left skid marks, the method for defining vehicle speed based on skid marks cannon be applied, even though the type and condition of the pavement are known and could be used to determine the deceleration of the vehicle.

At the moment of impact with the dummy, the vehicle (a commercial van and not a car) did not brake and the dummy represented a child. Therefore, the conditions for applying the method for calculating speed based on the pedestrian throw distance were not met in this case. The speed calculated using the empirical equation designated [3] in this paper, was 64.84 km/h and using the Kramer's equation 67.3 km/h.

The second crash test simulated a collision between a Hyundai Accent car and an adult dummy at the speed of 64.00 km/h. The dummy throw distance was 30.80 m. It was raining and the surface was therefore slippery. In this case, the dummy was wearing a hat that after the collision landed within 1.0 m from the impact location, and we can therefore conclude that the hat theory applies to this case.



***Figure 5**. Damage to the vehicle in the second crash test*

Figure 5 shows a damaged front bumper, a large dent on the hood and a cracked windshield in the bottom left part whose shape indicates that it was caused by the dummy's head. Based on the damage and the illustration of the speed estimation according to the head-on-vehicle contact shown in Figure 1, we can conclude that the impact speed ranged from 50 to 60 km/h, which indicates some deviation from the actual impact speed of 64 km/h.

Skid marks in the length of 24.10 were documented in the scene investigation report. The average deceleration of 5.4 m/s^2 corresponding to the type and condition of the surface was taken from the literature and applied. The speed calculated based on skid marks was 58.01 km/h, deviating by approximately 6 km/h, which can be explained by the deceleration tolerance, which according to literature can range in this case from 4.0 to 6.8 m/s^2, and the minimum vehicle deceleration resulting from the collision with the dummy. Since the vehicle began braking only after it had struck the dummy, it can be assumed that the speed at the start of the skid marks was also the impact speed. At the moment of impact, the vehicle did not brake. Therefore, the conditions for applying the method for calculating speed based on pedestrian throw distance are also not met in this case, although the calculated speed of 66.6 km/h does not deviate significantly from the actual value. If using Kramer's formula for the calculation, the resulting speed is 69.4 km/h.

The third test was a collision between a Hyundai Accent car and an adult dummy at the speed of 80.00 km/h. The dummy throw distance was 38.00 m and it was also rainy.



Figure 6. *Damage to the vehicle in the third crash test*

Figure 6 shows a cracked front bumper, cracked front right headlight, a dent and damaged paint on the hood, a dent on the right A-pillar and a cracked windshield with penetration into the cabin around the central right part. Judging from its shape, the penetration was caused by the dummy's head. Based on the damage and the illustration of the speed estimation according to the head-on-vehicle contact shown in Figure, we can conclude that the impact speed ranged from 60 to 70 km/h, which indicates a deviation from the actual impact speed of 80 km/h. For the impact speed of 80 km/h, the head-on-vehicle point of contact would be on the very top of the windshield. There is no record of skid marks in the investigation report; therefore, the method for calculating speed based on skid marks cannot be applied. At the moment of impact with the dummy, the vehicle did not brake, so the conditions for applying the method for calculating speed based on the empirical equation for pedestrian throw distance were also not met in this case, although the results do not deviate significantly from the actual value. The vehicle speed calculated using the empirical equation was 74.00 km/h and using the Kramer's equation 77.99 km/h.

Conducted calculations show that the methods relevant to these examples are the methods for defining speed based on skid marks, based on pedestrian throw distance and Kramer's equation. Other methods are not relevant since there was no record in the investigation report of the accident traces that could be applied in these methods, or the conditions for the application of such traces in a specific case were not met. Table 1 shows all calculated results expressed as km/h.

	Test 1	*Test 2*	*Test 3*
Skid marks	-----	*58.07*	-----
Pedestrian throw distance	*64.84*	*66.60*	*74.00*
Kramer	*67.30*	*69.40*	*77.99*
Based on head-on-vehicle contact	-----	*50-60*	*60-70*
Speed calculated in PC-Crash	*54.50*	*64.90*	*81.10*
Actual impact speed	*54.00*	*64.00*	*80.00*

Table 1. *Results of impact speed calculations using different methods*

As can be seen in Table 1, none of the relevant methods for defining the speed of the vehicle provided satisfactory results in the first example, i.e. for the commercial van, except the simulation conducted using PC-Crash software. There was no record of skid marks left by the commercial van in the scene investigation report, thus this method could not be applied. Speed calculations based on pedestrian throw distance and Kramer's formula considerably deviate from the actual impact speed. Since the vehicle in question was a commercial van, the pedestrian head-to-vehicle contact chart was also excluded as a method for determining the impact speed.

In the second example, the greatest imprecision with regard to the impact speed of the vehicle is evident in the data obtained based on the head-to-vehicle contact (50-60 km/h). In this example, the speed calculated based on pedestrian throw distance deviates the least from the actual impact speed if we take into account just the conventional methods. The most accurate speed calculation was again obtained by using the PC-Crash simulation tool.

In the third example where the actual impact speed was 80.00 km/h, the method based on skid marks again cannot be applied, since no skid marks were documented. The impact speed determined based on head-to-vehicle contact deviates considerably from the actual speed, i.e. it is 10-20 km/h slower. The most relevant conventional method applicable in this example is the method for calculating speed using Kramer's formula, where the calculated speed deviates from the actual speed by 2.01 km/h. An even more accurate result was obtained using PC-Crash simulation software.

As the above results show, the vehicle impact speed in a vehicle-pedestrian collision can be most accurately determined by using simulation software. PC-Crash simulation program uses established mathematical and empirical methods for calculating vehicle impact speed. It is thus evident that it provides the most accurate result.

6. Conclusion

Traffic accidents are one of the leading causes of death in the world. Each year, 1,240,000 road users on average die in traffic, of which 270,000 (22%) are pedestrians.

According to the conducted research presented in this paper, we can conclude that the traffic accidents involving pedestrians are the most complex type of traffic accident to analyse. The type of pedestrian collision dictates which method will be selected for calculating vehicle speed and the most accurate speed calculation will be obtained if several different calculation models are used. As can be seen in the paper, the most accurate calculation of impact speed was obtained by using PC-Crash simulation software.

An issue that became evident during the writing of this paper is that the models that are still used in the analysis of pedestrian accidents are outdated. These models were developed some fifty years ago which, given the technological advances in infrastructure and vehicles, reduces the relevance of the calculations. The models that correlate the vehicle speed and the pedestrian throw distance were empirically derived from tests and real-life traffic accidents. From today's standpoint, the equipment used to test and validate these models is inaccurate and technologically obsolete. The issue in defining models based on tests lies in the fact that the collision with the pedestrian is conducted on a test dummy that is supposed to mimic the human body and its movements in the collision. The joints of the test dummies used did not have the flexibility of human joints. Additionally, these dummies resemble the human body only in terms of mass and height, and no other properties mimic the actual pedestrian's movements on impact with the vehicle.

Yet another issue is the fact that the vehicles that were used in defining the models are today considered old-timers. As a result, the pedestrian throw distances were significantly different due to the front profiles of the vehicles and the materials used to manufacture the front parts of the vehicle.

To calculate the impact speed of the vehicle as precisely as possible, simulation tools have to be used as they ensure the most accurate calculation of vehicle speed. A downside to the simulation tools is their complexity and the extensive knowledge that their application requires.

7. References

[1] European Transport Safety Council, "How safe is walking and cycling in Europe?," no. 38, p. 1 file, 2020, [Online]. Available: www.e.eu/pin

[2] T. S. Pokazatelja, "Statistički p r e g l e d," *Ministarstvo unutarnjih poslova*, 2021.

[3] H. Burg and A. Moser, *Handbook of Accident Reconstruction*, First edit. Linz, 2013.

[4] G. Sturtz, "Kinematic of real pedestrian and two-wheel rider accidents and special aspect of the pedestrian accident," Jul. 1976.

[5] Ernst Tomasch, "Accident Reconstruction Guidelines Part of Deliverable D4," 2003.

[6] Evu, "Burg - Experience with Data Readout from the Event Data Recorder (EDR).pdf," 2016.

[7] J.-P. Depriester, C. Perrin, T. Serre, and S. Chalandon, "COMPARISON OF SEVERAL METHODS FOR REAL PEDESTRIAN ACCIDENT RECONSTRUCTION," 2005, p. 14.

[8] F. Rotim and Z. Peran, *Forenzika prometnih nesreća*, Svezak 1. Zagreb: Hrvatsko znanstveno društvo za promet, 2013.

[9] Ł. Gosławski *et al.*, "ANALYSIS OF BRAKING MARKS LEFT BY VEHICLES EQUIPPED WITH ABS WITH IR SPECTROSCOPY," 2019. doi: https://doi.org/10.14669/AM.VOL84.ART3.

[10] K. Pinter and Z. Szalay, "Comparison of data required for accident reconstruction based on crash test," in *Lecture Notes in Mechanical Engineering*, vol. 0, no. 9783319756769, Pleiades Publishing, 2018, pp. 476–486. doi: 10.1007/978-3-319-75677-6_41.

[11] J. Xu, Y. Li, G. Lu, and W. Zhou, "Reconstruction model of vehicle impact speed in pedestrian-vehicle accident," *International Journal of Impact Engineering*, vol. 36, no. 6, pp. 783–788, Jun. 2009, doi: 10.1016/j.ijimpeng.2008.11.008.

[12] D. Vangi, F. Begani, R. Toldo, and A. Fusiello, "Photogrammetry 3D vehicle reconstruction for energy loss evaluation," 2014.

[13] G. Sturtz, E. G. Suren, L. Gotzen, S. Behrens, and K. Richter, "Biomechanics of Real Child Pedestrian Accidents," Feb. 1976. doi: 10.4271/760814.

[14] N. Saulić, Z. Papić, and Z. Ovcin, "View of Pedestrian Throw Distance Prediction from Vehicle Damage Intensity," *Promet - Traffic&Transportation*, vol. 32, 2020.

[15] T. Aberle, "EDR for motorcycles, advantageous in terms of cost," 2012.

[16] J. de Bruyne and C. Vanleenhove, "The Rise of Self-Driving Cars: Is the Private International Law Framework for non-contractual obligations posing a bump in the road?," *IALS Student Law Review*, vol. 5, no. 1, pp. 14–26, 2018, doi: 10.14296/islr.v5i1.2819.

[17] A. Moser, H. Hoschopf, H. Steffan, and G. Kasanicky, "Validation of the PC-Crash Pedestrian Model," Mar. 2000. doi: 10.4271/2000-01-0847.

[18] S. Richardson *et al.*, "Pedestrian Throw Distance Impact Speed Contour Plots Using PC-Crash," in *SAE Technical Papers*, Apr. 2015, vol. 2015-April, no. April. doi: 10.4271/2015-01-1418.

Using algorithms to solve problems in urban transport optimization Case study: Prishtina

Sallauka Astrit*, LikajRame, Gashi Blendi
Faculty of Mechanical Engineering, University of Prishtina, BreguiDiellit, p.n. 10000 Prishtina, Kosovo
* Corresponding author e-mail: astrit.sallauka@gmail.com

Abstract**:** *The scope of this paper is using Dijkstra algorithm in Python to get the urban transport optimization one step further, by finding the best route, besides analysing the shortest one. Studying urban transport routes has been first analysed by Dijkstra algorithm taking into consideration two parameters, the number of stations and distances between stations. After this, the code of Dijkstra algorithm has been implemented in Python, adding the demand for travelling in each station.*
KEYWORDS: URBAN *TRANSPORT ANALYSIS, LINE SHORT PATH ANALYSIS, LINE OPTIMIZATION MODEL, PYTHON, DIJKSTRA*

1. Introduction

Optimizing urban transport routes is a significant problem in planning the network of transport routes. In general, users of the urban transport face problems such as the long-time of waiting in the station, bus arrival schedule inaccuracies, incompatibility between bus routes and passenger's trails, and the insufficient capacity. These problems have generally led to the use of private transport which in return creates non-favourable effect by increasing the consumption of fuels, environment pollution, traffic jams, occupation of parking public spaces, and number of accidents. An optimization of bus network would gradually lead to a decreasing of the above-mentioned phenomena, as it would make the selection of the most reasonable routes according to the frequency of use by citizens.

Considering that each transport problem should be seen as a whole, no transport model can be applied in another situation. In this paper we have initially analysed the existing route, and the coverage of the respective city area; then we performed finding the shortest routes from the departure bus stop to the arrival one, in order to decrease the bus itinerary; then we analysed the walking distances from the surrounding residences to the closest bus stop. [1]

Geographic Information System - GIS has been employed to conduct the analysis of all these steps. For the finding of the shortest distances, we have calculated the distances between stops, which have been saved in the database and have later used in the Dijkstra algorithm. This algorithm allows the finding of the shortest distances in the urban transport routes from one departure stop to another destination stop in the entire city map. Except calculating the shortest route, using Dijkstra algorithm, and referring to the studied map, we have calculated also the most optimal route based on the frequency of travellers in each bus stop. This has been done by implementing Dijkstra on Python.

2. Data collection

For a better and more accurate analysis of the urban transport modelling in the city of Prishtina, seventy-seven bus stops of the urban transport network have been used in the analysis. Their coordinates can be found in the following table and their location can easily be verified if they are put in any of the online map services or GIS systems.

The following figure shows the above-mentioned locations extracted from the Open Street Map - OSM application. The dots represent the locations of the bus stops. They are also attached the respective coordinates which serve us for further analysis.

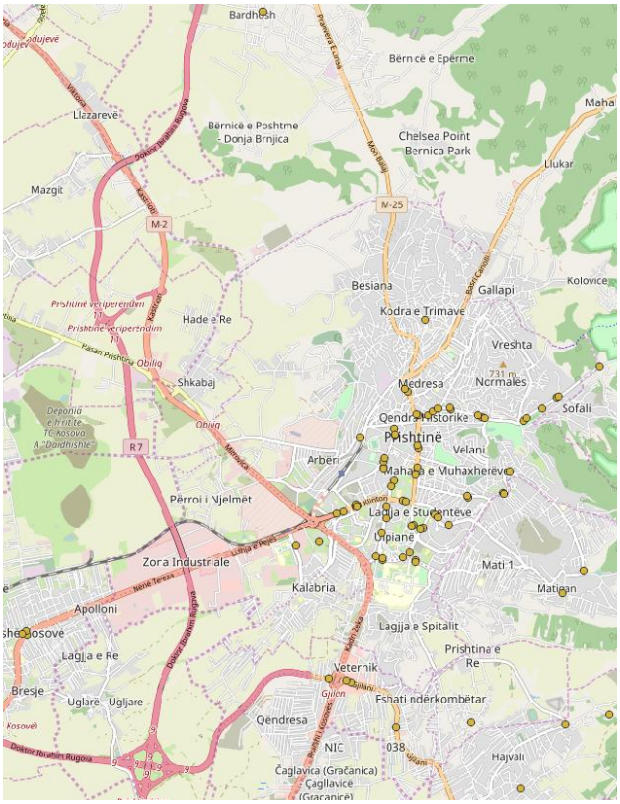


Figure 1. Urban transport bus stops extracted from Open Street Map

Table 1. Some of the bus stops coordinate

Bus stops		
longitude	latitude	osm_id
21.1586457	42.6596867	4870504746
21.0933585	42.6371888	3502701121
21.1999393	42.6263928	4987259828
21.1746672	42.6253341	5032771323
21.136493	42.7210963	5040838124
21.1526946	42.6306523	5320470421
21.1645186	42.6472796	4321932197
21.151867	42.63093	5320470521
21.1634699	42.6483035	4321932198
21.1914291	42.6427801	5377640038
21.198251	42.6733365	4331977901
21.1953934	42.6458422	5377640040
21.1621979	42.647671	4342371169
21.1650763	42.6623588	4434318892
21.1649044	42.6626514	4434319590
21.1648593	42.6596793	4434324490
21.1740565	42.655638	4434327690

Table 1 is compound of the coordinates for each bus stop, which are defined by osm_id using OSM for some of the stops, so the algorithm can easily identify each bus stop for further calculations.

Figure 2 gives a description of the data saving process in Structured Query Language, which will serve to calculate the shortest route using Python.

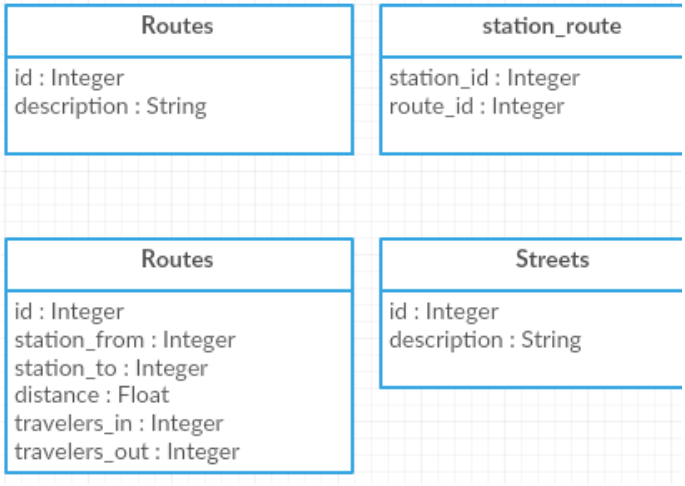


Figure 2. *Data saving process*

In order to effectively calculate the shortest routes from different locations in the network, we have created the matrix of distances between all stops in Prishtina route network. These distances will be used as parameters in function of optimizing existing routes and creating new routes accordingly.

Table 2. *The matrix of distances between bus stops*

osm_input_id	osm_target_id	distance(m)
4870504746	3502701121	5908.427
4870504746	4987259828	5014.722
4870504746	5032771323	4035.962
4870504746	5040838124	7059.213
4870504746	5320470421	3262.026
4870504746	4321932197	1459.963
4870504746	5320470521	3242.472
4870504746	4321932198	1324.942
4870504746	5377640038	3279.321
4870504746	4331977901	3583.478

The analysis for findings the shortest distance and going by as few as possible stops, has resulted very effective. This analysis considers as parameters the distances between bus stops and through Dijkstra algorithm can be found the shortest distance. [2] In the following table are indicated bus stops named alphabetically from A to O and the distances between them. Only fifteen bus stops have been taken as samples to visualize Dijkstra algorithm in finding the shortest distance between stations. [3]

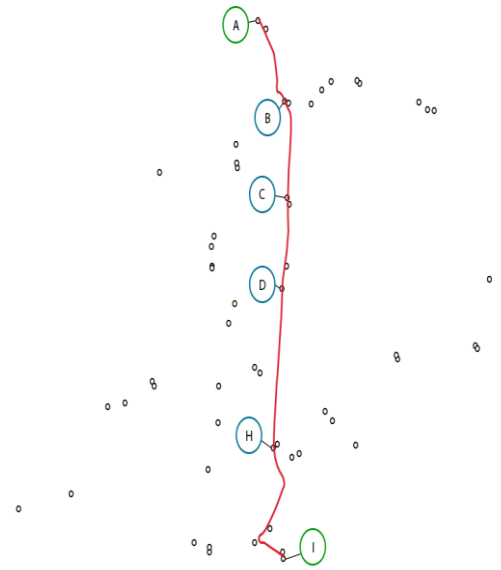


Figure 3. Visualising the shortest route found by Dijkstra

Table 3. Bus stop distances

Start	End	Distance (m)
A*	B	454
B	C	479
C	D	441
D	E	566
E	F	718
F	G	327
D	H	774
H	***I****	714
H	J	552
J	L	327
L	M	658
M	N	713
N	O	322
H	K	369

3. Implementation and addressing the problem

Number of passengers or the factor of using the existing routes has been considered for optimizing, changing, or adding new routes. Number of passengers has been calculated for each bus stop, where N_t represents the total number of passengers per route, and N_i represents the number of passengers per respective bus stop:

$$N_t = \sum_{i=1}^{11} N_i \qquad (1)$$

Table 4. *Number of passengers of the route "Linja 1"*

Linja 1 - AB	
Bus stop	*Number of passengers*
1	10
2	13
3	14
4	15
5	16
6	24
7	24
8	24

Linja 1 - BA	
Bus stop	*Number of passengers*
1	3
2	20
3	30
4	39
5	39
6	36
7	36
8	35

9	27
10	24
11	0

9	32
10	24
11	0

According to the table of results, in the first route direction there are forty-seven passengers in the network, while on the return route, there are sixty-five passengers. Nevertheless, not all the bus stops have had the same number of passengers. The following table shows that some of the stops are much less frequented.

Table 5. *Number of passengers entering and exiting the network of urban transport*

Linja 1 - AB			**Linja 1 - BA**		
Bus stop	*Number of passengers*		*Bus stop*	*Number of passengers*	
	Enter	*Exit*		*Enter*	*Exit*
1	10	0	1	3	0
2	6	3	2	18	1
3	1	0	3	14	4
4	2	1	4	12	3
5	3	2	5	3	3
6	9	1	6	10	13
7	4	4	7	0	0
8	3	3	8	2	3
9	5	2	9	1	4
10	4	7	10	2	10
11	0	24	11	0	24

To optimize this route, in finding the shortest distance between two points, we can consider as potential parameters also the number of passengers per bus stop. This can be used as a weight which takes absolute value based on the differences between the number of passengers entering and those exiting the network of the urban transport. [4]

In this way, to conduct the calculation of passengers served in one station, we can calculate the number of passengers who enter the network I_i and the number of passengers who exit the networkO_i:

$$S = \sum_{i=1}^{n} I_i + O_i \qquad (2)$$

Table 6. *Number of served passengers per bus stop*

Linja 1 - AB	
Bus stop	*Number of passengers*
1	10
2	9
3	1
4	3
5	5
6	10
7	8
8	6
9	7
10	11
11	24

Linja 1 - BA	
Bus stop	*Number of passengers*
1	3
2	19
3	18
4	15
5	6
6	23
7	0
8	5
9	5
10	12
11	24

Table 7. *Normalized values of distances and number of passengers per bus stop*

osm_id_prej	osm_id_deri	Distance (m)	Normalized distance	Passengers number	Normalized passengers number	Selection ratio
4436375390	1458787667	454	0.657223796	13	0.705882353	0.681553074
1458787667	4434319590	479	0.621813031	2	0.058823529	0.34031828
4434319590	4434334789	441	0.675637394	5	0.235294118	0.455465756
4434334789	4436261491	566	0.498583569	8	0.411764706	0.455174138
4436261491	4436381092	718	0.283286119	10	0.529411765	0.406348942
4436292791	1458787612	788	0.184135977	5	0.235294118	0.209715047
4436381092	4436431589	327	0.837110482	3	0.117647059	0.47737877
4434334789	2070906981	774	0.203966006	4	0.176470588	0.190218297
2070906981	4461986290	714	0.288951841	9	0.470588235	0.379770038
2070906981	4342371169	552	0.518413598	12	0.647058824	0.582736211
4342371169	4469391589	327	0.837110482	8	0.411764706	0.624437594
4469391589	4436274090	658	0.368271955	6	0.294117647	0.331194801
4436274090	4436292791	713	0.290368272	12	0.647058824	0.468713548
4436292791	1458787612	322	0.844192635	2	0.058823529	0.451508082
2070906981	4434334790	369	0.777620397	3	0.117647059	0.447633728

According to table 6, the values for the number of passengers and the values for the distances between stations are different; therefore, it is necessary to normalize the values. This normalization of values is done for the values between 0 and 1:

$$X_{new} = \frac{X - X_{min}}{X_{max} - X_{min}} \qquad (3)$$

Due to the high values that large distances create after the normalization; it is necessary to minus for 1 point the value extracted through the formula (3). After the values normalization for the number of passengers and the distance between stations, we get values as shown in the following table. During the creation of the route, the chance of selecting the next stop can be done through calculating the average of normalized values of the distance and the number of passengers, where M_i represents the value of the distances and N_i represents the value of the number of passengers:

$$S_i = \frac{M_i + N_i}{2} \quad (4)$$

For assessing the route performance, we can calculate the average value of each selected stop:

$$S = \frac{1}{n}\sum_{i=1}^{n} \frac{M_i + N_i}{2} \quad (5)$$

According to the analysed data, we take the minimal value one passenger served in one bus stop and maximal value of twenty-four passengers served in one bus stop. Whereas, as the shortest distance we have selected the value of 212 and for the longest, we have selected the value of 918. These values can be changed depending on the data to be extracted in different given times and locations. [5]

In the above reviewed case where the solution is given as **A – B – C – D – H – I**through Dijkstra algorithm, we can see that some of the selected bus stops had smaller value of selection, but that appear to be the shortest and most optimal route.

The following table shows how the matrix of distances between bus stops can be formed according to the above-described method.

Table 8. *The selection weight between bus stops*

osm_id_prej	osm_id_deri	Shkalla e zgjedhjes
4436375390	1458787667	**0.681553074**
1458787667	4434319590	**0.34031828**
4434319590	4434334789	**0.455465756**
4434334789	4436261491	**0.455174138**
4436261491	4436381092	**0.406348942**
4436292791	1458787612	**0.209715047**
4436381092	4436431589	**0.47737877**
4434334789	2070906981	**0.190218297**
2070906981	4461986290	**0.379770038**
2070906981	4342371169	**0.582736211**
4342371169	4469391589	**0.624437594**
4469391589	4436274090	**0.331194801**
4436274090	4436292791	**0.468713548**
4436292791	1458787612	**0.451508082**
2070906981	4434334790	**0.447633728**

4. Results of implementing Dijkstra on Python

The built code for solving this problem has been implemented on Python. To execute the code, it is necessary to write the name of the Dijkstra function, which accepts two parameters, the origin and the destination, and the created graph through the matrix of distances.

After executing the code, where as a parameter two stations are given, S_{origin}='4436375390' as a start and $S_{destination}$='4461986290' as the end of the route, we can see that the most optimal route calculated by Dijkstra is:

```
1. ['4436375390', '1458787667', '4434319590', '4434334789', '
   2070906981', '4461986290']
```

5. Conclusion

The paper has been conducted analysing and studying the movements of citizens and the use of the urban transport routes, extracting statistics. From the in-field work we have analysed the route with the highest frequency of use and formed the model for urban transport routes optimization in Prishtina. Applying this model would facilitate the traffic situation and would create premises for a better use of urban transport. This would also affect the increase of route rationale for both the costs and itinerary. The code of Dijkstra algorithm implemented on Python was built to be applicable in any given transport problem, using several parameters of the route, the distance between bus stops and the demand of passengers per each bus stop. This algorithm gives us the opportunity to build optimal solutions for the routes.

6. References

[1] C. f. U. T. Research, “Best Practices in Transit Service Planning”, Florida Department of Transportation, Florida, 2009.

[2] Ravi N., Sireesha V., (2010), "Using Modified Dijkstra’s Algorithm for Critical Path Method in a Project Network", International Journal of Computational and Applied Mathematics, Volume 5 number 2 pp. 217-225.

[3] H. L. H. AL-TAMEEMI, «USING DIJKSTRA ALGORITHM IN CALCULATING ALTERNATIVE SHORTEST PATHS FOR PUBLIC TRANSPORTATION WITH TRANSFERS AND WALKING 2014 FAQE 17-20».

[4] RAMË LIKAJ, (KOAUTORS: A.SHALA, M. MEHMETAJ, P. HYSENI, XH. BAJRAMI), APPLICATION OF GRAPH THEORY TO FIND OPTIMAL PATHS FOR THE TRANSPORTATION PROBLEM, ORIGINAL RESEARCH ARTICLE, JOURNAL: IFAC PROCEEDINGS, VOLUMES, VOLUME 46, ISSUE 8, 2013, PAGES 235-240, INDEXED ON ACADEMIC DATABASES SCOPUS.

[5] A. Sallauka, X. Bajrami, R. Likajdhe B. Gashi, «APPLICATION GENETICS ALGORITHM FOR FINDING SHORTEST PATH IN SEVEN CITIES,»*International Journal of Civil Engineering & Technology (IJCIET)*, vëll. i 9, nr. 4, pp. 1516-1526, 2018.

Energy analysis of two-cylinder steam turbine from nuclear power plant

Mrzljak Vedran[1], Prpić-Oršić Jasna[1], Baressi Šegota Sandi[1], Medica-Viola Vedran[1]
[1]Faculty of Engineering, University of Rijeka, Vukovarska 58, 51000 Rijeka, Croatia
E-mail: vedran.mrzljak@riteh.hr, jasna.prpic-orsic@riteh.hr, sbaressisegota@riteh.hr, vmedica@riteh.hr

Abstract: *In this paper, two-cylinder steam turbine, which operates in nuclear power plant is analyzed from the energy viewpoint. Along with the whole turbine, energy analysis is performed for each turbine cylinder (High Pressure Cylinder – HPC and Low Pressure Cylinder – LPC). A comparison of both cylinders shows that the dominant mechanical power producer is LPC, which also has much higher energy loss and much lower energy efficiency. Therefore, any potential improvement of this steam turbine should be based dominantly on the LPC, which also has a dominant influence on energy analysis parameters of the whole observed turbine. The whole turbine produces real (polytropic) mechanical power equal to 1247.69 MW, has energy loss equal to 352.70 MW and energy efficiency equal to 77.96%. According to obtained energy efficiency value it can be concluded that the whole analyzed steam turbine is comparable to main marine propulsion steam turbines, while its energy efficiency is much lower in comparison to steam turbines from conventional steam power plants which operates by using superheated steam.*

KEYWORDS: TWO-CYLINDER STEAM TURBINE, NUCLEAR POWER PLANT, ENERGY LOSSES, ENERGY EFFICIENCIES

1. Introduction

The highest percentage of electrical power worldwide is produced by using various steam turbines. Steam turbines today can be found not only in many different power plants [1-5] but also it can be used in ship steam propulsion systems [6-8], for simultaneous production of heat and electrical power [9, 10], and for various other purposes.

Nuclear power plants also use steam turbines for the electrical power production. The specificity of such steam turbines can be found in a fact that they dominantly operate with wet steam, while the most steam turbines from other power plants dominantly operate by using superheated steam [11]. The reason of wet steam usage in nuclear power plants is steam temperature and pressure, which are much lower in comparison to conventional steam power plants and which are limited according to nuclear reactor specifications. On the other side, nuclear reactors produced high steam mass flow rate, much higher than is produced in conventional steam power plants [12, 13]. Due to condensate droplets, wet steam brings several additional losses in the turbine inner process which did not occur when turbine operates by using superheated steam.

In this paper is performed energy analysis of a steam turbine from nuclear power plant. It is detected which cylinder has the dominant influence of the whole turbine energy analysis parameters. Also, it is detected cylinder which should be a baseline for further improvement of the analyzed steam turbine and its process. According to obtained energy analysis parameters, the whole observed steam turbine is compared with other steam turbines from conventional and marine steam power plants.

2. Scheme and operating characteristics of two-cylinder steam turbine from nuclear power plant

The scheme of the analyzed steam turbine, which operates in nuclear power plant is presented in Fig. 1. Steam turbine consists of two cylinders: High Pressure Cylinder (HPC) and Low Pressure Cylinder (LPC). Both cylinders are connected to the same shaft which drives an Electrical Generator (EG).

Steam produced in the nuclear reactor cycle is delivered from steam generators to the HPC. HPC has one steam extraction through which a certain steam mass flow rate is delivered to high pressure feed water heating system. Remaining steam mass flow rate, after expansion in HPC, is sent to reheating system.

Reheating process in the analyzed nuclear power plant is performed in a standard configuration – this process consists of moisture separation firstly and then steam reheating. In a moisture separation process, obtained condensate from wet steam is delivered to high pressure feed water heating system, therefore the steam mass flow rate at the HPC outlet (operating point 3, Fig. 1) will be higher than the steam mass flow rate at the LPC inlet (operating point 4, Fig. 1). Steam reheating is performed with a certain amount of additional steam of the highest temperature and pressure in the process, taken directly from steam generators. So, reheater in nuclear power plant is steam-steam heat exchanger [14]. Moisture separation and steam reheating processes occur between HPC and LPC.

LPC of the analyzed turbine has four steam extractions. Steam mass flow rate extracted in each LPC extraction is delivered to low pressure condensate heating system. After expansion in the LPC, remaining steam mass flow rate is delivered to the main condenser for condensation [15]. It should be highlighted that in this analysis all additional losses related to a steam turbine and both of its cylinders (steam mass flow rate leakage through gland seals, losses in power transmission, heat losses, etc. [16, 17]) are neglected.

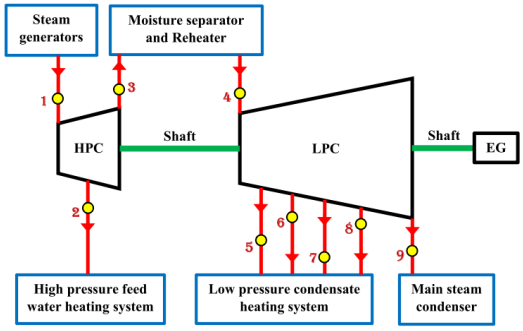


Fig. 1. *Scheme of the two-cylinder steam turbine from nuclear power plant and operating points necessary for the energy analysis*

3. Steam operating parameters required for the analysis and h-s diagram of the analyzed turbine

Steam operating parameters (pressure, temperature, mass flow rate and quality) in each operating point from Fig. 1 are found in [18] and presented in Table 1.

Table 1. *Steam operating parameters of the observed turbine for real (polytropic) expansion*

O.P.*	Temperature (°C)	Pressure (bar)	Specific enthalpy (kJ/kg)	Specific entropy (kJ/kg·K)	Quality	Mass flow rate (kg/s)
1	282.10	66.220	2771.4	5.832	0.9961	1943.04
2	219.22	22.850	2602.2	5.886	0.8933	161.49
3	186.62	11.650	2519.2	5.959	0.8676	1781.55
4	237.70	11.080	2911.3	6.820	Superheated	1456.71
5	164.30	4.960	2777.6	6.893	Superheated	66.96
6	125.77	2.378	2654.5	6.920	0.9727	83.36
7	96.41	0.891	2499.9	6.938	0.9250	116.34
8	55.05	0.158	2386.9	7.339	0.9100	69.92
9	40.61	0.0763	2325.5	7.450	0.8964	1120.13

* O.P. = Operating Point (according to Fig. 1)

Steam quality equal to 1 denotes dry saturated steam, while steam quality equal to 0 denotes condensate. Steam specific enthalpy and steam specific entropy in each operating point from Fig. 1 are also presented in Table 1 – they are calculated from known steam pressure, temperature and quality by using NIST REFPROP 9.0 software [19]. All the operating parameters presented in Table 1 are related to real (polytropic) steam expansion process.

Ideal (isentropic) steam expansion process of any cylinder (valid for any cylinder of any turbine, not only for the observed turbine) is the process which begins at the same operating point as the real (polytropic) expansion process. In ideal steam expansion process in each cylinder, steam expand between the same pressures with identical steam mass flow rates as in the real process, but assuming always the same steam specific entropy as at the beginning of the expansion. Therefore, steam operating parameters for the ideal (isentropic) expansion process are obtained mathematically and presented in Table 2. In Table 2 can be clearly seen that the pressures and mass flow rates are identical as in Table 1, while steam specific entropies are always the same for each cylinder. Operating points related to ideal (isentropic) steam expansion process are marked with the same numbers as in Table 1 and Fig. 1, but with an addition of abbreviation – is.

Table 2. *Steam operating parameters of the observed turbine for ideal (isentropic) expansion*

O.P.*	Pressure (bar)	Mass flow rate (kg/s)	Specific entropy (isentropic expansion) (kJ/kg·K)	Specific enthalpy (isentropic expansion) (kJ/kg)
1	66.220	1943.04	5.8317	2771.4
2is	22.850	161.49	5.8317	2575.2
3is	11.650	1781.55	5.8317	2460.7
4	11.080	1456.71	6.8195	2911.3
5is	4.960	66.96	6.8195	2746.1
6is	2.378	83.36	6.8195	2614.6
7is	0.891	116.34	6.8195	2456.2
8is	0.158	69.92	6.8195	2216.4
9is	0.0763	1120.13	6.8195	2127.6

* O.P. = Operating Point (according to Fig. 2)

According to data from Table 1 and Table 2 is drawn h-s diagram for the ideal (isentropic) and real (polytropic) steam expansion processes through both analyzed turbine cylinders, Fig. 2. Between the HPC and LPC occur moisture separation and steam reheating processes which resulted with an increase in steam specific enthalpy (between operating points 3 and 4). It also should be noted that almost entire steam expansion process in both observed turbine cylinders occurs under the saturation line (only operating points 4 and 5 are in the superheated steam area), Fig. 2. Almost the entire turbine operation under the saturation line is the characteristic not only for the observed, but also for any other steam turbine which operate in nuclear power plant [20].

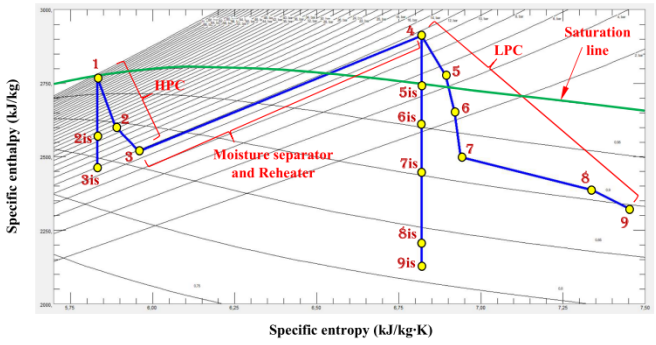


Fig. 2. *Ideal (isentropic) and real (polytropic) steam expansion processes in h-s diagram through both analyzed turbine cylinders (drawn according to data from Table 1 and Table 2, using [19])*

4. Energy analysis equations

4.1. General energy analysis equations and balances

The first law of thermodynamics defines energy analysis of any system or a control volume [21, 22]. While disregarding potential and kinetic energies, which have a low influence on the entire energy balance, energy balance equation of any system or a control volume can be written as [23]:

$$\left(\dot{Q} + P + \sum \dot{E}n\right)_{\text{inlet}} = \left(\dot{Q} + P + \sum \dot{E}n\right)_{\text{outlet}}. \tag{1}$$

In the above equation, P is mechanical power and $\dot{Q}$ is energy transfer by heat. $\dot{E}n$ is a total energy power of fluid flow, defined according to [24] as:

$$\dot{E}n = \dot{m} \cdot h. \tag{2}$$

In Eq. 2, $\dot{m}$ is a fluid mass flow rate and h is fluid specific enthalpy (fluid energy content). During any system or a control volume operation, fluid mass flow rate leakage usually did not occur, therefore the valid mass flow rate balance is [25]:

$$\sum \dot{m}_{\text{inlet}} = \sum \dot{m}_{\text{outlet}}. \tag{3}$$

The overall definition of any system or a control volume energy efficiency is [26]:

$$\eta_{\text{en}} = \frac{\text{cumulative energy outlet}}{\text{cumulative energy inlet}}. \tag{4}$$

Presented equations and balances will be used in energy analysis of the whole observed steam turbine and each of its cylinders.

4.2. Energy analysis equations of the observed steam turbine

Markings in all the equations presented in this section will be related to operating points from Fig. 1 and Fig. 2.

High Pressure Cylinder (HPC)

- Real (polytropic) and ideal (isentropic) mechanical power:

$$P_{\text{re,HPC}} = \dot{m}_1 \cdot (h_1 - h_2) + (\dot{m}_1 - \dot{m}_2) \cdot (h_2 - h_3), \tag{5}$$

$$P_{\text{id,HPC}} = \dot{m}_1 \cdot (h_1 - h_{2\text{is}}) + (\dot{m}_1 - \dot{m}_2) \cdot (h_{2\text{is}} - h_{3\text{is}}). \tag{6}$$

- Energy loss:

$$\dot{E}n_{\text{loss,HPC}} = P_{\text{id,HPC}} - P_{\text{re,HPC}}. \tag{7}$$

- Energy loss per unit of produced mechanical power:

$$\dot{E}n_{\text{loss,power,HPC}} = \frac{\dot{E}n_{\text{loss,HPC}}}{P_{\text{re,HPC}}} \cdot 100. \tag{8}$$

- Energy efficiency:

$$\eta_{\text{en,HPC}} = \frac{P_{\text{re,HPC}}}{P_{\text{id,HPC}}}. \tag{9}$$

Low Pressure Cylinder (LPC)

- Real (polytropic) and ideal (isentropic) mechanical power:

$$P_{\text{re,LPC}} = \dot{m}_4 \cdot (h_4 - h_5) + (\dot{m}_4 - \dot{m}_5) \cdot (h_5 - h_6) + (\dot{m}_4 - \dot{m}_5 - \dot{m}_6) \cdot (h_6 - h_7) + (\dot{m}_4 - \dot{m}_5 - \dot{m}_6 - \dot{m}_7) \cdot (h_7 - h_8) + \dot{m}_9 \cdot (h_8 - h_9), \tag{10}$$

$$P_{\text{id,LPC}} = \dot{m}_4 \cdot (h_4 - h_{5\text{is}}) + (\dot{m}_4 - \dot{m}_5) \cdot (h_{5\text{is}} - h_{6\text{is}}) + (\dot{m}_4 - \dot{m}_5 - \dot{m}_6) \cdot (h_{6\text{is}} - h_{7\text{is}}) + (\dot{m}_4 - \dot{m}_5 - \dot{m}_6 - \dot{m}_7) \cdot (h_{7\text{is}} - h_{8\text{is}}) + \dot{m}_9 \cdot (h_{8\text{is}} - h_{9\text{is}}). \tag{11}$$

- Energy loss:

$$\dot{E}n_{\text{loss,LPC}} = P_{\text{id,LPC}} - P_{\text{re,LPC}}. \tag{12}$$

- Energy loss per unit of produced mechanical power:

$$\dot{E}n_{\text{loss,power,LPC}} = \frac{\dot{E}n_{\text{loss,LPC}}}{P_{\text{re,LPC}}} \cdot 100. \tag{13}$$

- Energy efficiency:

$$\eta_{\text{en,LPC}} = \frac{P_{\text{re,LPC}}}{P_{\text{id,LPC}}}. \quad (14)$$

Whole Turbine (WT)

- Real (polytropic) and ideal (isentropic) mechanical power:

$$P_{\text{re,WT}} = P_{\text{re,HPC}} + P_{\text{re,LPC}}, \quad (15)$$

$$P_{\text{id,WT}} = P_{\text{id,HPC}} + P_{\text{id,LPC}}. \quad (16)$$

- Energy loss:

$$\dot{E}n_{\text{loss,WT}} = P_{\text{id,WT}} - P_{\text{re,WT}}. \quad (17)$$

- Energy loss per unit of produced mechanical power:

$$\dot{E}n_{\text{loss,power,WT}} = \frac{\dot{E}n_{\text{loss,WT}}}{P_{\text{re,WT}}} \cdot 100. \quad (18)$$

- Energy efficiency:

$$\eta_{\text{en,WT}} = \frac{P_{\text{re,WT}}}{P_{\text{id,WT}}}. \quad (19)$$

5. Results and discussion

Real (polytropic) steam expansion process involves several losses which did not occur in ideal (isentropic) steam expansion process. The expected result is that mechanical power of the whole turbine and each turbine cylinder is lower in the real in comparison to ideal expansion process, Fig. 3.

As can be seen from Fig. 3, the dominant mechanical power producer from the observed turbine is LPC which mechanical power is approximately two times higher (in both real and ideal expansion processes) in comparison to HPC.

The whole observed turbine develop 1247.69 MW of mechanical power (real steam expansion process), while in an ideal situation the whole turbine can develop 1600.39 MW of mechanical power. Therefore, the ideal (isentropic) steam expansion process shows maximum mechanical power potential of the whole turbine (or each cylinder) which can be developed if all the losses are neglected.

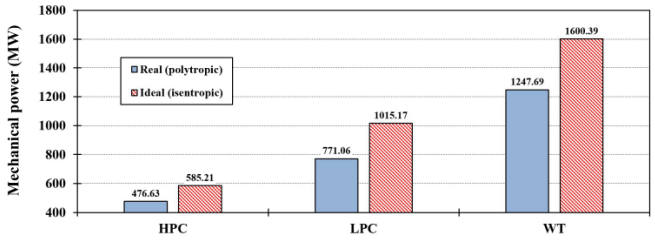


Fig. 3. *Real (polytropic) and ideal (isentropic) mechanical power of the whole analyzed turbine and each its cylinder*

The difference between ideal and real mechanical power of the whole analyzed steam turbine and each of its cylinders represents an energy loss. As shown in Fig. 4, the dominant mechanical power loss, if observing both cylinders, occurs in LPC (more than two times higher in comparison to HPC). Energy loss of the whole turbine is equal to 352.70 MW.

Energy loss per unit of produced mechanical power is the variable related to specific fuel consumption in internal combustion engines [27]. Specific fuel consumption allows comparison of, for example, high power slow speed marine two stroke diesel engines and low power automotive fast speed four stroke diesel or gasoline engines. Energy loss per unit of produced mechanical power allows comparison of different steam turbines (or its cylinders), regardless of steam operating parameters, developed power, size, or any other parameter related to each turbine.

Energy loss per unit of produced mechanical power equals 22.78%, 31.66% and 28.27% for the HPC, LPC and the whole observed steam turbine, respectively. Comparison of HPC and LPC shows that per unit of produced mechanical power LPC has a much higher energy loss. The energy loss per unit of produced mechanical power of the whole turbine is much closer to LPC than to HPC, which means that the dominant influence on this parameter for the whole turbine has LPC.

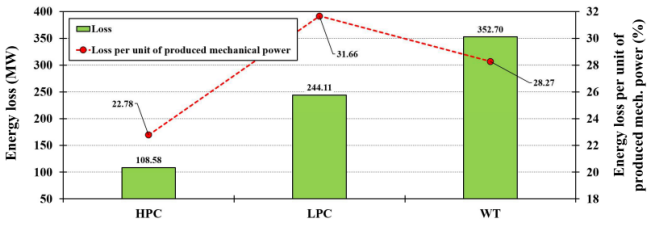


Fig. 4. *Energy loss and energy loss per unit of produced mechanical power for the whole analyzed turbine and each its cylinder*

Considering both cylinders of the analyzed steam turbine, LPC which is the dominant mechanical power producer and which has higher energy loss, also has much lower energy efficiency in comparison to HPC, Fig. 5. The energy efficiency of the HPC is 81.45%, while of the LPC is 75.95%. Whole turbine energy efficiency is equal to 77.96% what again confirms that LPC has the dominant influence on the whole turbine energy analysis parameters.

According to obtained energy efficiency of the whole analyzed steam turbine from nuclear power plant, it can be concluded that such energy efficiency is comparable to the energy efficiency of main marine steam turbines at the highest loads [28]. Also, it is expected that such turbine from nuclear power plant has much lower energy efficiency in comparison to steam turbines from conventional steam power plants [29] because in nuclear power plant steam turbine operates dominantly by using wet steam. Operation with wet steam (steam under the saturation line) brings several additional losses in the turbine operation (inner turbine losses) [30].

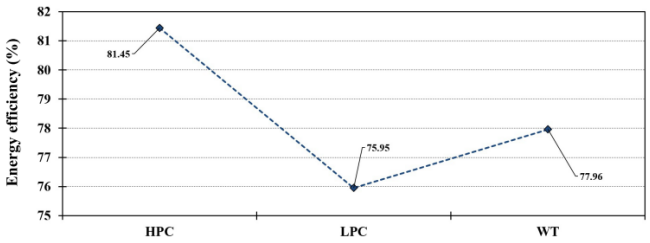


Fig. 5. *The energy efficiency of the whole analyzed turbine and each its cylinder*

Further research of the observed steam turbine from nuclear power plant will be performed by using various artificial intelligence approaches [31-33]. If possible, it will be performed optimization. Low pressure cylinder of the observed turbine, which has a much higher energy loss and much lower energy efficiency in comparison to the high pressure cylinder will be the baseline for any further research and improvement.

6. Conclusions

In this paper is performed energy analysis of the two-cylinder steam turbine, which operates in nuclear power plant. Mechanical power, energy loss, energy loss per unit of produced mechanical power as well as energy efficiency are calculated for each cylinder and the whole observed turbine. The most important conclusions from the performed analysis are:

- The dominant mechanical power producer from the observed turbine is LPC which mechanical power is approximately two times higher in comparison to HPC. The whole observed turbine develop 1247.69 MW of mechanical power in the real (polytropic) steam expansion process.
- Comparison of both turbine cylinders shows that LPC has much higher energy loss and energy loss per unit of produced mechanical power in comparison to HPC. Energy loss of the whole turbine is

352.70 MW, while energy loss per unit of produced mechanical power of the whole turbine is 28.27%.

- Energy efficiency of the whole turbine is 77.96%, which makes it comparable to main marine steam turbines at the highest loads. Such energy efficiency is notably lower in comparison to steam turbines from conventional steam power plants, what is an expected occurrence because steam turbine in nuclear power plant operates with wet, not superheated steam.
- LPC has much lower energy efficiency in comparison to HPC (75.95% in comparison to 81.45%), so any possible improvement of this turbine should be based firstly on the LPC.

7. Acknowledgment

This research has been supported by the Croatian Science Foundation under the project IP-2018-01-3739, CEEPUS network CIII-HR-0108, European Regional Development Fund under the grant KK.01.1.1.01.0009 (DATACROSS), project CEKOM under the grant KK.01.2.2.03.0004, CEI project "COVIDAi" (305.6019-20), University of Rijeka scientific grants: uniri-tehnic-18-275-1447, uniri-tehnic-18-18-1146 and uniri-tehnic-18-14.

8. References

[1] Erdem, H. H., Akkaya, A. V., Cetin, B., Dagdas, A., Sevilgen, S. H., Sahin, B., ... & Atas, S. (2009). Comparative energetic and exergetic performance analyses for coal-fired thermal power plants in Turkey. International Journal of Thermal Sciences, 48(11), 2179-2186. (doi:10.1016/j.ijthermalsci.2009.03.007)

[2] Elhelw, M., Al Dahma, K. S., & el Hamid Attia, A. (2019). Utilizing exergy analysis in studying the performance of steam power plant at two different operation mode. Applied Thermal Engineering, 150, 285-293. (doi:10.1016/j.applthermaleng.2019.01.003)

[3] Ersayin, E., & Ozgener, L. (2015). Performance analysis of combined cycle power plants: A case study. Renewable and Sust. Energy Reviews, 43, 832-842. (doi:10.1016/j.rser.2014.11.082)

[4] Lorencin, I., Anđelić, N., Mrzljak, V., & Car, Z. (2019). Genetic Algorithm Approach to Design of Multi-Layer Perceptron for Combined Cycle Power Plant Electrical Power Output Estimation. Energies, 12(22), 4352. (doi:10.3390/en12224352)

[5] Aljundi, I. H. (2009). Energy and exergy analysis of a steam power plant in Jordan. Applied thermal engineering, 29(2-3), 324-328. (doi:10.1016/j.applthermaleng.2008.02.029)

[6] Mrzljak, V., Poljak, I., & Prpić-Oršić, J. (2019). Exergy analysis of the main propulsion steam turbine from marine propulsion plant. Brodogradnja: Teorija i praksa brodogradnje i pomorske tehnike, 70(1), 59-77. (doi:10.21278/brod70105)

[7] Behrendt, C., & Stoyanov, R. (2018). Operational Characteristic of Selected Marine Turbounits Powered by Steam from Auxiliary Oil-Fired Boilers. New Trends in Production Engineering, 1(1), 495-501. (doi:10.2478/ntpe-2018-0061)

[8] Medica-Viola, V., Mrzljak, V., Anđelić, N., & Jelić, M. (2020). Analysis of Low-Power Steam Turbine With One Extraction for Marine Applications. NAŠE MORE: znanstveni časopis za more i pomorstvo, 67(2), 87-95. (doi:10.17818/NM/2020/2.1)

[9] Kamate, S. C., & Gangavati, P. B. (2010). Energy and exergy analysis of a 44-MW bagasse-based cogeneration plant in India. Cogeneration and distributed generation journal, 25(1), 35-51. (doi:10.1080/15453661009709861)

[10] Burin, E. K., Vogel, T., Multhaupt, S., Thelen, A., Oeljeklaus, G., Gorner, K., & Bazzo, E. (2016). Thermodynamic and economic evaluation of a solar aided sugarcane bagasse cogeneration power plant. Energy, 117, 416-428. (doi:10.1016/j.energy.2016.06.071)

[11] Naserbegi, A., Aghaie, M., Minuchehr, A., & Alahyarizadeh, G. (2018). A novel exergy optimization of Bushehr nuclear power plant by gravitational search algorithm (GSA). Energy, 148, 373-385. (doi:10.1016/j.energy.2018.01.119)

[12] Al-Zareer, M., Dincer, I., & Rosen, M. A. (2017). Development and assessment of a novel integrated nuclear plant for electricity and hydrogen production. Energy Conversion and Management, 134, 221-234. (doi:10.1016/j.enconman.2016.12.004)

[13] Ray, T. K., Datta, A., Gupta, A., & Ganguly, R. (2010). Exergy-based performance analysis for proper O&M decisions in a steam power plant. Energy Conversion and Management, 51(6), 1333-1344. (doi:10.1016/j.enconman.2010.01.012)

[14] Wang, C., Yan, C., Wang, J., Tian, C., & Yu, S. (2017). Parametric optimization of steam cycle in PWR nuclear power plant using improved genetic-simplex algorithm. Applied Thermal Eng., 125, 830-845. (doi:10.1016/j.applthermaleng.2017.07.045)

[15] Škopac, L., Medica-Viola, V., & Mrzljak, V. (2020). Selection Maps of Explicit Colebrook Approximations according to Calculation Time and Precision. Heat Transfer Engineering, 1-15. (doi:10.1080/01457632.2020.1744248)

[16] Cangioli, F., Chatterton, S., Pennacchi, P., Nettis, L., & Ciuchicchi, L. (2018). Thermo-elasto bulk-flow model for labyrinth seals in steam turbines. Tribology international, 119, 359-371. (doi:10.1016/j.triboint.2017.11.016)

[17] Mrzljak, V., Kudláček, J., Begić-Hajdarević, Đ., & Musulin, J. (2020). The Leakage of Steam Mass Flow Rate through the Gland Seals–Influence on Turbine Produced Power. Pomorski zbornik, 58(1), 39-56. (doi:10.18048/2020.58.03.)

[18] Marques, J. G., Costa, A. L., Pereira, C., & Fortini, Â. (2019). Energy and Exergy Analyses of Angra 2 Nuclear Power Plant. Brazilian Journal of Radiation Sciences, 7(2B). (doi:10.15392/bjrs.v7i2B.647)

[19] Lemmon, E. W., Huber, M. L., & McLinden, M. O. (2010). NIST Standard Reference Database 23, Reference Fluid Thermodynamic and Transport Properties (REFPROP), version 9.0, National Institute of Standards and Technology. R1234yf. fld file dated December, 22, 2010.

[20] Kostyuk, A., & Frolov, V. (1988). Steam and gas turbines. Mir Publishers.

[21] Kanoğlu, M., Çengel, Y. A., & Dinçer, İ. (2012). Efficiency evaluation of energy systems. Springer Science & Business Media.

[22] Mrzljak, V. (2018). Low power steam turbine energy efficiency and losses during the developed power variation. Tehnički glasnik, 12(3), 174-180. (doi:10.31803/tg-20180201002943)

[23] Mrzljak, V., Blecich, P., Anđelić, N., & Lorencin, I. (2019). Energy and Exergy Analyses of Forced Draft Fan for Marine Steam Propulsion System during Load Change. Journal of Marine Science and Engineering, 7(11), 381. (doi:10.3390/jmse7110381)

[24] Medica-Viola, V., Baressi Šegota, S., Mrzljak, V., & Štifanić, D. (2020). Comparison of conventional and heat balance based energy analyses of steam turbine. Pomorstvo, 34(1), 74-85. (doi:10.31217/p.34.1.9)

[25] Mrzljak, V., Anđelić, N., Poljak, I., & Orović, J. (2019). Thermodynamic analysis of marine steam power plant pressure reduction valves. Pomorski zbornik, 56(1), 9-30. (doi:10.18048/2019.56.01)

[26] Koroglu, T., & Sogut, O. S. (2018). Conventional and advanced exergy analyses of a marine steam power plant. Energy, 163, 392-403. (doi:10.1016/j.energy.2018.08.119)

[27] Mrzljak, V., Medica, V., & Mrakovčić, T. (2015). Simulation of diesel engine cylinder process using quasi-dimensional numerical model. Pomorstvo, 29(2), 165-169.

[28] Mrzljak, V., & Poljak, I. (2019). Energy Analysis of Main Propulsion Steam Turbine from Conventional LNG Carrier at Three Different Loads. NAŠE MORE: znanstveno-stručni časopis za more i pomorstvo, 66(1), 10-18. (doi:10.17818/NM/2019/1.2)

[29] Ahmadi, G. R., & Toghraie, D. (2016). Energy and exergy analysis of Montazeri steam power plant in Iran. Renewable and Sust. Energy Reviews, 56, 454-463. (doi:10.1016/j.rser.2015.11.074)

[30] Tanuma, T. (Ed.). (2017). Advances in Steam Turbines for Modern Power Plants. Woodhead Publishing.

[31] Anđelić, N., Baressi Šegota, S., Lorencin, I., Poljak, I., Mrzljak, V., & Car, Z. (2021). Use of Genetic Programming for the Estimation of CODLAG Propulsion System Parameters. Journal of Marine Science and Engineering, 9(6), 612. (doi:10.3390/jmse9060612)

[32] Mrzljak, V., Anđelić, N., Lorencin, I., & Sandi Baressi Šegota, S. (2021). The influence of various optimization algorithms on nuclear power plant steam turbine exergy efficiency and destruction. Pomorstvo, 35(1), 69-86. (doi:10.31217/p.35.1.8)

[33] Baressi Šegota, S., Lorencin, I., Anđelić, N., Mrzljak, V., & Car, Z. (2020). Improvement of Marine Steam Turbine Conventional Exergy Analysis by Neural Network Application. Journal of Marine Science and Engineering, 8(11), 884. (doi:10.3390/jmse8110884)